1-1-2012

Cardiac PI3Kα Signaling and K+ Channel Regulation in Cardiac Hypertrophy and Heart Failure

Kai-Chien Yang
Washington University in St. Louis

WASHINGTON UNIVERSITY IN ST. LOUIS

Division of Biology and Biomedical Sciences

Molecular Genetics and Genomics

Dissertation Examination Committee:
Jeanne Nerbonne, Chair
Patrick Jay
Douglas Mann
Colin Nichols
Jean Schaffer
Gary Stormo

Cardiac PI3Kα Signaling and K^+ Channel Regulation in Cardiac Hypertrophy and Heart Failure

by

Kai-Chien Yang

A dissertation presented to the
Graduate School of Arts and Sciences
of Washington University in
partial fulfillment of the
requirements for the degree
of Doctor of Philosophy

May 2012

Saint Louis, Missouri

ABSTRACT OF THE DISSERTATION

Cardiac PI3Kα Signaling and K^+ Channel Regulation in Cardiac Hypertrophy and Heart Failure

by

Kai-Chien Yang

Doctor of Philosophy in Biology and Biomedical Sciences

Molecular Genetics and Genomics

Washington University in St. Louis, 2012

Professor Jeanne Nerbonne, Chairperson

Pathologic biomechanical stresses cause cardiac hypertrophy, which is associated with QT prolongation and increased risk of life-threatening ventricular arrhythmias. Previous studies demonstrated that repolarizing K^+ current densities are decreased in pressure overload-induced left ventricular hypertrophy, resulting in action potential and QT prolongation. Cardiac hypertrophy also occurs with exercise training, but this "physiological hypertrophy" is not associated with electrical abnormalities or increased arrhythmia risk, suggesting that repolarizing K^+ currents are upregulated, in parallel with the increase in myocyte size, to maintain normal cardiac function. To explore this hypothesis directly, two mouse models of physiological hypertrophy, one produced by chronic exercise (swim-) training of wild type mice and the other by cardiac-specific expression of constitutively active phosphoinositide-3-kinase-p110α (caPI3Kα), were utilized. Electrophysiological experiments revealed that repolarizing K^+ current amplitudes were increased and K^+ current densities were normalized in hypertrophied ventricular myocytes from swim-trained or caPI3Kα animals. Molecular analyses revealed that increases in K^+ currents reflect the upregulation of the transcripts encoding

the underlying K^+ channel subunits. Importantly, additional experiments demonstrated that the transcriptional upregulation of myocardial K^+ channel expression in response to exercise or augmented PI3Kα signaling is independent of cellular hypertrophy and Akt signaling.

The hypothesis that increased PI3Kα signaling can counteract the adverse electrophysiological remodeling, including decreased K^+ current densities and impaired repolarization associated with pathological hypertrophy and heart failure was also explored. These experiments revealed that increased PI3Kα signaling, but not renin-angiotensin system blockade, results in transcriptional upregulation of repolarizing K^+ channel subunits and normalization of K^+ current densities in transverse aortic constriction (TAC)-induced pathological hypertrophy, as well as in a transgenic mouse model of dilated cardiomyopathy/heart failure. Increased PI3Kα signaling, therefore, normalizes ventricular action potential durations, QT intervals and cardiac electrical functioning in the hypertrophied and failing heart.

Additional studies here applied a combined miRNA- and RNA-sequencing approach to define the impact of enhanced PI3Kα signaling on myocardial transcriptome structure in the setting of pressure overload-induced pathological left ventricular hypertrophy. These analyses revealed that enhanced PI3Kα signaling normalized miRNAs and mRNAs that were aberrantly expressed in pathological hypertrophy and that increased PI3Kα signaling reduces cardiac fibrosis in pathological hypertrophy through the modulation of TGF-β signaling and miR-21 expression.

In conclusion, enhanced PI3Kα signaling results in the transcriptional upregulation of K^+ channel subunits and the maintenance of cardiac excitability in physiological hypertrophy, and the impact of increased PI3Kα signaling on K^+ channel regulation is independent of cellular hypertrophy and Akt. In addition, enhancing PI3Kα signaling

increases repolarizing K^+ currents and K^+ channel subunit expression in mouse models of pathological hypertrophy and heart failure, ameliorating arrhythmogenic electrical remodeling. Augmentation of PI3Kα signaling, therefore, may be a useful and unique strategy to protect against the increased risk of ventricular arrhythmias and sudden death associated with cardiomyopathy. The results here also demonstrate the power and robustness of next-generation sequencing in efforts to define the cardiac transcriptome architecture and dynamics in physiological and pathological contexts, as well as to identify novel molecular mechanisms important in cardiovascular pathophysiology.

Acknowledgements

It is my great and humble pleasure to acknowledge many people who have made this thesis work possible. First and foremost, I would like to thank all the present and past members of the Nerbonne Lab, who made each day in the lab a pleasant adventure, in both science and culture. You have been a wonderful source of friendships as well as scientific advice and collaboration during my graduate studies at Washington University. In particular, I wish to express my sincere gratitude to my mentor, Drs. Jeanne Nerbonne, for the continuous support of my research, for her patience, enthusiasm, inspiration, and immense knowledge in electrophysiology and science. I appreciate all her contributions of time, ideas and funding that make my research experience productive and stimulating. I am also grateful for the excellent example she has provided as a great researcher who thinks critically about science. I would like to thank the members of my thesis committee for their time, interest, insightful questions and helpful comments. In addition, I wish to thank fellow scientists who generously provided reagents: Dr Patrick Jay and Julie McMullen for the gift of the caPI3Kα mice, Dr Tony Muslin for the gift of the Akt1$^{-/-}$ mice, and Dr. Yi-Tang Tseng for the gift of the icaPI3Kα animals. For the sequencing experiments, I would like to thank Jeffrey Ku and Dr. Mike Lovett for all the support and inspirational discussions. This work would not have been possible without the financial support of the National Institutes of Health (HL034161) and the Midwest Affiliate of the American Heart Association (09PRE2050215). Last but not least, I would like to thank my parents for all their love, encouragement and support, all my friends in St Louis who made my life here so enjoyable, and most of all thanks to my loving, supportive, encouraging and patient wife Irene whose faithful support during the years of my graduate studies is so appreciated. Thank you.

Table of Content

List of Figures and Tables

List of Abbreviations

α, pore-forming; ACE, angiotensinn converting enzyme; Akt1$^{-/-}$, Akt1 knock-out; α-MHC, α-myosin heavy chain; APA, action potential amplitude; APD_{25}, action potential duration at 25% recovery; APD_{50}, action potential duration at 50% recovery; APD_{90}, action potential duration at 90% recovery; BNP: brain natriuretic peptide; CaMKII, calmodulin kinase II; caPI3Kα: constitutively active phosphoinositide-3-kinase p110α; Cav, voltage-gated Ca^{2+}; ECG, electrocardiogram; CS, Citrate synthase; C_T, threshold cycle; Dox, doxycycline; EGTA, ethylene glycol tetraacetic acid; ERK, extracellular signal regulated kinase; FDR: false discovery rate; FOXO, Forkhead family of transcriptional factors; GAPDH, glyceraldehyde 3-phosphate dehydrogenase; GH: growth hormone; GO: gene ontology; GPCR: G-protein coupled receptor; GSK3β, Glycogen synthase kinase 3 beta; HP, holding potential; HPRT, Hypoxanthine-guanine phosphoribosyltransferase; I_{Ca}, voltage-gated inward Ca^{2+} currents; icaPI3Kα, inducible constitutively active phosphoinositide-3-kinase p110α; IGF1, insulin-like growth factor 1; IGF1R: insulin-like growth factor 1 receptor; I_K, delayed rectifier K^+ current; I_{Kr}, rapid delayed rectifier K^+ current; I_{Ks}, slow delayed rectifier K^+ current; I_{K1}, inwardly rectifying K^+ current; $I_{K,slow}$, slow-inactivating outward K^+ current; $I_{K,peak}$, peak outward K^+ current; I_{ss}, non-inactivating steady state outward K^+ current; I_{to}, transient outward K^+ current; $I_{to,f}$, fast transient outward K^+ current; $I_{to,s}$, slow transient outward K^+ current; K2P, two (2) pore-domain K^+; KChIP, K^+ Channel Interacting Protein; Kir, inwardly rectifing K^+; Kv, voltage-gated K^+; *Lmna,* nuclear membrane protein lamin A/C; LV, left ventricle; LVA, left ventricular apex; LVH, left ventricular hypertrophy; LVW/TL: LV weight to tibia length ratio; miRNA-Seq: microRNA sequencing; MinK, minimal K^+ channel; MiRP1, MinK Related Peptide 1; mRNA-Seq: messanger RNA sequencing; Nav, voltage-gated Na^+; Navβ1, voltage-gated Na^+ β1 subunit; PBS, phosphate buffered saline; PDK1, phosphatidylinositol-

dependent kinase 1; PIP2, phosphatidylinositol-4,5-bisphosphate; PIP3, phosphatidylinositol-3,4,5-trisphosphate; PKA, cAMP-dependent protein kinase; PKC, protein kinase C; PMMR, sequences per million mapped reads; qRT-PCR: quantitative real time polymerase chain reaction; QT_C, corrected QT; RPKM, reads per kilobase of exon per million mapped reads; RV, right ventricle; SDS-PAGE, sodium dodecyl sulfate polyacrylamide gel electrophoresis; TAC: transverse aortic constriction; TCN, triciribine; τ_d , decay time constant; TTX, Tetrodotoxin; WT, wild type

Chapter 1: Introduction

1.1 Ionic basis of cardiac excitability and contractile function

The normal contractile function of the mammalian heart depends on proper myocardial electrical activity, including the sequential activation of cells in specialized conducting system, the normal propagation of electrical activity through the myocardium, and the generation of action potentials in individual cardiomyocytes (Fozzard, 1991; Roden *et al.*, 2002). The normal cardiac cycle begins with the action potential originating in the sinoatrial node, propagating through the atria to the atrioventriular node; the electrical activity then spreads through the His bundle and conducting Purkinje fibers to the cardiac apex and excites the working ventricular myocardium (Figure 1.1) (Nerbonne & Kass, 2005). The propagation of myocardial electrical activity also depends on electrical coupling mediated by gap junctions, ensuring the coordination of the electromechanical functioning of the atrial and ventricular myocardium (Kanno & Saffitz, 2001). Myocardial action potentials are generated by the sequential activation and inactivation of ion channels conducting depolarizing, Na^+ and Ca^{2+}, and repolarizing, K^+, currents (Fozzard, 1991; Roden *et al.*, 2002). During the action potential, Ca^{2+} influx through voltage-gated Ca^{2+} channels trigger the release of Ca^{2+} ions from the sarcoplasmic reticulum into the cytosol, where Ca^{2+} binds to the protein troponin-C of the troponin-tropomyosin complex, leading to cardiomyocyte longitudinal shortening. The synchronous shortening of the ventricular myocytes results in the contraction of the heart and the systolic ejection of blood (ter Keurs, 2011).

The subsequent diastolic relaxation of the myocytes depends on the repolarization of membrane potential and the removal of Ca^{2+} from the sarcomere (ter Keurs, 2011). Myocardial action potential repolarization is determined by multiple outward K^+ currents through voltage-gated K^+ (Kv) and inwardly rectifying K^+ (Kir) channels. The relative

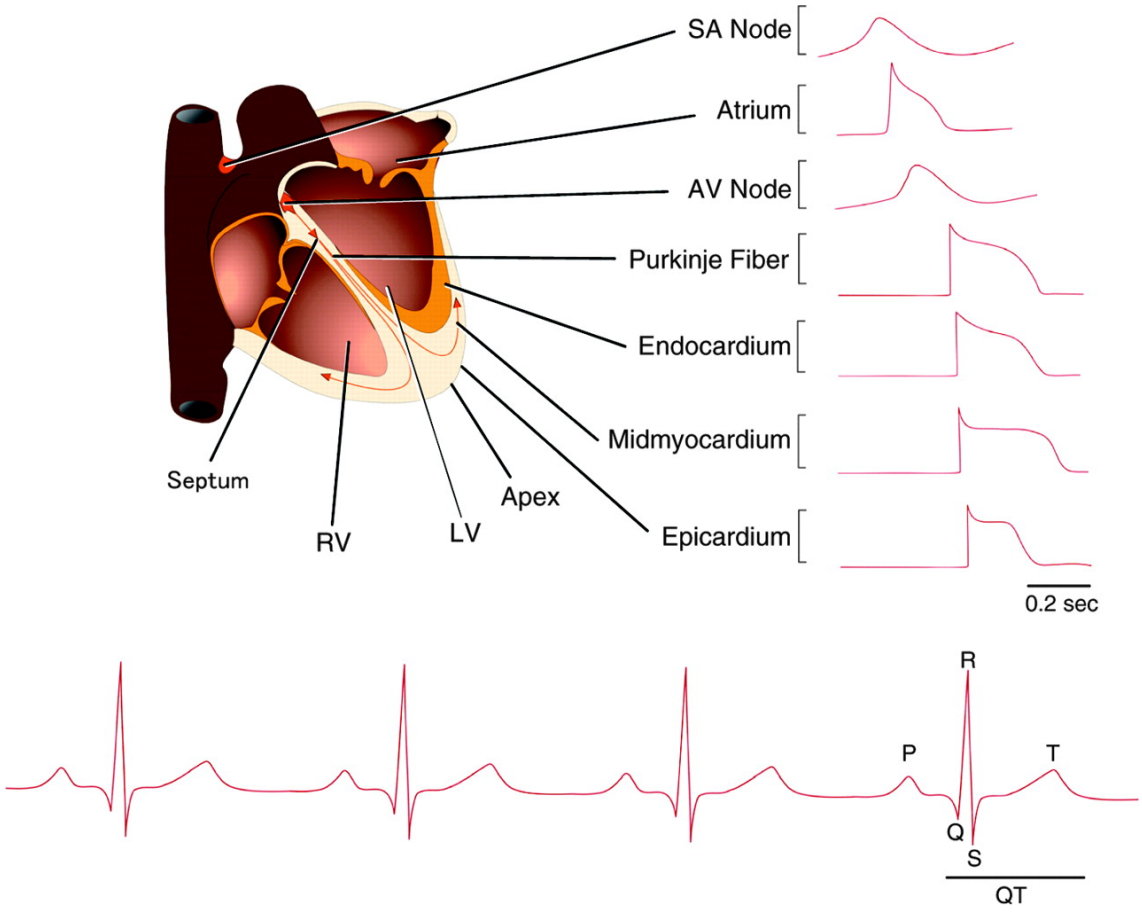

Figure 1.1 Electrical activity in the myocardium

Top: Schematic of a human heart with action potential waveforms recorded in different regions illustrated. *Bottom*: Schematic of a surface electrocardiogram; four sequential beats are displayed. Reprinted from (Nerbonne & Kass, 2005) with permission from the American Physiological Society.

expression levels of Kv channels vary in myocytes from different regions (eg. atrial vs ventricle, epicardium vs endocardium), resulting in the distinct action potential waveforms in atrial and ventricular myocytes, as well as the gradient of repolarization through the ventricular myocardium (**Figure 1.1**) (Nerbonne & Guo, 2002; Nerbonne & Kass, 2005). The transmural ventricular repolarization gradient plays a critical role in the propagation of myocardial electrical activity and the maintenance of normal contractile function (Akar *et al.*, 2000).

1.2 Multiple K^+ currents determine myocardial action potential repolarization

Multiple voltage-gated K^+ (Kv) channels, as well as non-voltage-gated Kir channels, have been identified and demonstrated to contribute to myocardial action potential repolarization (Roden *et al.*, 2002; Nerbonne & Kass, 2005). Based on differences in time- and voltage-dependent properties and pharmacological sensitivities, two types of Kv channels have been distinguished: transient outward Kv (I_{to}) and delayed rectifier Kv (I_K) currents. Currents classified as I_{to} activate and inactivate rapidly upon membrane depolarization and underlie early (phase I) repolarization, whereas I_K currents activate on depolarization with variable kinetics and underlie late (phase III) repolarization (Nerbonne & Kass, 2005). The heterogeneities in the biophysical properties and expression levels of various K^+ currents contribute to the inter-species and inter-regional differences in action potential waveforms (Schram *et al.*, 2002; Nerbonne & Kass, 2005). The I_{to} densities, for example, are high in murine ventricular myocytes, dominating the early repolarization and contributing to the short action potential durations (APD) in mouse cardiomyocytes (**Figure 1.2**, right panel). In contrast, I_{to} in human ventricular myocytes (**Figure 1.2**, left panel) partially repolarizes the membrane potential,

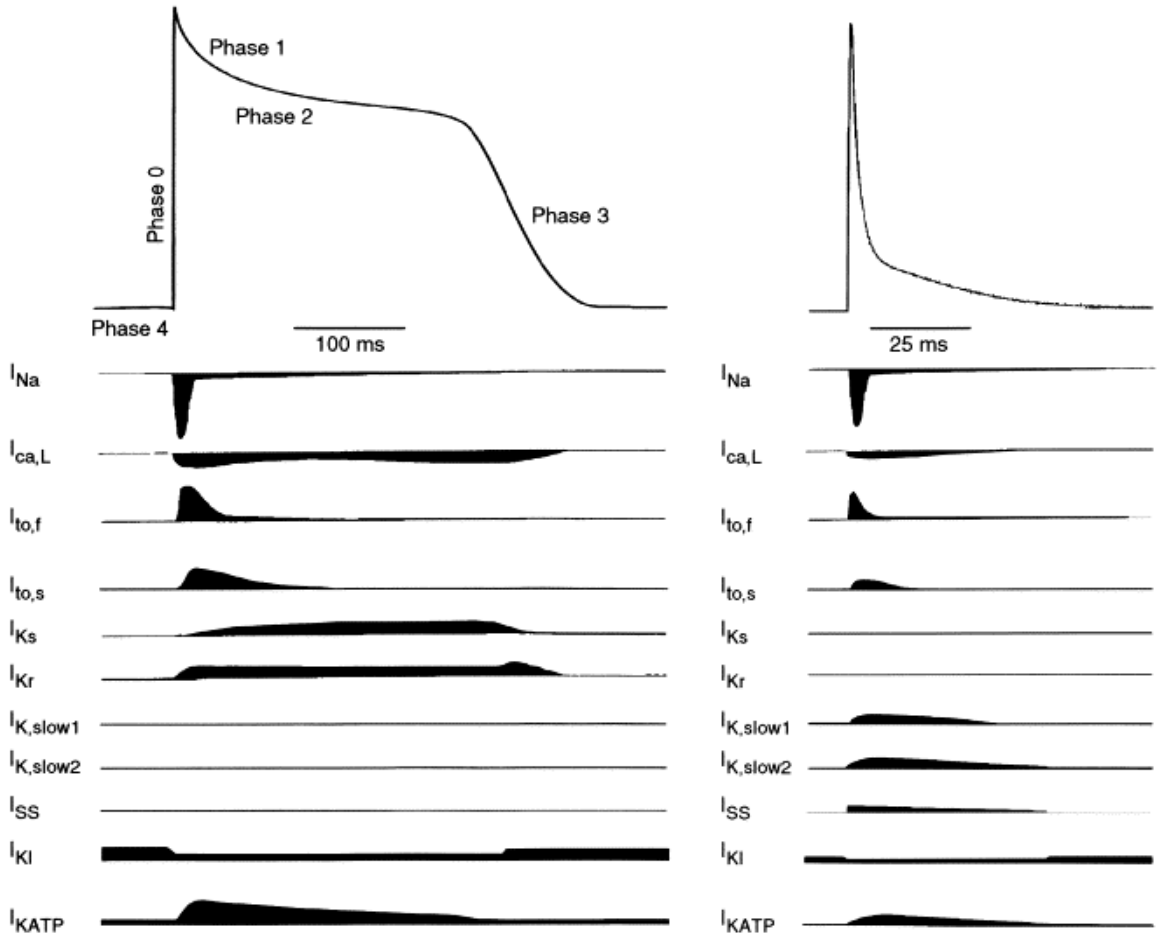

Figure 1. 2 Schematic of action potential waveforms and underlying ionic currents in adult human (left) and mouse (right) ventricular myocytes.

As illustrated, the diversity of outward K^+ currents in myocardial cells is greater than that for the inward Na^+ and Ca^{2+} currents, and the various K^+ currents play distinct roles in action potential repolarization in human and mouse ventricular cells. Reprinted from (Nerbonne, 2004) with permission from Elsevier.

determining phase 1 repolarization and the early plateau potential, yet only influencing APD indirectly (van der Heyden *et al.*, 2006).

Action potential waveforms are typically shorter in the mammalian epicardium (Figure 1.1) than in endocardium, reflecting regional differences in I_{to} and/or I_K densities (Litovsky & Antzelevitch, 1988; Furukawa *et al.*, 1992; Bryant *et al.*, 1998; Nerbonne & Guo, 2002; Costantini *et al.*, 2005). Importantly, while the expression of individual I_{to} and I_K components varies in different cardiac regions and in different species, the biophysical properties and pharmacological sensitivities of the individual current types are similar, suggesting that each is encoded by a unique molecular entity, and that the regional differences in action potential waveforms reflect largely the differences in the expression levels of the various channel types (Nerbonne & Kass, 2005). In the adult mouse ventricular myocardium, two different types of I_{to} ($I_{to,f}$ and $I_{to,s}$) are expressed, along with two distinct slowly inactivating Kv current components, $I_{K,slow1}$ and $I_{K,slow2}$, and a non-inactivating, steady-state current, I_{ss} (**Figure 1.3**) (Guo *et al.*, 1999). While the densities of $I_{K,slow}$ and I_{ss} are expressed at similar levels throughout the ventricles, the expression of $I_{to,f}$ and $I_{to,s}$ varies in different regions (Guo *et al.*, 1999). The expression of $I_{to,f}$, for example, is highest in the right ventricle (RV), intermediate in the left ventricle (LV) (Brunet *et al.*, 2004), lower in ~80% of the interventricular septum (IVS) cells, and undetectable in ~20% of IVS cells (Guo *et al.*, 1999). In addition, $I_{to,s}$ is expressed in all IVS cells, but not detectable in LV or RV myocytes (Brunet *et al.*, 2004).

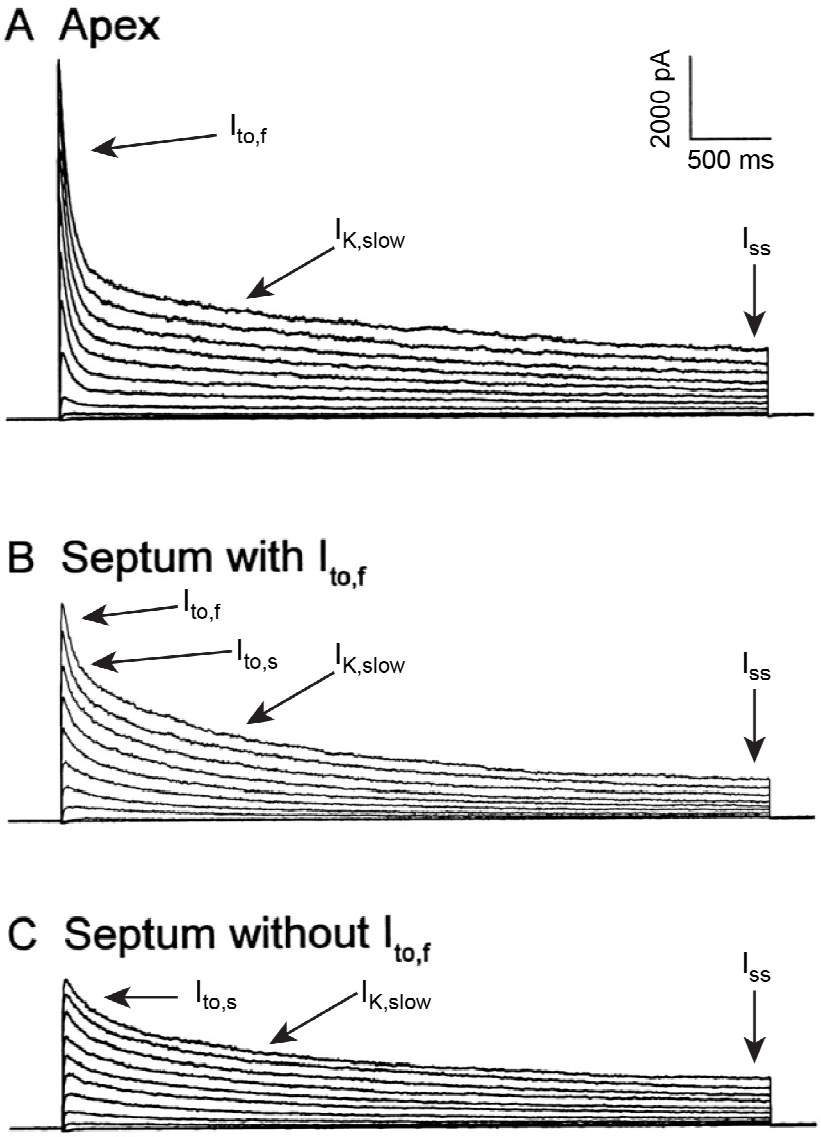

Figure 1.3 Regional differences in Ca^{2+}-independent, depolarization-activated K^+ currents in isolated adult mouse left ventricular myocytes.

Outward K^+ currents were recorded during 4.5-s depolarizing voltage steps to potentials between −40 and +60 mV from a holding potential of −70 mV. The records displayed were from three different cells: one isolated from the apex (A) of the left ventricle (LV) and the other two from the interventricular septum (B and C). The Kv current components, $I_{to,f}$, $I_{to,s}$, $I_{K,slow}$ and I_{ss} are indicated. $I_{to,f}$, which is prominent in cells isolated from the LV apex (A), is expressed at a significantly lower level or is absent in cells isolated from the interventricular septum (B and C). Reprinted and adapted from (Xu *et al.*, 1999b) with permission from the Rockefeller University Press.

While Kv currents contribute importantly to the repolarization of action potentials in mammalian ventricular myocardium, the inwardly rectifying (Kir) currents also contribute to shaping the resting and active membrane properties of cardiomyocytes. Among the several types of Kir currents expressed in adult mouse heart, I_{K1} contributes to the terminal phase of repolarization and the maintenance of resting membrane potentials in mouse ventricular cells (**Figure 1.2**) (Nichols & Lopatin, 1997; Lopatin & Nichols, 2001; Nerbonne & Kass, 2005)

1.3 Molecular determinants of repolarizing K^+ currents in ventricular myocytes

Functional K^+ channels are integral membrane protein complexes consisting of pore-forming (α) subunits, multiple accessory (β) subunits and regulatory proteins (Roden *et al.*, 2002; Nerbonne & Kass, 2005). The α subunits of Kv channels are six-transmembrane-spanning domain (S1-S6) proteins, and functional Kv channels are composed of four α-subunits. A large number of Kv α subunit genes have been identified (Nerbonne & Kass, 2005), and heterologous expression of the various Kv α subunits reveals functional Kv currents with distinct time- and voltage-dependent properties (Po *et al.*, 1993; Snyders, 1999; Nerbonne & Kass, 2005). In heterologous expression systems, Kv α subunits of the same subfamily have been shown to form heteromeric channels, contributing to the diversity of Kv channels (Covarrubias *et al.*, 1991; Po *et al.*, 1993). In addition, a number of different types of Kv channel accessory subunits have been identified and shown to interact with Kv α subunits to modulate channel biophysical properties and cell surface expression (Nerbonne & Kass, 2005; Abbott *et al.*, 2007), further increasing Kv channel diversity.

Using transgenic and targeted gene knock out strategies and biochemical approaches, it has been demonstrated that in adult mouse ventricles, the pore forming (α) subunit Kv4.2 underlies $I_{to,f}$ (Barry *et al.*, 1998; Guo *et al.*, 2000; Kuo *et al.*, 2001) and that Kv1.4 encodes $I_{to,s}$ (Guo *et al.*, 1999; Guo *et al.*, 2000). Biochemical studies have revealed that the Kv channel accessory (β) subunit, KChIP2, associates with Kv4.2 α subunits in mouse ventricular tissues, modulating the cell surface expression and gating properties of Kv4 channels (Kuo *et al.*, 2001; Guo *et al.*, 2002; Li *et al.*, 2005; Foeger *et al.*, 2012). Exploiting similar strategies, it has been shown that the two components of $I_{K,slow}$, $I_{K,slow1}$ and $I_{K,slow2}$, are encoded by Kv1.5 and Kv2.1, respectively (Xu *et al.*, 1999a; London *et al.*, 2001a; Kodirov *et al.*, 2004; Li *et al.*, 2004). Recent studies in rat ventricular myocytes have also suggested that the two-pore domain K^+ (K2P) channel subunit, *KCNK3* (TASK1), underlies I_{ss} currents (Putzke *et al.*, 2007; Wang *et al.*, 2012).

Similar to the Kv channels, multiple functionally distinct types of Kir channel pore-forming α-subunits (Kir1-6) have been identified. The Kir α-subunits, like Kv channels, assemble as tetramers to form functional Kir channels (Nichols & Lopatin, 1997; Lopatin & Nichols, 2001; Nerbonne & Kass, 2005), although Kir α-subunits have only two, instead of six, transmembrane domains. It has been shown that murine cardiac I_{K1} channels appear to reflect the heteromeric assembly of the Kir α-subunits, Kir 2.1 and Kir 2.2 (Nichols *et al.*, 1996; Zaritsky *et al.*, 2000; Zaritsky *et al.*, 2001; McLerie & Lopatin, 2003; Zobel *et al.*, 2003).

Accumulating evidence suggests that myocardial repolarizing K^+ channels function as components of macromolecular protein complexes, comprising different pore-forming and accessory channel subunits and other regulatory proteins that mediate interactions

with the actin cytoskeleton, extracellular matrix and/or signaling proteins (Nerbonne & Kass, 2005), each of which likely plays a role in determining repolarizing K^+ channel properties and functional K^+ channel cell surface expression.

1.4 Repolarizing K^+ current remodeling in cardiac hypertrophy and heart failure

Cardiac hypertrophy, defined as thickening of the myocardial wall along with enlargement of the heart, is associated with increased cardiomyocyte size secondary to pathological stresses (valvular heart diseases, hypertensioin, myocardial infarction etc.), physiological loading (exercise training or pregnancy) or intrinsic sarcomeric protein mutations (Lorell & Carabello, 2000). Cardiac hypertrophy induced by pathological stresses (pathological hypertrophy), although initially a compensatory response to increased load, results in impaired, deteriorating cardiac function. In addition, decompensated cardiac hypertrophy leads to left ventricular (LV) dilatation, increased interstitial fibrosis, and ultimately heart failure (Levy *et al.*, 1990). By contrast, exercise training-induced physiological hypertrophy is associated with maintained (or enhanced) cardiac function, normal histological features with no evidence of interstitial fibrosis, and does not progress to failure (Kaplan *et al.*, 1994; Pluim *et al.*, 2000).

At the molecular level, pathological hypertrophy is associated with upregulation of the fetal gene program, including atrial natriuretic peptide (ANP), B-type natriuretic peptide (BNP), and fetal forms of contractile proteins, such as skeletal α-actin and β-myosin heavy chain (β-MHC). These changes are accompanied by downregulation of adult cardiac proteins, such as α-MHC and sarcoplasmic reticulum Ca^{2+}-ATPase (McMullen &

Jennings, 2007). In contrast, this molecular remodeling is not observed in physiological hypertrophy induced by exercise training (McMullen *et al.*, 2003).

Pathological hypertrophy is also associated with increased risk of cardiac arrhythmias and sudden cardiac death. Large-scaled epidemiological studies have revealed higher rates of ventricular arrhythmias and atrial fibrillation in individuals (patients) with pathological hypertrophy (Messerli *et al.*, 1984; Levy *et al.*, 1987; McLenachan *et al.*, 1987). The Framingham Heart Study, for example, reported that pathological hypertrophy is associated with >2 fold increase in risk for sudden cardiac death, independent of the development of heart failure. Several mechanisms have been proposed to account for the increased arrhythmogenicity associated with pathological hypertrophy, including impaired myocardial perfusion (Harrison *et al.*, 1991; Houghton *et al.*, 1992), fibrosis-related pro-arrhythmic substrates (Mammarella *et al.*, 2000), and abnormal electrophysiological properties of the hypertrophied cardiomyocytes (Nordin *et al.*, 1989; Rials *et al.*, 1997; Swynghedauw *et al.*, 1997). Consistent with the latter hypothesis, pathological hypertrophy results in prolonged ventricular action potential durations (APD) and increased APD dispersion, changes that are reflected (prolonged QT internal and increased QT dispersion) in surface ECG recordings (Gillis *et al.*, 2000), and that appear to reflect impaired myocardial repolarization secondary to the reduction in repolarizing K^+ current densities (Volk *et al.*, 2001a; Wang *et al.*, 2007). The impaired repolarization and increased APD dispersion result in increased electrical heterogeneity in the myocardium and increased arrhythmia susceptibility (Volk *et al.*, 2001a; Marionneau *et al.*, 2008b).

Recent studies in a mouse model of pressure overload-induced left ventricular hypertrophy (LVH) produced by transverse aortic constriction (TAC) revealed that the observed reductions in the densities of repolarizing K^+ currents are not associated with K^+ channel subunit gene/protein downregulation (Marionneau *et al.*, 2008b). Rather, in TAC LV myocytes, increased myocyte size is the main factor in determining the reductions in K^+ current densities. The observed decreases in functional K^+ current densities, therefore, result directly from the failure to upregulate K^+ channel subunit expression levels in proportion to the increase in myocyte size (Marionneau *et al.*, 2008b).

Heart failure, irrespective of the underlying etiology, is associated with increased risk of life-threatening arrhythmias (Tomaselli *et al.*, 1994; Haider *et al.*, 1998). Sudden cardiac death, presumably due to lethal ventricular arrhythmias, accounts for approximately 50% of deaths in individuals with heart failure (Tomaselli *et al.*, 1994). The increased incidence of life-threatening ventricular arrhythmias in heart failure patients is a consequence of complex pathological remodeling in cardiac structural (Akar *et al.*, 2004), neurohumoral (Vaseghi & Shivkumar, 2008) and electrophysiological properties (Beuckelmann *et al.*, 1993; Marionneau *et al.*, 2008b). Electrical remodeling in heart failure (Beuckelmann *et al.*, 1993) results, at least in part, from reductions in the densities of repolarizing K^+ currents, I_{to} (Beuckelmann *et al.*, 1993; Kaab *et al.*, 1998; Tomaselli & Marban, 1999; Li *et al.*, 2002; Akar *et al.*, 2005), delayed rectifier (Tsuji *et al.*, 2000; Li *et al.*, 2002) and I_{K1} (Beuckelmann *et al.*, 1993; Li *et al.*, 2002; Akar *et al.*, 2005), which can lead to action potential prolongation and increased dispersion of repolarization, both of which are arrhythmogenic. Molecular studies have revealed that the decreases in many of the repolarizing K^+ currents in failing hearts reflect the

downregulation of the subunits encoding the underlying channels/currents (Nattel *et al.*, 2007; Nass *et al.*, 2008).

In contrast to pathological hypertrophy or heart failure, exercise training-induced physiological hypertrophy, regardless of the magnitude of hypertrophic growth, is not associated with impaired repolarization, increased QT intervals/dispersion (Mayet *et al.*, 1999), life-threatening arrhythmias, or sudden cardiac death (Pelliccia *et al.*, 2000; Serra-Grima *et al.*, 2000; Biffi *et al.*, 2008). The absence of electrical abnormalities and the immunity against ventricular arrhythmias in physiological hypertrophy suggest that there are fundamental differences in the electrophysiological properties of myocytes in pathological and physiological hypertrophy. Delineating the mechanism(s) underlying the differences in the electrophysiological responses of the myocardium in physiological and pathological hypertrophy is key to advancing our understanding and to developing therapeutic strategies to prevent arrhythmias associated with pathological hypertrophy. These topics are the focus of the studies presented in **Chapter 3 and 4**.

1.5 Physiological cardiac hypertrophy and PI3Kα signaling

Chronic exercise training activates the insulin-like growth factor 1 (IGF1)-phosphoinositide-3-kinase p110α (PI3Kα)-Akt signaling pathway, and accumulating evidences have shown that IGF1-PI3Kα-Akt signaling axis is essential in mediating exercise training-induced physiological hypertrophy (DeBosch *et al.*, 2006b; McMullen & Jennings, 2007; Weeks & McMullen, 2011). Studies focused on defining the effects of growth factors on cardiac hypertrophy revealed that cardiac IGF1, but not endothelin-1 or angiotensin II, was elevated in the hearts of athletes, compared with healthy

sedentary controls (Neri Serneri *et al.*, 2001), and that serum levels of IGF1 were increased in humans and animals with chronic exercise training (Yeh *et al.*, 1994; Koziris *et al.*, 1999). It has also been shown that cardiac IGF1 levels correlated positively with LV mass and size in the hearts of athletes as well as controls (Neri Serneri *et al.*, 2001). These results suggest a pivotal role for IGF1 in mediating exercise-induced physiological cardiac hypertrophy. Consistent with this suggestion, transgenic mice with cardiac-specific overexpression of IGF1 receptor (α-MHC IGF1R) develop physiological hypertrophy, with 35-40% increase in cardiac size and normal cardiac function (McMullen *et al.*, 2004), whereas mice lacking IGF1R ($IGF1R^{-/-}$) were resistant to chronic exercise-induced cardiac hypertrophy (Kim *et al.*, 2008). Taken together, these observations demonstrate that IGF1-mediated signaling plays a critical role in the development of physiological hypertrophy.

IGF1 acts through IGF1R, a receptor tyrosine kinase on the cell surface, and activates phosphoinositide-3-kinase p110α (PI3Kα). PI3Kα, the Class IA component of the PI3K enzyme family, converts the plasma membrane lipid phosphatidylinositol-4,5-bisphosphate (PIP2) to phosphatidylinositol-3,4,5-trisphosphate (PIP3), which initiates the activation of downstream signaling constituents at the plasma membrane such as phosphatidylinositol-dependent kinase 1 (PDK1) and Akt (Cantley, 2002). Transgenic mice with enhanced cardiac PI3Kα signaling develop cardiac hypertrophy similar to exercise-induced physiological hypertrophy (Shioi *et al.*, 2000). In contrast, mice with reduced PI3Kα activity, either transgenic mice expressing dominant negative PI3Kα (dnPI3Kα) or knock-out mice lacking both p85α and p85β, the regulatory subunits of PI3Kα, display a blunted hypertrophic response to exercise training, but not to pathological stimuli, such as pressure overload (McMullen *et al.*, 2003; Luo *et al.*, 2005).

In addition, crossbreeding dnPI3Kα with α-MHC IGF1R transgenic mice blunted the development of cardiac hypertrophy that was normally observed in IGF1R transgenic animals (McMullen *et al.*, 2004). These observations suggest that PI3Kα, acting downstream of IGF1, plays a critical role in regulating physiological hypertrophy induced by exercise training.

Akt is a well-characterized serine threonine kinase downstream of PI3Kα, and is activated (hyperphosphorylated) in animal models of physiological hypertrophy (McMullen *et al.*, 2003; McMullen *et al.*, 2004; Kemi *et al.*, 2008). There are three Akt isoforms, Akt1, 2 and 3, although only Akt1 and Akt2 are highly expressed in the heart (Nakatani *et al.*, 1999). Akt1 has been shown to regulate normal cardiac growth (Cho *et al.*, 2001b) and is absolutely required for the development of physiological hypertrophy induced by chronic exercise training (DeBosch *et al.*, 2006b). The hypertrophic response normally observed in wild-type animals with chronic exercise training is completed abrogated in mice ($Akt1^{-/-}$) lacking Akt1 (DeBosch *et al.*, 2006b). Akt2, on the other hand, plays a critical role in insulin-regulated glucose homeostasis, as well as in cardiomyocyte survival (Cho *et al.*, 2001a; Garofalo *et al.*, 2003; Etzion *et al.*, 2010). Mice ($Akt2^{-/-}$) lacking Akt2 display a severe diabetic phenotype, but the hypertrophic response to IGF1 stimulation is preserved (DeBosch *et al.*, 2006a).

In addition to acting through Akt, PI3K-mediated signaling has been shown to regulate various cellular processes by modulating the cell surface expression and the functioning of membrane ion channels. PIP2 and PIP3, lipid products of the PI3Ks, for example, reportedly affect the activity of the cystic fibrosis transmembrane conductance regulator (CFTR) (Himmel & Nagel, 2004), Kv channels (Loussouarn *et al.*, 2003) and Kir

channels (Hilgemann *et al.*, 2001; Lopes *et al.*, 2002). PI3Ks also mediate the activation of L-type Ca^{2+} channels in vascular smooth muscle cells upon stimulation of M2-muscarinic (Callaghan *et al.*, 2004), α2-adrenergic (Roberts, 2003) and angiotensin II receptors (Le Blanc *et al.*, 2004). In addition, PI3Ks have been shown to enhance the cell surface expression of voltage-dependent Ca^{2+} currents in neurons by promoting channel subunit trafficking (Viard *et al.*, 2004). Because the activation of PI3Kα signaling is necessary and sufficient to induce physiological hypertrophy, it is possible that the maintenance of normal electrical functioning and the immunity against arrhythmogenecity observed in physiological hypertrophy is also attributed to the activation of PI3Kα signaling.

As described above, the impaired repolarization and increased arrhythmogenecity associated with pathological hypertrophy are attributed to the failure to upregulate K^+ currents and K^+ channel subunits in parallel with the hypertrophic growth. The absence of electrical abnormalities or arrhythmia risk observed in physiological hypertrophy, in contrast, suggests that repolarizing K^+ currents are upregulated in parallel with the increase in myocyte size with physiological hypertrophy to maintain normal myocardial electrical functioning. The studies presented in **Chapter 3** were designed to test this hypothesis directly. Additional studies were carried out to determine the role of PI3Kα-Akt signaling in the regulation of repolarizing K^+ currents and K^+ channel subunit expression in physiological hypertrophy (**Chapter 3**). In addition, the hypothesis that enhanced PI3Kα signaling can protect against the effects of pathological hypertrophy and heart failure to maintain K^+ channel expression, was also tested (**Chapter 4**). Finally, using the molecular and bioinformatic pipeline optimized for transcriptomal profiling with next-generation high-throughput sequencing technologies, the hypothesis that increased

PI3Kα signaling provides protective effects in pathological hypertrophy by reversing aberrant myocardial miRNA and mRNA expression, secondary to pathological stress, was tested (**Chapter 5**).

Chapter 2: Materials and Methods

2.1 Experimental animals

Animals were handled in accordance with the *Guide for the Care and Use of Laboratory Animals* (NIH). All protocols involving animals were approved by the Animal Studies Committee at Washington University Medical School.

For data presented in **Chapter 3**, initial experiments were performed on adult (8-10 week) male wild type (WT) FVB/N mice subjected to chronic swim-training (McMullen *et al.*, 2003), as well as on adult (8-12 week) male mice with cardiac-specific expression of constitutively active phosphoinositide-3-kinase p110α (caPI3Kα) (n=25) (Shioi *et al.*, 2000) and WT littermate controls (n=35). Additional experiments were carried out on adult (8-10 week) $Akt1^{-/-}$ mice (C57Bl/6) (Cho *et al.*, 2001b; DeBosch *et al.*, 2006b) subjected to chronic swim-training (trained n=14, untrained control n=15) (McMullen *et al.*, 2003) and on a mouse model of cardiac-specific expression of caPI3Kα transgene driven by a tet-responsive (tet-off) α-MHC promoter (in FVB/N background) (icaPI3Kα n=30, WT control n=15) (Yano *et al.*, 2008). Double transgenic animals carrying both tTA and caPI3Kα transgenes (icaPI3Kα) were maintained with doxycycline-containing (Dox; 200mg doxycycline/kg) diet to repress transgene expression. The expression of caPI3Kα transgene was induced by removing Dox diet for 4 weeks in adult (8-10 weeks) icaPI3Kα animals and the activation of PI3Kα signaling in these animals was confirmed by Western blot.

For data presented in **Chapter 4**, initial experiments were carried out on eight to twelve-week-old male caPI3Kα and WT mice subjected to transverse aortic constriction (TAC) to produce pressure overload-induced LVH (Marionneau *et al.*, 2008b). In addition, experiments were also performed in a transgenic mouse model (TG9) of heart failure

(Buerger *et al.*, 2006). Electrophysiological studies were conducted on 10 week male WT, TG9, double transgenic (caPI3KαxTG9) mice as well as on TG9 mice following chronic 4 weeks swim training. Additional experiments were carried out on 10 week TG9 animals treated with the angiotensin-converting enzyme (ACE) inhibitor, captopril (50mg/L in the drinking water for 4 weeks).

For data presented in **Chapter 5**, experiments were conducted in eight to twelve-week-old male WT FVB/N and caPI3Kα mice subjected to TAC or sham operation.

2.2 Chronic swim training and citrate synthase activity measurement

Animals (WT FVB/N, Akt1$^{-/-}$, or TG9) were placed in a small tank (surface area of 225 cm^2) filled with water maintained at 30-32ºC to avoid thermal stress. Initial swim time was 20 min, increasing by 10 min per day until 90 min sessions were reached. Once attained, the 90 min training schedule was continued twice a day (separated by 4-5 hr), 7 days a week, for 4 weeks. Citrate synthase (CS) activity was measured in gastrocnemius muscles dissected from swim-trained and untrained experimental animals (Harrison *et al.*, 2002), weighed and frozen in liquid nitrogen. Frozen samples were homogenized on ice in 100 mM Tris-HCl, and protein concentrations were determined using the BCA protein Assay Kit (Pierce). Individual tissue homogenates (5µl) were then added to a (1 ml) reaction mix containing: 100 mM Tris-HCl, 1.0 mM dithio-bis(2-nitrobenzoic acid), 10 mM oxaloacetate and 0.2 mM acetyl CoA. The absorbance of each sample at 412 nm was recorded at 25 °C every 30 seconds for 5 minutes. Mean absorbance change per minute was recorded and citrate synthase activity (in µmol*mg protein^{-1}*min^{-1}) was calculated using the extinction coefficient (13.6 mM^{-1}*cm^{-1}) of 5-thio-2-nitrobenzoic acid at 412 nm (Harrison *et al.*, 2002).

2.3 Induction of pressure overload-induced pathological left ventricular hypertrophy

Eight to twelve-week-old male caPI3Kα and WT mice were subjected to transverse aortic constriction (TAC) to produce pressure overload-induced LVH (Zhang *et al.*, 2003; Marionneau *et al.*, 2008b). Animals were anesthetized with a mixture of xylazine (16 mg/kg, intraperitoneally[i.p.]) and ketamine (80 mg/kg, i.p.). Once deep anesthesia was confirmed by the absence of toe pinch reflex, the chest was opened and the thoracic aorta was identified. A 7-0 silk suture was placed around the transverse aorta and tied around a 26-gauge needle, which was then removed. Seven days after surgery, caPI3Kα and WT animals, with and without TAC, were analyzed.

2.4 Electrophysiological recordings

Surface electrocardiograms (ECG) were recorded from anesthetized (Tribromoethanol, 0.25 mg/kg, i.p.) swim-trained WT, control WT, swim-trained and untrained $Akt1^{-/-}$, caPI3Kα control, caPI3Kα+TAC, WT+TAC, TG9 and caPI3KαxTG9 animals, using needle electrodes connected to a dual bioamplifier (AD Instrument, PowerLab 26T). Lead II recordings were analyzed (Yang *et al.*, 2010). QT intervals were measured as the time interval between the initiation of the QRS complex and the end of the T wave, and corrected for heart rate using the formula $QTc=QT/(\sqrt{RR}/100)$ (Mitchell *et al.*, 1998).

Body weights, tibia lengths and LV weights were measured and recorded at the time of tissue harvesting. Hearts were removed from anesthetized animals, mounted on a Langendorf-apparatus and perfused retrogradely through the aorta with 25 ml of (0.8 mg/ml) collagenase-containing (type II, Worthington) solution (Marionneau *et al.*, 2008b; Yang *et al.*, 2010). Following perfusion, the LV apex was separated, mechanically

dispersed, plated on laminin-coated coverslips and maintained in a 95% air-5% CO_2 incubator. Whole-cell current- and voltage-clamp recordings were obtained from LV apex myocytes within 24 hr of isolation at room temperature (22-24°C). All voltage- and current-clamp experiments were performed using an Axopatch 1B patch clamp amplifier (Molecular Devices) interfaced to a microcomputer with a Digidata 1332 analog/digital interface and the pCLAMP9 software package (Molecular Devices); Data were filtered at 5kHz before storage.

For recordings of whole-cell K^+ currents, pipettes contained (in mM): KCl 135; EGTA 10; HEPES 10; K_2ATP 5 and glucose 5 (pH 7.2; 310 mOsm). The bath solution contained (in mM): NaCl 136; KCl 4; $MgCl_2$ 2; $CaCl_2$ 1; $CoCl_2$ 5; tetrodotoxin (TTX) 0.02; HEPES 10 and glucose 10 (pH 7.4; 300 mOsm). For recordings of whole-cell voltage-gated Ca^{2+} (I_{Ca}) currents, the $CoCl_2$ was omitted from the bath and the KCl in the pipette and bath solutions was replaced with CsCl (140 mM) and TEACl (4mM), respectively. The TTX and the $CoCl_2$ were omitted from the bath solution for current-clamp recordings.

Whole-cell voltage-gated outward K^+ (Kv) currents were recorded in response to 4.5 s voltage steps to test potentials between -60 and +40 mV from a holding potential (HP) of -70 mV. Currents (I_{K1}) through inward rectifier K^+ (Kir) channels, evoked in response to hyperpolarization to -120 mV from the same HP, were also recorded in each cell. Whole-cell voltage-gated inward Ca^{2+} currents (I_{Ca}), evoked in response to 250 ms voltage steps to test potentials between -30 and +50 mV from a prepulse to -40 mV, presented from the holding potential (-70 mV) to inactivate the voltage-gated Na^+ currents; the paradigm is illustrated in the legend to **Figure 3.9**. Action potentials were elicited in response to brief (<5 ms) depolarizing current injections of varying amplitudes, delivered at 1 Hz.

Voltage-clamp data were compiled and analyzed using Clampfit (Version 9.2, Molecular Devices) and Excel (Microsoft). Integration of the capacitative transients recorded during brief ± 10 mV voltage steps from the holding potential (-70 mV) provided the whole-cell membrane capacitance (C_m). Leak currents were always <100 pA, and were not corrected. Series resistances (<9 MΩ) were routinely compensated electronically (>80%). Voltage errors resulting from the uncompensated series resistance were ≤8 mV and were not corrected. Peak Kv current and I_{K1} amplitudes were measured as the maximal amplitudes of the outward and inward currents, respectively, evoked at each test potential under the recording conditions described above. Peak I_{Ca} amplitudes were measured as the differences between the peak inward current and the current at the end of the depolarizing voltage step. Current amplitudes were normalized to whole-cell membrane capacitances (in the same cell) to provide current densities (in pA/pF). The time constants of inactivation (τ_{decay}) and the amplitudes of the individual Kv current components, $I_{to,f}$, $I_{K,slow}$ and I_{ss} were determined from double exponential fits to the decay phase of the outward K^+ currents, as described previously (Brunet *et al.*, 2004). Resting membrane potentials, action potential amplitudes and action potential durations at 25%, 50% and 90% repolarization were also measured.

2.5 Histology

Swim-trained and WT mice were anesthetized with intraperitoneal injection of ketamine (86 mg/kg) and xylazine (13 mg/kg) and perfused with 4% paraformaldehyde in 0.1 mol/L phosphate buffer. Isolated ventricular tissue was embedded in paraffin, sectioned and stained with Masson trichrome (DeBosch *et al.*, 2006b). Ventricular myocyte cross-sectional area was measured using an Axioskop microscope (Carl Zeiss, Inc, Chester, VA) and the Axiovision 4.0 software (DeBosch *et al.*, 2006b).

2.6 Quantitative transcript analyses

Total RNA from the LV of experimental animals was isolated and DNase treated using described methods (Marionneau *et al.*, 2005). RNA concentrations were determined by optical density measurements. For experiments in **Chapter 3 and 4**, equal amounts of mRNA were used for each sample for transcript analyses of genes encoding ion channel pore-forming (α) and accessory subunits, markers of pathological hypertrophy, as well as of control genes, including glyceraldehyde 3-phosphate dehydrogenase (*Gapdh*), hypoxanthine guanine phosphoribosyl transferase (*Hprt*), and the nuclear membrane protein lamin A/C (*Lmna*) **(Table 2.1)** using SYBR green RT-PCR in a two-step process (Marionneau *et al.*, 2005; Marionneau *et al.*, 2008b). All data were analyzed using the threshold cycle (C_T) relative quantification method. These data were normalized to the value measured (in the same sample) for *Lmna,* which encodes the nuclear membrane protein lamin A/C, to reference the transcript expression data to the number of nuclei (i.e. the number of myocytes) in the sample. Because only myocyte size (not number) is increased in cardiac hypertrophy (Hannan *et al.*, 2003), this method provided relative differences in transcript expression levels on a per myocyte basis. For each transcript, these normalized values were then expressed relative to the mean value determined for the control LV samples, and mean ± SEM normalized values are presented. Expression of each channel subunit transcript was also normalized to the total cellular RNA in the same sample, which increases with cardiac hypertrophy (Hannan *et al.*, 2003). This method allows direct comparisons of the observed changes in channel subunit expression levels relative to the overall increase in RNA.

Table2. 1 Sequence specific primers used in SYBR Green RT-PCR

Gene		Forward Primer	Reverse Primer
Kv4.2	*(Kcnd2)*	5'-TGAATCACGTTTGTGTCATTAGTGA	5'-TTCAACTTGCGCTCATCTTAGG
Kv4.3	*(Kcnd3)*	5'-GCCGCAGCACCTAGTCGTT	5'-CACCACGTCGATGATACTCATGA
KChIP2	*(Kcnip2)*	5'-GGCTGTATCACGAAGGAGGAA	5'-CCGTCCTTGTTTCTGTCCATC
Kvβ1	*(Kcnab1)*	5'-AAATACCCAGAAAGGCAAGTGT	5'-ATCTAGCATGTGCCGAGGAA
Kv1.5	*(Kcna5)*	5'-CCTGCGAAGGTCTCTGTATGC	5'-TGCCTCGATCTCTCTTTACAAATCT
Kv2.1	*(Kcnb1)*	5'-CACACAGCAATAGCGTTCAACTT	5'-AGGCGTAGACACAGTTCGGC
TASK1	*(Kcnk3)*	5'-GCTTCCGCAACGTCTATGC	5'-GGGATGGAGTACTGCAGCTTCT
Kir2.1	*(Kcnj2)*	5'-AAGAGCCACCTTGTGGAAGCT	5'-CTTCTGAAGTGATCCTAGATTTGAGA
Kir2.2	*(Kcnj12)*	5'-AGCACCACCCTGACCACAAT	5'-CTGAGCAACCCTACCCCAA
KvLQT1	*(Kcnq1)*	5'-ACCATCGCCTCCTGTTTCTCT	5'-CCCGCTGGGAGTGCAA
mERG	*(Kcnh2)*	5'-CCGGGTGCGGGAGTTTAT	5'-CGAGGCGCTGGCGTAAT
Mink	*(Kcne1)*	5'-CCCAATTCCACGACTGTTCTG	5'-CCGCCCTGTTCAGCTGTCT
MiRP2	*(Kcne3)*	5'-TGCTGTGCTGAAGGCTCTGA	5'-CAGGCCGGCAGAGCAA
Nav1.5	*(Scn5a)*	5'-AGTGCCACCAATGCCTTGTAC	5'-GCGGAGGGTCGTGTTGTG
Navβ1	*(Scn1b)*	5'-TGGCAGAGATGGTGTACTGC	5'-TCCACTGCAGAACTGTGAGG
Cav1.2	*(Cacna1c)*	5'-CCCTTCTTGTGCTCTTCGTC	5'-ACACCCAGGGCAACTCATAG
Cavβ2	*(Cacnb2)*	5'-GTACCTTCCATGCGACCAGT	5'-ATTGTATCCGCGTCAAGGAC
Cavα2δ1	*(Cacna2d1*	5'-CACTGCTGTGGCAAGTGTTT	5'-TTACATCCTGAGCGTTGCTG
ANF	*(Nppa)*	5'-CACTGTGGCGTGGTGAACA	5'-TCGTGATAGATGAAGGCAGGAA
Cx43	*(Gja1)*	5'-ACAAGTCCTTCCCCATCTCTCA	5'-GTGTGGGCACAGACACGAAT
Cx40	*(Gja5)*	5'-CCAAACCAGGAGCAGATTCC	5'-GCGTACTCTGGCTTCTGGCTAT
HPRT	*(Hprt)*	5'-TGAATCACGTTTGTGTCATTAGTGA	5'-TTCAACTTGCGCTCATCTTAGG
GAPDH	*(Gapdh)*	5'-ACTCCACTCACGGCAAATTC	5'-TCTCCATGGTGGTGAAGACA
Lamin A/C	*(Lmna)*	5'-GGCTACAGACGCTGAAGGAG	5'-CTGTTCCACCTGGTCCTCAT

In **Chapter 5**, total RNA isolated from the LV of individual animals (as described above) was reserve transcribed into cDNA using NCode VILO miRNA cDNA synthesis Kit (Life Technologies). Quantitative real-time PCR (RT-PCR) for mmu-miR-21, mmu-miR-127, mmu-miR-146b, mmu-miR-199-5p, mmu-miR-411, mmu-miR-541, mmu-miR-34c, mmu-miR-214, mmu-miR-410, mmu-miR-300 and endogenous control 5S rRNA for each sample was carried out using EXPRESS SYBR GreenER miRNA qRT-PCR Kit (Life Technologies) with NCode universal reverse primer and forward primers designed specifically for each of the miRNAs (**Table 2.2**). All data, analyzed using the threshold cycle relative quantification ($\Delta\Delta C_T$) method, were normalized to the value measured (in

the same sample) for 5S rRNA. For each miRNA, the normalized values were then expressed relative to the mean of the control (WT Sham) LV samples.

Table2. 2 Primer sequences for miRNA-specific RT-PCR

Gene	Mature sequence	Forward primer sequence
mmu-miR-21	Uagcuuaucagacugauguuga	5' CTAGCTTATCAGACTGATGTTGAA
mmu-miR-127	Cugaagcucagagggcucugau	5'TGAAGCTCAGAGGGCTCTGAT
mmu-miR-146b	Ugagaacugaauuccauaggcu	5'GCTGAGAACTGAATTCCATAGGCT
mmu-miR-199a-5p	Cccaguguucagacuaccuguuc	5' CCAGTGTTCAGACTACCTGTTCAA
mmu-miR-411	Uaguagaccguauagcguacg	5' GGTAGTAGACCGTATAGCGTACGAA
mmu-miR-541	Aagggauucugauguuggucacacu	5' GGGATTCTGATGTTGGTCACACTA
mmu-miR-34c	Aggcaguguaguuagcugauugc	5' GAGGCAGTGTAGTTAGCTGATTGC
mmu-miR-214	Ugccugucuacacuugcugugc	5' GCCTGTCTACACTTGCTGTGC
mmu-miR-410	Agguugucugugaugaguucg	5' GAGGTTGTCTGTGATGAGTTCGA
mmu-miR-300	Uugaagagagguuauccuuugu	5' GCTTGAAGAGAGGTTATCCTTTGTAA
5S rRNA		5'AATACCGGGTGCTGTAGGCTTT
miR-cluster 16	Cacggcggcuggaauuccc	5' GGCGGCTGGAATTCCC
miR-cluster 4	Accaucugugggauuaugacugaacg	5' CATCTGTGGGATTATGACTGAACG
miR-cluster 54	Gggggcguggaauuaucgggu	5' GGCGTGGAATTATCGGGT

2.7 Quantitative protein analyses

Protein lysates were prepared from the LV of experimental animals using described methods (Guo *et al.*, 2005). Protein concentrations were determined using the BCA protein Assay Kit (Pierce). For Western blot analyses, equal amounts of total proteins prepared from individual control and experimental animals were loaded on SDS-PAGE gels. The following commercially available antibodies were used: rabbit polyclonal anti-Kv4.2, anti-Kir2.2 (Millipore, Billerica, MA, USA); rabbit polyclonal anti-TASK1 (Alomone labs, Jerusalem, Israel); mouse monoclonal anti-GAPDH (Abcam, Cambridge, MA, USA); rabbit polyclonal anti-phospho-Akt(S473), anti-total Akt, anti-phospho-ribosomal protein S6(S235/236), and anti-phospho-GSK3β(S9) (Cell Signaling Technology, Danvers, MA); goat polyclonal anti-*Sprouty 1* and rabbit polyclonal anti-lamin A/C (Santa Cruz Biotechnology, Santa Cruz, CA). The mouse monoclonal anti-KChIP2 and anti-Kv2.1 antibodies were developed by and obtained from the UC Davis/NIH NeuroMab

Facility, supported by NIH grant U24NS050606 and maintained by the University of California, Davis, CA 95616. The specificities of the anti-Kv4.2, anti-KChIP2, anti-Kv2.1, and anti-TASK1 antibodies have all been tested on protein extracts from mice in which the genes encoding these subunits have been eliminated by homologous recombination. In each case, no signals corresponding to the targeted channel subunit were detected.

After washing, the membrane strips were incubated for 2 hr at room temperature with alkaline phosphatase-conjugated secondary antibody diluted in blocking buffer, and bound antibodies were detected using a chemiluminescent alkaline phosphatase substrate. Protein band intensities were quantified by densitometry (Quantity One Basic Software, Bio-Rad Laboratory, Hercules, CA), and the measured abundances were normalized to the expression of lamin A/C (evident as a doublet at 62- and 69-kD) in the same sample on the same blot. For each protein, these values were then expressed relative to the mean control LV value; mean ± SEM normalized values are presented. Channel subunit protein expression levels were also normalized to the total cellular protein (in the same sample) to allow direct comparison of observed changes relative to the global increases in cellular protein associated with cardiac hypertrophy (Hannan *et al.*, 2003).

2.8 Construction of barcoded short-read RNA libraries and sequencing

2.8.1 Small RNA library construction and sequencing

Total RNA from the LV of individual animals was isolated with Trizol (Life Technologies) using described protocols (Marionneau *et al.*, 2008b; Yang *et al.*, 2010), and the quality and integrity of total RNA samples were confirmed using Agilent 2100 bioanalyzer (Agilent Technologies). Small RNA libraries were prepared using TrueSeq Small RNA

Sample Prep Kits (Illumina) in accordance with the manufacturer's instructions. In short, 3' and 5' adapters were sequentially ligated to small RNAs (from 1 μg total RNA), followed by a reverse transcription reaction to create single stranded cDNA. The cDNA samples were then PCR amplified and barcoded using a common primer and a primer containing unique six-base index sequence. The amplified libraries were size-selected/gel-purified and quantified using Qubit dsDNA HS Assay kit (Life Technologies). Six to eight barcoded libraies were pooled in equimolar (10 nmol/L) amounts and diluted to 8 pmol/L for cluster formation on a single flow cell lane, followed by single-end sequencing on an Illumina HiSeq 2000 sequencer.

2.8.2 Messenger RNA library preparation and sequencing

Messenger RNA libraries were prepared using TrueSeq RNA Sample Prep Kits (Illumina) in accordance with the manufacturer's recommendations. In brief, 3μg of total LV RNA was twice oligo(dT) selected using poly-T oligo-attached magnetic beads. The poly-A(+) RNA was then eluted, fragmented and reverse transcribed into first strand cDNA using random hexamers, followed by second-strand cDNA synthesis. Double-stranded (ds) cDNAs were end-repaired and single-adenylated at 3' ends. Barcoded adapters containing unique six-base index sequences and T-overhangs were ligated to the cDNA samples from individual mouse LV. Individual cDNA libraries was PCR amplified and purified; six barcoded libraries were pooled in equimolar (10 nmol/L) amounts and diluted to 4 pmol/L for cluster formation on a single flow cell lane, followed by single-end sequencing on an Illumina HiSeq 2000 sequencer.

2.9 Analyses of miRNA and mRNA sequencing data

2.9.1 Small RNA sequencing data analyses

Sequencing data from samples pooled in the same flow cell lane were separated (demultiplexed) using CASAVA 1.6 software (Illumina). A total of 165.5 million reads were obtained from sequencing 15 small RNA libraries (Table 1). The sequence reads were analyzed using the miRanalyzer program (Hackenberg *et al.*; Hackenberg *et al.*, 2009), where the raw sequencing data were transformed and filtered to keep only sequences containing 17-26 bases. Filtered reads were then successively mapped (using Bowtie) (Langmead *et al.*, 2009) to: (1) miRBase (Griffiths-Jones, 2006) v.16 mouse database (allowing up to two mismatches), to detect known miRNAs; (2) the RefSeq and Rfam database, to detect contamination from other RNA species; and (3) the mouse genome to detect potential novel miRNAs. The sequences matching known miRNAs were clustered and counted; the read counts of each known miRNAs were then normalized to the total counts of sequences mapped to the miRbase v.16 database and presented as PMMR (sequences per million mapped reads).

2.9.2 Novel miRNA discovery

Sequence reads that are counterparts of known mature miRNAs, but that have not been previously reported in the miRBase database, were identified and defined as novel miRNA-star (miRNA*). Sequence reads that did not match known miRNAs or known transcripts from the RefSeq and Rfam database were mapped against the mouse genome (M37). Once aligned, sequence reads that share characteristics of miRNAs were identified and clustered using the computational algorithms provided by miRAnalyzer (Hackenberg *et al.*, 2009). These clusters were further filtered to exclude contamination from repetitive sequences and from mRNA or noncoding RNA

degradation products. Only clusters with a read depth ≥100 reads were chosen for further analyses. The filtered candidate miRNAs and their precursors were further examined using the following criteria (Griffiths-Jones *et al.*, 2006; Fehniger *et al.*, 2010): (1)non-homologous to any known non-coding RNAs; (2)predicted with stem-loop hairpin structure with a $-\Delta G \leq 15$; (3)mature miRNA length of 17-26 bases mapped to the stem of the predicted hairpin structure without extension into the loop or outside of the stem-loop fold; and (4) lack of a bulged secondary structure larger than 50% of the mature sequence within the stem of the hairpin. The structures of putative miRNA precursors were examined using the RNA-folding prediction software, RNAfold WebServer (http://rna.tbi.univie.ac.at/cgi-bin/RNAfold.cgi). Candidate miRNAs (and their precursors), fulfilling the described criteria, were grouped as putative novel miRNAs. The putative novel miRNAs were first checked against the latest miRBase v.18 database (released in Nov 2011); candidate miRNAs not found in the miRBase v.16, but reported in the miRBase v.18 were reassigned to the group of known miRNAs.

2.9.3 mRNA sequencing data processing

After demultiplexing sequencing data, adapter sequences were removed and individual libraries were converted to FASTQ format. Sequence reads were mapped to the mouse genome (mm9) with Bowtie (Langmead *et al.*, 2009), allowing up to two mismatches. Sequence reads aligned to the mouse genome were imported into Partek Genomics Suite version 6.5 (Partek, St Louis, MO) for sequencing read clustering, counting and annotation. The RefSeq transcript database was chosen as the annotation reference and subsequent data analyses were focused on sequence reads mapping to coding exons. The read counts of each known transcript were normalized to the length of individual transcript and the total mapped read counts in a given sample and expressed as RPKM (reads per kilobase of exon per million mapped reads). Sequence reads

mapped to different isoforms of individual genes were pooled together for subsequent comparative analyses.

2.9.4 Methods for sequencing data compiling and presentation

Gene symbols and PMMR/RPKM values were imported into MultiExperiment Viewer (MeV v4.7.4) for comparison of miRNA and mRNA expression values, computation of significant levels/false discovery rates, preparation of heat-map, hierarchical clustering and self-organizing trees analyses. Gene ontology analyses were performed using g:Profiler (http://biit.cs.ut.ee/gprofiler/) (Reimand *et al.*, 2007). Correlation coefficients and linear regression for comparison of miRNA/mRNA expression between biological replicates were calculated using Excel (Microsoft).

2.10 Statistical analyses

All averaged electrophysiological, transcript, sequencing and Western blot data are presented as means ± SEM. The statistical significance of differences among experimental groups was evaluated by one-way analysis of variance (ANOVA), followed by post-hoc Tukey's multiple comparison correction. In some cases, Student's *t* test or Mann-Whitney *U* test were used to evaluate the differences between groups. A two-tailed *P* value <0.05 was considered statistically significant.

2.11 Principal contributions to the work as a whole

Kai-Chien Yang in collaboration with Jeanne Nerbonne contributed to the design of these studies and Kai-Chien Yang carried out the experiments presented here. Expert technical assistance was received from Rick Wilson in the maintenance and screening of the mouse lines used in this study.

Chapter 3: Enhanced PI3Kα Signaling Mediates Electrical Remodeling in Physiological Hypertrophy through an Akt-independent Mechanism

3.1 Abstract

Pathologic biomechanical stresses cause cardiac hypertrophy, which is associated with QT prolongation and arrhythmias. Previous studies have demonstrated that repolarizing K^+ current densities are decreased in pressure overload-induced left ventricular hypertrophy, resulting in action potential and QT prolongation. Cardiac hypertrophy also occurs with exercise training, but this physiological hypertrophy is not associated with electrical abnormalities or increased arrhythmia risk, suggesting that repolarizing K^+ currents are upregulated, in parallel with the increase in myocyte size, to maintain normal cardiac function. To explore this hypothesis directly, electrophysiological recordings were obtained from ventricular myocytes isolated from two mouse models of physiological hypertrophy, one produced by swim-training of wild type mice and the other by cardiac-specific expression of constitutively active phosphoinositide-3-kinase-p110α (caPI3Kα). Whole-cell voltage-clamp recordings revealed that repolarizing K^+ current amplitudes were higher in ventricular myocytes isolated from swim-trained and caPI3Kα, compared with wild type, animals. The increases in K^+ current amplitudes paralleled the observed cellular hypertrophy, resulting in normalized or increased K^+ current densities. Electrocardiographic parameters, including QT intervals, as well as ventricular action potential waveforms in swim-trained animals/myocytes were indistinguishable from controls, demonstrating preserved electrical function. Additional experiments revealed that inward Ca^{2+} current amplitudes/densities were also increased in caPI3Kα, compared with WT, LV myocytes. The expression of transcripts encoding K^+, Ca^{2+} and other ion channel subunits was increased in swim-trained and caPI3Kα ventricles, in parallel with the increase in myocyte size and with the global increases in total cellular RNA expression. In contrast to pathological hypertrophy, therefore, the functional expression of repolarizing K^+ (and depolarizing Ca^{2+}) channels is increased with physiological hypertrophy, reflecting upregulation of the underlying ion channel

subunit transcripts and resulting in increased current amplitudes and the normalization of current densities and action potential waveforms. These results suggest that activation of PI3Kα signaling preserves normal myocardial electrical functioning and could be protective against the increased risk of arrhythmias and sudden death that are prevalent in pathological cardiac hypertrophy.

Additional experiments were undertaken to test the hypothesis that Akt1, which underlies PI3Kα-induced cellular hypertrophy, also mediates the effects of augmented PI3Kα signaling on the transcriptional regulation of cardiac ion channels. In contrast to wild-type animals, chronic exercise (swim) training of mice ($Akt1^{-/-}$) lacking Akt1 did not result in ventricular myocyte hypertrophy. Ventricular K^+ current amplitudes and the expression of K^+ channel subunits, however, were increased markedly in $Akt1^{-/-}$ animals with exercise training. Expression of the transcripts encoding inward (Na^+ and Ca^{2+}) channel subunits were also increased in $Akt1^{-/-}$ ventricles following swim training. Using a transgenic mouse model of inducible cardiac-specific expression of constitutively active PI3Kα (icaPI3Kα), further experiments revealed that short-term activation of PI3Kα signaling in the myocardium also led to the transcriptional upregulation of ion channel subunits. Inhibition of cardiac Akt activation with triciribine in the context of enhanced PI3Kα signaling did not prevent the upregulation of myocardial ion channel subunits. The results here demonstrate that chronic exercise training and enhanced PI3Kα expression/activity result in transcriptional upregulation of myocardial ion channel subunits independent of cellular hypertrophy and Akt signaling.

3.2 Introduction

Cardiac hypertrophy, an adaptive response of the myocardium to increased load, occurs in a variety of disease states, including hypertension and myocardial infarction, and is associated with an increased risk of life-threatening ventricular arrhythmias (Haider *et al.*, 1998). Abnormal electrical function in cardiac hypertrophy (Mayet *et al.*, 1996; McIntyre & Fry, 1997) reflects at least in part reductions in repolarizing K^+ current densities (Nabauer *et al.*, 1996; Marionneau *et al.*, 2008b). Reduced K^+ currents can prolong the action potential and increase repolarization dispersion. Both effects are arrhythmogenic and predispose individuals to life-threatening arrhythmias (McIntyre & Fry, 1997; Oikarinen *et al.*, 2004).

Recent studies in a mouse model of pressure overload-induced left ventricular hypertrophy (LVH) produced by transverse aortic constriction (TAC) revealed that the observed reductions in the densities of repolarizing K^+ currents are not associated with K^+ channel subunit gene/protein downregulation (Marionneau *et al.*, 2008b). Rather, in TAC LV myocytes, increased myocyte size is the main factor in determining the reductions in K^+ current densities. The observed decreases in functional K^+ current densities, therefore, result directly from the failure to upregulate K^+ channel subunit expression levels in proportion to the increase in myocyte size (Marionneau *et al.*, 2008b). Interestingly, exercise also causes cardiac hypertrophy, especially in trained athletes, although this physiological hypertrophy is not associated with electrical abnormalities or increased arrhythmia risk (Mayet *et al.*, 1999; Biffi *et al.*, 2008). These observations suggest that repolarizing K^+ currents are upregulated in parallel with the increase in myocyte size in physiological hypertrophy to maintain normal myocardial function. The studies presented here tested this hypothesis directly.

Initial experiments here were carried out in mice subjected to 4 weeks of exercise (swimming) training (McMullen *et al.*, 2003). QT intervals, a reflection of ventricular depolarization and repolarization, in swim-trained mice were indistinguishable from controls, as determined from surface electrocardiograms. Ventricular action potential waveforms were also not significantly different in swim-trained and control LV myocytes. In addition, whole-cell voltage-clamp experiments revealed that amplitudes of the repolarizing K^+ currents were higher in swim-trained LV myocytes, and that repolarizing K^+ current densities were maintained (or increased) in spite of marked increases in LV myocyte size.

Chronic exercise training activates the insulin-like growth factor 1 (IGF-1)-phosphoinositide-3-kinase p110α (PI3Kα) signaling pathway, and PI3Kα is the key signaling molecule mediating exercise training-induced physiological hypertrophy (McMullen *et al.*, 2003). Marked upregulation of repolarizing K^+ currents was also evident in a transgenic mouse model (caPI3Kα) of physiological hypertrophy produced by cardiac-specific expression of constitutively active PI3Kα (Shioi *et al.*, 2000).

Molecular and biochemical analyses in both models of physiological hypertrophy revealed increases in the transcript and protein expression levels of the subunits encoding myocardial ion channels, in parallel with the increase in myocyte size and global increases in cellular protein/RNA expression, suggesting that increased myocardial ion channel subunit expression underlies the upregulated ionic currents and the maintenance of normal electrical function in physiological hypertrophy.

PI3Kα, the Class IA component of the PI3K enzyme family, converts the plasma membrane lipid phosphatidylinositol-4,5-bisphosphate (PIP2) to phosphatidylinositol-

3,4,5-trisphosphate (PIP3), which initiates the activation of downstream signaling constituents at the plasma membrane such as phosphatidylinositol-dependent kinase 1 (PDK1) and Akt (Cantley, 2002). Akt is a well-characterized serine threonine kinase downstream of PI3Kα, and consists of three different isoforms, Akt1, 2 and 3; of the three Akt isoforms, only Akt1 and Akt2 are highly expressed in the heart (Nakatani *et al.*, 1999). Akt1 has been shown to regulate normal cardiac growth (Cho *et al.*, 2001b) and is absolutely required for the development of physiological hypertrophy induced by chronic exercise training (DeBosch *et al.*, 2006b). Akt2, on the other hand, plays a critical role in insulin-regulated glucose homeostasis, as well as in cardiomyocyte survival (Cho *et al.*, 2001a; Garofalo *et al.*, 2003; Etzion *et al.*, 2010). Because of the pivotal role of PI3Kα-Akt1 signaling axis in mediating physiological hypertrophy, we hypothesized that electrical remodeling upon enhanced PI3Kα signaling also depends on Akt1.

Genetic and pharmacological approaches were utilized in experiments designed to explore this hypothesis directly. Unexpectedly, these experiments revealed that PI3Kα-mediated electrical remodeling, reflecting transcriptional upregulation of ion channel subunits, is independent of cellular hypertrophy and Akt signaling.

3.3 Results

3.3.1 Exercise-induced ventricular myocyte hypertrophy and K^+ current upregulation

As previously reported (McMullen *et al.*, 2003), the experiments here revealed that chronic swim-training in mice results in marked ventricular hypertrophy. The mean ± SEM left ventricular mass to tibia length ratio (LVM/TL), for example, is significantly

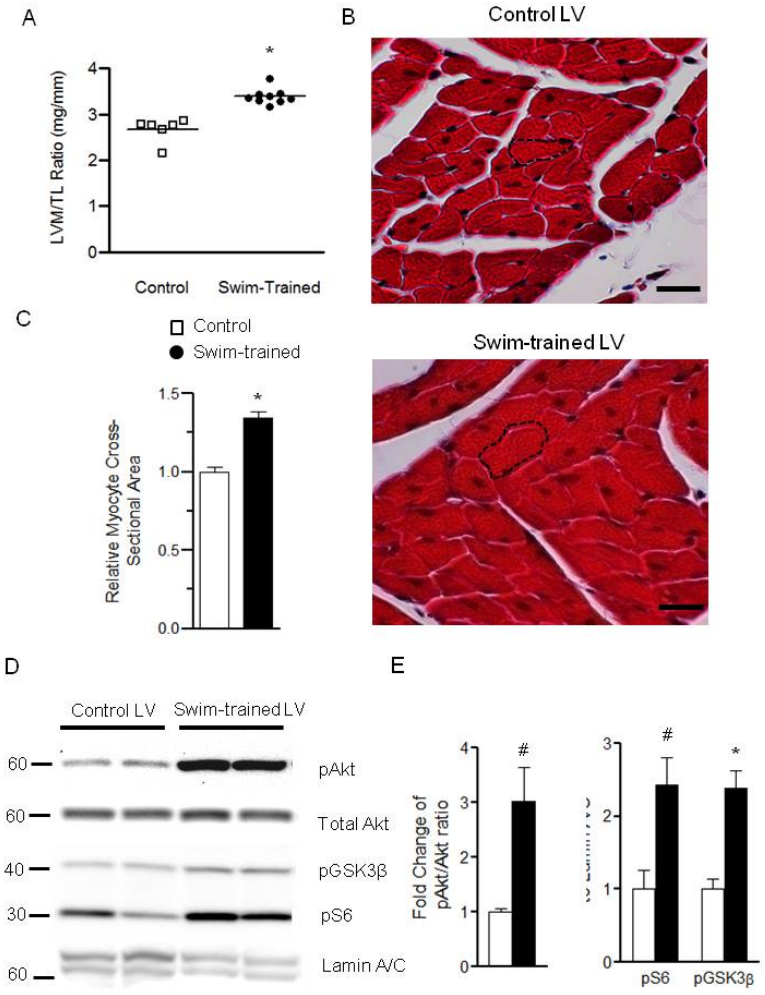

Figure 3. 1 Chronic (4 week) swim-training results in LV myocyte hypertrophy and increased phosphorylation of the downstream targets of the PI3Kα, Akt, ribosomal protein S6 and GSK3β.

A, LV mass/tibia length (LVM/TL) ratios were determined in control (n= 6) and swim-trained (n= 9) animals; individual and mean ±s.e.m. values are plotted. B, representative transverse LV sections from control and swim-trained animals, stained with Masson Trichrome, are shown. The black dashed lines outline individual myocytes; scale bar = 20 μm. C, mean ± s.e.m. cross-sectioned area of LV myocytes in control (n= 50) and swim-trained (n= 50) LV. Mean values in A and C are significantly different (*P < 0.001). D, representative Western blots of fractionated LV proteins from control (n= 4) and swim-trained (n= 4) animals probed for phospho-Akt (pAkt), total Akt, phospho-GSK3β (pGSK3β), phospho-ribosomal protein S6 (pS6), and the nuclear membrane protein lamin A/C; equal amounts of proteins were loaded in each lane. E, the expression levels of each of these proteins were determined. pAkt levels were normalized to total Akt, whereas pS6 and pGSK3β levels were normalized to lamin A/C in the same sample. The mean ±s.e.m. relative expression levels of pAkt, pS6 and pGSK3β are significantly (#P < 0.01, *P < 0.001) higher in swim-trained, compared with control, LV.

(*P*<0.001) higher (by 27 ± 4 %) in swim-trained, compared with untrained (**Figure 3.1A**), animals. Histological measurements in trichrome-stained transverse LV sections revealed that mean ± SEM LV myocyte cross-sectional area is significantly (*P*<0.001) larger in swim-trained, compared with control, hearts (**Figure 3.1B** and **3.1C**). Also consistent with previous reports (Hannan *et al.*, 2003; McMullen *et al.*, 2003), therefore, swim-training induced physiological hypertrophy is associated with increased LV myocyte size without an increase in myocyte number.

Biochemical experiments were also conducted to examine the extent of phosphorylation of Akt, ribosomal protein S6 and glycogen synthase kinase 3β (GSK3β), previously shown to be increased with swim training induced-hypertrophy (McMullen *et al.*, 2003). As illustrated in **Figure 3.1D**, Western blot analyses revealed increased phosphorylation of Akt, ribosomal protein S6 and GSK3β in swim-trained, compared with control, LV, consistent with the activation of PI3Kα signaling with exercise (McMullen *et al.*, 2003). As also shown in **Figure 3.1D**, however, the relative expression of the nuclear membrane protein lamin A/C was lower in the samples from swim-trained, compared with control, animals. This observation is consistent with the suggestion (see above) that cardiac hypertrophy reflects an increase in myocyte size, but not in the numbers of (nuclei) myocytes (Hannan *et al.*, 2003) and suggests that normalizing protein expression data to lamin A/C (see methods) will allow comparison of protein expression levels based on the numbers of cells (nuclei) in each sample.

Whole-cell voltage-clamp recordings from LV myocytes isolated from control and swim-trained mice revealed that the amplitudes of the peak outward Kv ($I_{K,peak}$) and the inwardly rectifying Kir (I_{K1}) currents are significantly (*P*<0.01) higher in LV myocytes from the swim-trained animals (**Figure 3.2A** and **3.2B**). Kinetic analyses of the decay phases

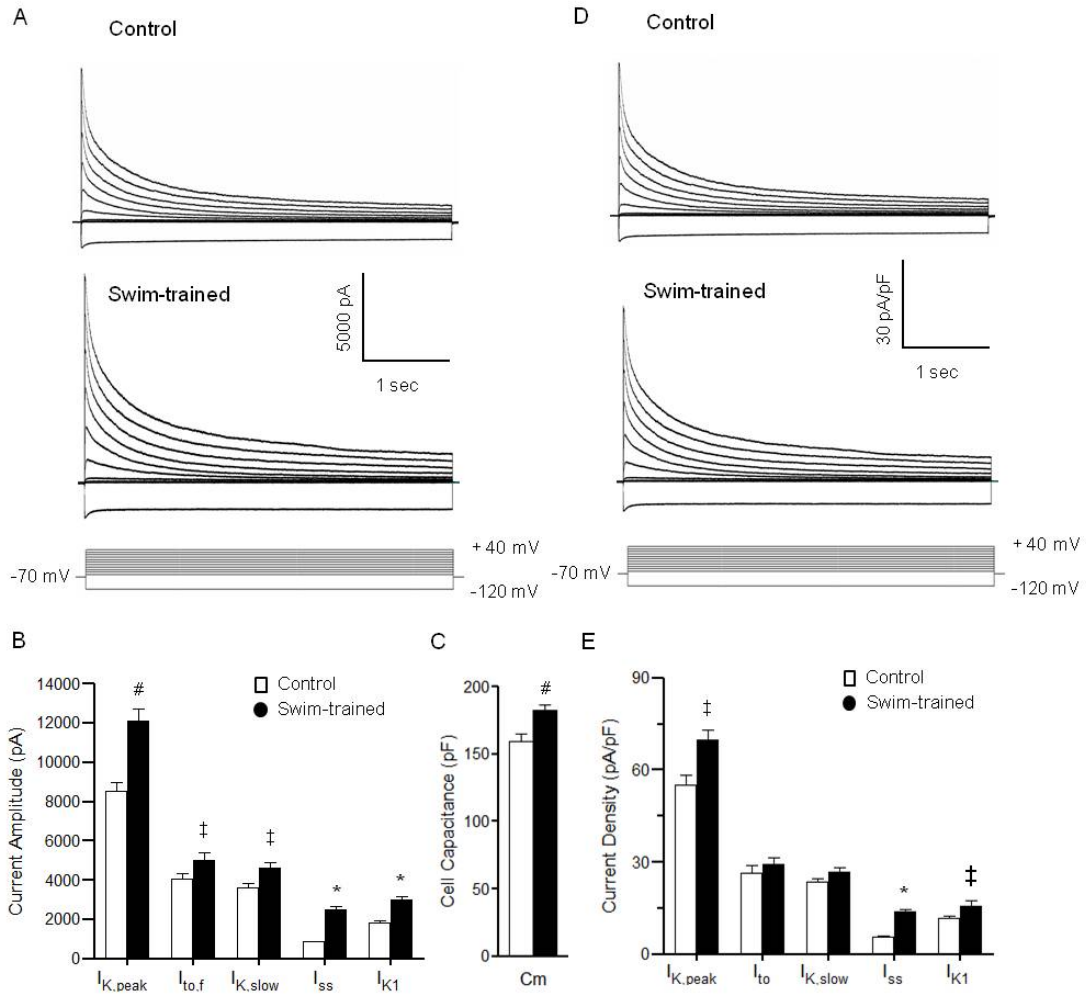

Figure 3. 2 Repolarizing K^+ current amplitudes are increased in ventricular myocytes from swim-trained mice.

(A) Representative whole-cell K^+ currents recorded from myocytes isolated from the apex of the left ventricles (LV) of control and swim-trained mice. Currents were evoked in response to (4.5 s) voltage steps to test potentials between -120 and +40 mV from a holding potential (HP) of -70mV; the paradigm is illustrated below the records. Mean ± SEM K^+ current amplitudes in LV myocytes from swim-trained animals are larger than in control LV myocytes (B). Mean ± SEM C_m is also significantly higher in cells from swim-trained animals (C), reflecting the increase in myocyte size. Normalizing current amplitudes for differences in cell size provided K^+ current densities (D, E). Mean ± SEM K^+ current densities in LV myocytes following swim-training are similar to (or higher than) control LV myocytes (see text). Values indicated are significantly ($^{‡}P<0.05$, $^{\#}P<0.01$, $^{*}P<0.001$) different in LV myocytes from control and swim-trained animals.

of the outward currents (Brunet *et al.*, 2004) provided the amplitudes of the individual components ($I_{to,f}$, $I_{K,slow}$ and I_{ss}) of the peak Kv currents, each of which is significantly higher in LV myocytes from swim-trained animals (**Figure 3.2B**). In contrast, there are no measurable differences in the time (**Table 3.1**) or the voltage- (data not shown) dependent properties of the Kv currents in cells from control and swim-trained mice. Consistent with the hypertrophic growth of the LV, however, whole-cell membrane capacitances (C_m) are significantly (P<0.01) higher in myocytes from swim-trained, compared with control, animals with mean ± SEM C_m values of 183 ± 4 pF (n=32) and 156 ± 5 pF (n=20), respectively (**Figure 3.2C**). The observed increases in current amplitudes (**Figure 3.2B**), however, are sufficient to offset the cellular hypertrophy (**Figure 3.2C**) to maintain repolarizing K^+ current densities similar to control levels (**Figure 3.2D and 3.2E**). Indeed, I_{ss} and I_{K1} densities are actually higher in LV myocytes from swim-trained, compared with control, animals (see **3.4 Discussion**).

3.3.2 Functional consequences of exercise training-induced physiological hypertrophy

To examine the functional consequences of exercise-induced ventricular hypertrophy, paired surface ECG recordings were obtained from animals before and after the 4-week training protocol. Analyses of these records revealed that the morphologies of the QRS complexes, P and T waves (**Figure 3.3A**), as well as the durations of the RR, PR, QRS and QT (and QTc) intervals (**Figure 3.3B**), measured before and after training, are indistinguishable. In addition, action potential waveforms in control and swim-trained LV myocytes are similar (**Figure 3.3C**), and mean ± SEM action potential durations at 25 (APD_{25}), 50 (APD_{50}) and 90 (APD_{90}) percent repolarization in control and swim-trained LV myocytes are not significantly different (**Figure 3.3D**).

Table 3. 1 Kv and Kir Currents in WT Control, Swim-Trained and caPI3Kα LV Myocytes.

		WT Control	Swim-trained	caPI3K	ANOVA
N		20	32	25	
Cm (pF)		156 ± 5	183 ± 4$^{\#}$	202 ± 7*	*P*<0.0001
I_{peak}	τ_d (ms)	—	—	—	
	Amplitude (pA)	8535 ± 462	11561 ± 519$^{\#}$	14941 ± 827*	*P*<0.0001
	Density (pA/pF)	55.0 ± 3.4	66.5 ± 3.5‡	77.6 ± 5.2$^{\#}$	*P*<0.0001
$I_{to,f}$	τ_d (ms)	88 ± 10	93 ± 10	90 ± 8	N.S.
	Amplitude (pA)	4042 ± 321	5016 ± 384‡	6052 ± 597$^{\#}$	*P*<0.01
	Density (pA/pF)	26.5 ± 2.5	27.3 ± 2.4	32.1 ± 3.5	N.S.
$I_{K,slow}$	τ_d (ms)	981 ± 40	1168 ± 72	1093 ± 44	N.S.
	Amplitude (pA)	3615 ± 226	4612 ± 288‡	7027 ± 512*	*P*<0.0001
	Density (pA/pF)	23.4 ± 1.4	25.4 ± 1.6	36.1 ± 2.7*	*P*<0.05
I_{ss}	τ_d (ms)	—	—	—	
	Amplitude (pA)	868 ± 35	2471 ± 169*	1862 ± 145*	*P*<0.0001
	Density (pA/pF)	5.7 ± 0.3	13.8 ± 0.8*	9.4 ± 0.6*	*P*<0.0001
I_{K1}	τ_d (ms)	—	—	—	
	Amplitude (pA)	-1811 ± 106	-2946 ± 156*	-2694 ± 150*	*P*<0.0001
	Density (pA/pF)	-11.7 ± 0.7	-15.4 ± 1.6‡	-13.8 ± 0.9‡	*P*<0.05

* All values are means ± SEM. Kv and Kir current amplitudes/densities were determined at +40 mV and -120mV, respectively. The ANOVA column refers to the statistical significance of a one-way ANOVA test across each row. Values in caPI3Kα, or in swim-trained LV myocytes that were compared are significantly (‡ *P*<0.05, $^{\#}$*P*<0.01 , **P*<0.001) different from the values in control WT cells in the post-hoc Tukey's multiple comparison test are indicated.

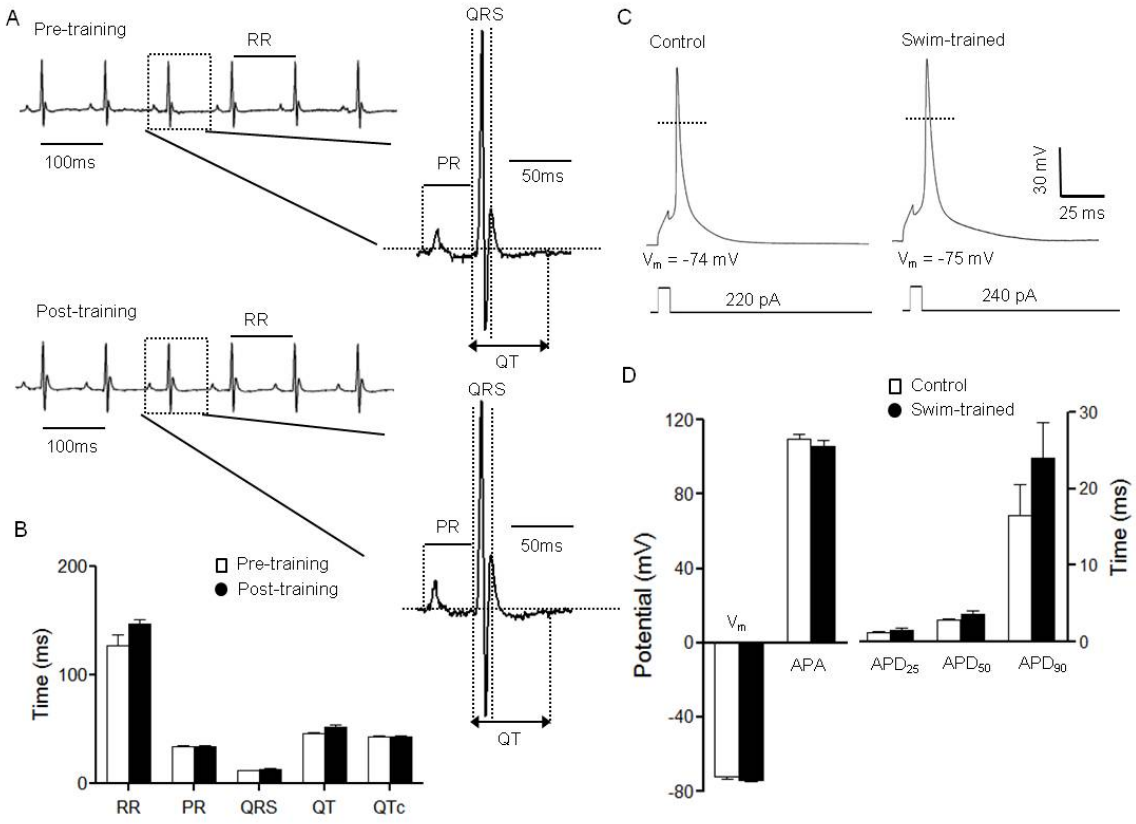

Figure 3. 3 ECG and action potential waveforms in swim-trained and control animals are indistinguishable.

(A) Representative ECG (lead II) waveforms from an anesthetized adult WT mouse before and 4 weeks after swim-training are illustrated. (B) Mean ± SEM RR, PR, QRS, QT and QTc intervals in animals before and after swim-training are not significantly different. (C) Mean ± SEM action potential amplitudes (APA) and action potential durations at 25% (APD_{25}), 50% (APD_{50}) and 90% (APD_{90}) repolarization in swim-trained and control LV myocytes are not significantly different (D).

3.3.3 Molecular basis of K^+ current upregulation in swim-trained LV

Physiological hypertrophy has been shown to be associated with global increases in total LV protein and RNA content (Hannan *et al.*, 2003), suggesting that the observed increases in K^+ current amplitudes in LV myocytes from swim-trained animals (**Figure 3.2A**) reflect increased expression of the subunits encoding the underlying K^+ channels. To explore this hypothesis directly, Western blot analyses, using K^+ channel subunit-specific antibodies, were performed on protein lysates prepared from the LV of swim-trained and control animals. Equal amounts of proteins from individual animals were fractionated, probed and quantified. Expression of lamin A/C was also probed (**Figure 3.4A**) and used for normalization (see Methods). Representative blots are presented in **Figure 3.4A**.

Quantitative analyses of these blots revealed that the mean ± SEM normalized (to lamin A/C) expression levels of each of the K^+ channel proteins examined (**Figure 3.4B**) were increased in swim-trained, compared with control, LV. Specifically, the mean ± SEM relative expression levels of Kv4.2, the Kv pore-forming subunit that underlies mouse ventricular $I_{to,f}$ (Guo *et al.*, 2005), and of the $I_{to,f}$ channel accessory subunit KChIP2 (Kuo *et al.*, 2001; Guo *et al.*, 2002), are increased significantly (P<0.05) in swim-trained, compared with control, LV (**Figure 3.4B**). Marked increases in the expression of Kv2.1 (P<0.05), which underlies one component of $I_{K,slow}$, $I_{K,slow2}$ (Xu *et al.*, 1999a), and of the I_{K1} channel subunit, Kir2.2 (P<0.01) (Zaritsky *et al.*, 2001), as well as of the two-pore domain subunit (K2P), TASK1 (P<0.05), suggested to encode ventricular I_{ss} channels (Putzke *et al.*, 2007), are also evident in swim-trained, compared with control, LV (**Figure 3.4B**). Consistent with previous reports (Hannan *et al.*, 2003), total protein is also increased significantly (P<0.001) in swim-trained (compared to control) LV (**Figure 3.4C**).

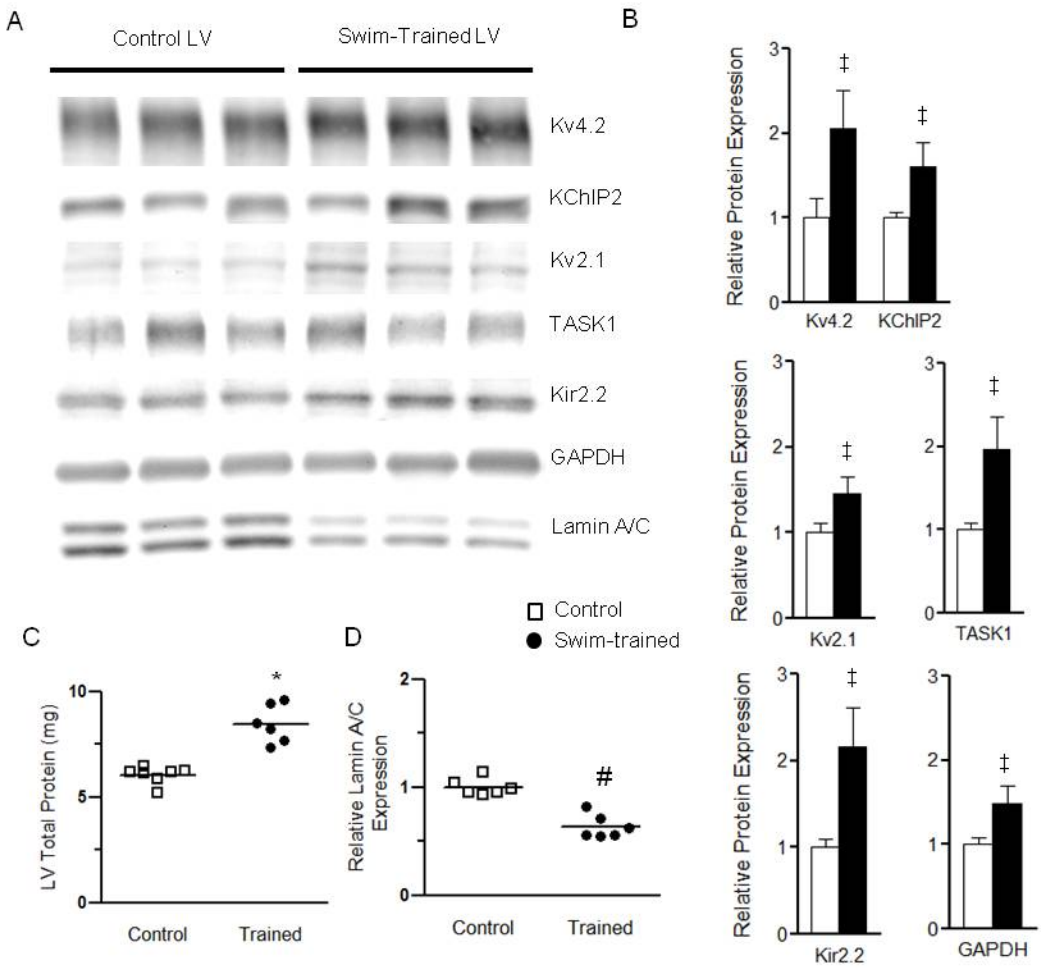

Figure 3. 4 Expression of K^+ channel subunits is increased in the LV of swim-trained animals in parallel with the increase in total protein.

(A) Representative Western blots of fractionated LV proteins from control (n=6) and swim-trained (n=6) animals probed with anti-K^+ channel subunit-specific antibodies, as well as anti-GAPDH and anti-nuclear membrane protein lamin A/C antibodies. (B) The expression of each protein on each blot was measured and normalized to the expression of lamin A/C (evident as a doublet at 62- and 69-kD) in the same sample on the same blot. Protein expression data were expressed relative to the mean value of the control LV samples. The mean ± SEM relative expression levels of several K^+ channel subunits, as well as GAPDH, are significantly ($^{‡}P<0.05$) higher in swim-trained, compared with control, LV. (C) Individual and mean ± SEM total protein content are significantly ($^{*}P<0.001$) higher in swim-trained (n=8), than in control (n=6), LV (left). (D) The individual and mean ± SEM relative (to total protein) lamin A/C protein expression levels are significantly ($^{\#}P<0.01$) lower in the LV from swim-trained (n=6), compared with control (n=6), animals (see text).

Normalization of the individual channel subunit protein expression levels to the total protein measured in the same sample revealed that each of the channel subunit proteins is increased in swim-trained LV in parallel with the overall increase in protein expression (**Supplemental Figure 3.1A**), thereby maintaining relative (compared to total protein) ion channel subunit expression levels similar to WT control levels. In contrast, when compared to total protein, the relative expression level of lamin A/C is lower in swim-trained, compared with control, LV (**Figure 3.4D**). The fact that the expression of lamin A/C is not increased in parallel with the global increase in protein expression is consistent with previous reports demonstrating increased myocyte size, but not myocyte number, in the hypertrophied heart (Hannan *et al.*, 2003) and with the suggestion above that lamin A/C expression can be exploited to normalize protein expression data to cell (nuclei) number.

Further experiments revealed that the expression levels of the transcripts encoding $I_{to,f}$ channel subunits, *Kcnd2* (Kv4.2) and *Kcnip2* (KChIP2), normalized to lamin A/C, are also increased (P<0.01) in swim-trained, compared with control, LV (**Figure 3.5A**), as is *Kcnd3* (Kv4.3) (P<0.01), the primary determinant of $I_{to,f}$ in large mammals (Kaab *et al.*, 1998; Kong *et al.*, 1998; Wang *et al.*, 1999). The expression level of the *Kcnb1* transcript, which encodes the $I_{K,slow,2}$ channel subunit, Kv2.1, but not of *Kcna5*,which encodes the $I_{K,slow,1}$ channel subunit, Kv1.5, (Xu *et al.*, 1999a; London *et al.*, 2001b), is also increased significantly (P<0.01) with exercise (Figure 3.5A). Similarly, expression of the I_{K1} channel transcripts, *Kcnj12* (Kir2.2) and *Kcnj2* (Kir2.1) (Zaritsky *et al.*, 2001), as well as of the putative I_{ss} encoding, K2P channel subunit, *Kcnk3* (TASK1) (Putzke *et al.*, 2007), are higher (P<0.05) in swim-trained, compared with control, LV (**Figure 3.5A**).

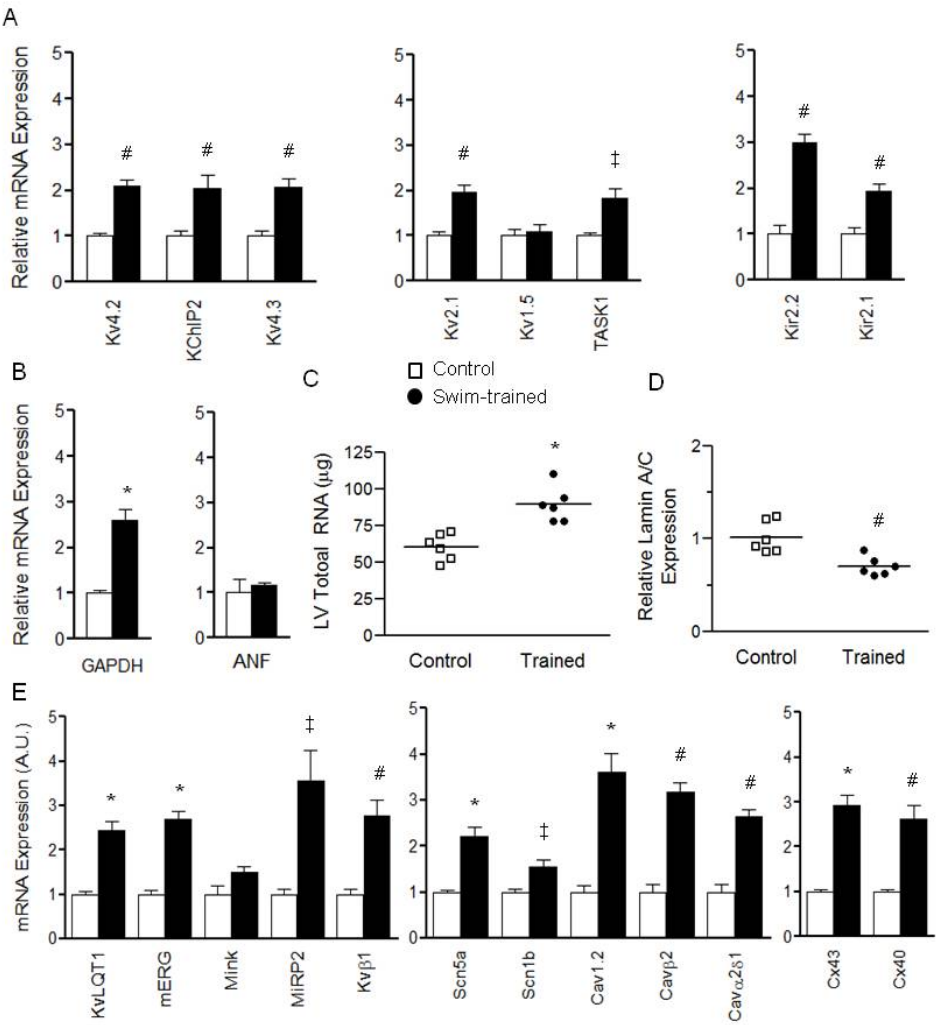

Figure 3. 5 Expression levels of K^+ channel subunit transcripts are also increased with swim-training.

(A) Individual and mean ± SEM total RNA levels are higher in swim-trained (n=6), compared with control (n=6), LV. Expression levels of K^+ channel subunit transcript expression levels were measured and normalized to *Imna* in the same sample. Transcript expression data were expressed relative to the mean value of control LV samples. The mean ± SEM relative expression levels of the transcripts encoding GAPDH (B) and several K^+ channel subunits (C) are significantly ($^{‡}P<0.05$, $^{\#}P<0.01$, $^{*}P<0.001$) higher in swim-trained LV, whereas expression of ANF (B), a marker of pathological hypertrophy, is similar in LV samples from control and swim-trained animals.

Expression of GAPDH is also increased with swim training, whereas atrial natriuretic factor (ANF), considered a marker of pathological hypertrophy (McMullen & Jennings, 2007), is not affected (**Figure 3.5B**). In parallel with the global increase in protein (**Figure 3.4C**), total RNA is also significantly (*P*<0.001) higher (1.4-fold on average) in swim-trained, than in control, LV (**Figure 3.5C**). Normalization of channel subunit transcript expression levels to the total cellular RNA measured in the same sample revealed that the increases in channel subunit transcript expression levels in swim-trained LV parallel the global increases in cellular RNA, maintaining relative (compared to total RNA) ion channel subunit expression levels at or near control levels (**Supplemental Figure 3.1B**).

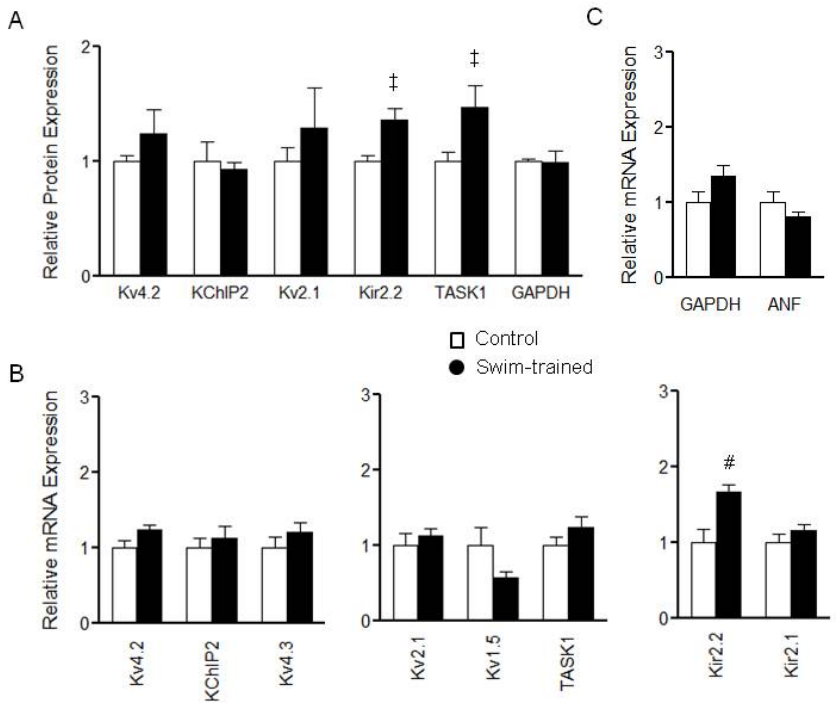

Supplemental Figure 3. 1 Myocardial K^+ channel subunit protein and transcript expression levels in LV samples from swim-trained and control animals increase in parallel with total cellular protein/RNA.

Protein (A) and transcript (B) expression levels of each of the K+ channel subunits were measured in LV samples from swim-trained and control LV, and normalized to the total protein or total RNA respectively determined in the same sample. Values determined in swim-trained LV were then expressed relative to the controls. Mean ± SEM normalized protein (A) and transcript (B) expression levels are plotted.

The expression levels of transcripts encoding several other ion channel subunits (normalized to lamin A/C) are also increased in the LV of animals following exercise (**Figure 3.5E**). For example, expression of *Kcnh2* (mERG) and *Kcnq1* (KvLQT1), the subunits which underlie the rapid and slow components of cardiac delayed rectification, I_{Kr} and I_{Ks} (Sanguinetti *et al.*, 1995; Sanguinetti *et al.*, 1996) in large mammals including humans, as well as voltage-gated Na^+ and Ca^{2+} channel and gap junction channel subunit transcripts, are also increased with swim-training (**Figure 3.5E**)

3.3.4 Activation of cardiac PI3Kα signaling also results in K^+ current upregulation

Chronic exercise training results in activation of PI3Kα and downstream signaling targets (**Figure 3.1**), as previously demonstrated (McMullen *et al.*, 2003; DeBosch *et al.*, 2006b; O'Neill *et al.*, 2007). It has also been reported that cardiac specific transgenic overexpression of constitutively active PI3Kα (caPI3Kα) produces ventricular hypertrophy with normal cardiac function (Shioi *et al.*, 2000). Subsequent experiments here, therefore, were aimed at determining if increasing cardiac PI3Kα signaling directly also results in the upregulation of repolarizing ventricular K^+ currents.

Similar to the results obtained in the experiments conducted on myocytes from animals following chronic swim training (**Figure 3.2**), $I_{K,peak}$ (P<0.001) and I_{K1} (P<0.001) amplitudes are significantly larger in caPI3K, compared with WT, LV myocytes (**Figure 3.6A and 3.6B**). Analysis of the currents revealed that the amplitudes of $I_{to,f}$, $I_{K,slow}$ and I_{ss} are all significantly (P<0.01) higher in caPI3Kα, than in WT, LV myocytes (**Figure 3.6B**), whereas the time- and voltage-dependent properties of the currents in caPI3Kα and WT cells are similar (**Table 3.1**). Consistent with the hypertrophic growth of caPI3Kα hearts, however, caPI3Kα LV myocytes are larger than WT cells. The mean ± SEM C_m determined for caPI3Kα (202 ± 7 pF, n=25) LV cells is significantly (P<0.001) higher than

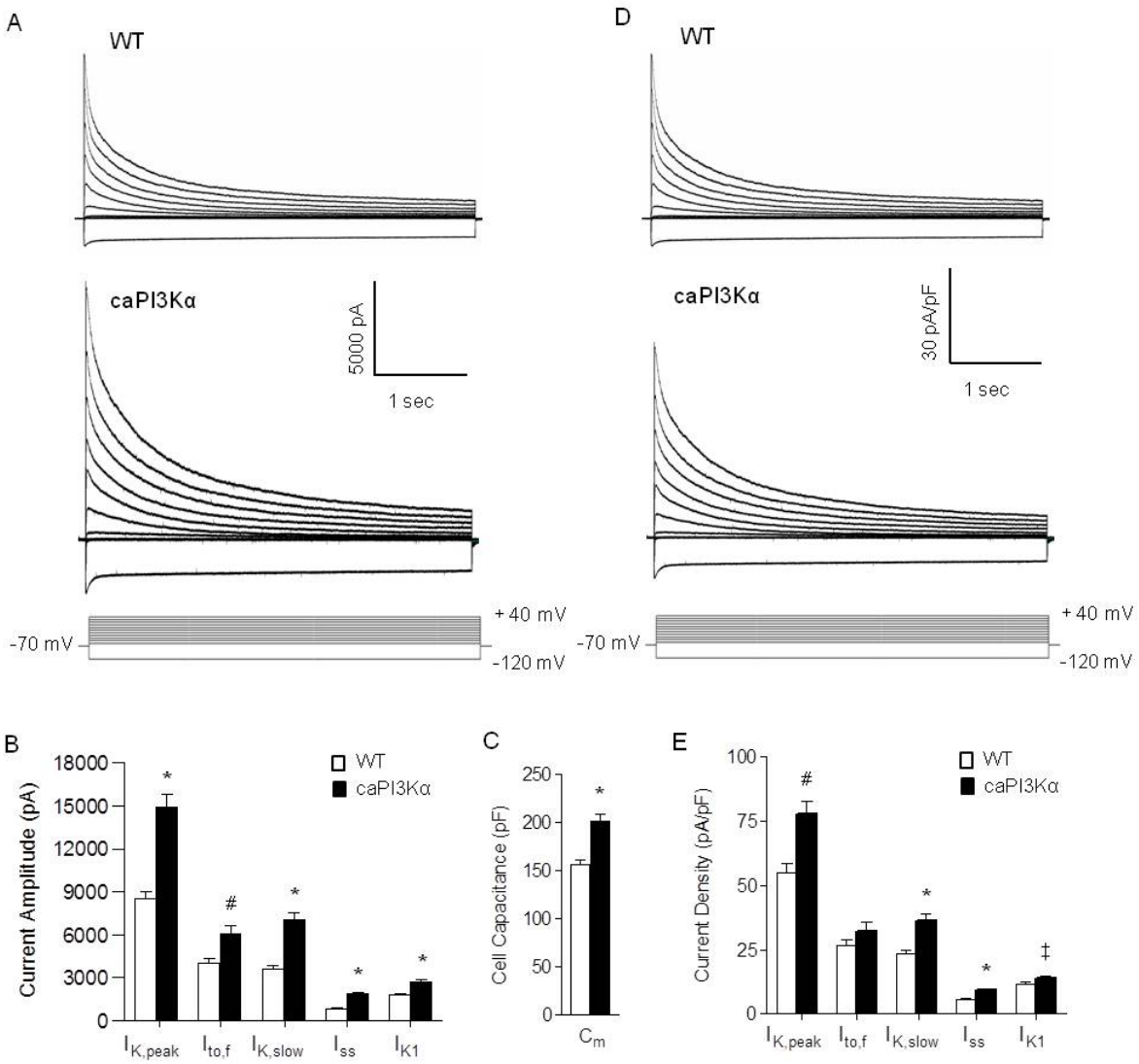

Figure 3. 6 Repolarizing K^+ currents are also upregulated in ventricular myocytes from adult caPI3Kα mice.

(A) Whole-cell K^+ currents were recorded as described in the legend to Figure 2 from myocytes isolated from the LV apex of caPI3Kα and WT mice. Mean ± SEM K^+ current amplitudes (B) and whole-cell C_m (C) are higher in caPI3Kα, than in WT, LV myocytes. After normalization for differences in cell size, K^+ current densities (D, E) in caPI3Kα LV myocytes are similar to, or higher than, the densities in WT cells. Values indicated are significantly ($^{‡}P<0.05$, $^{\#}P<0.01$, and $^{*}P<0.001$) higher in caPI3Kα LV myocytes compared with WT myoyctes.

the mean in WT (156 ± 5 pF, n=20) cells (**Figure 3.6C**). Normalization of the measured K^+ current amplitudes (**Figure 3.6B**) for differences in myocyte size (**Figure 3.6C**) revealed that repolarizing K^+ current densities in caPI3Kα LV myocytes are similar to, or actually higher than, the densities in WT LV cells (**Figure 3.6D and 6E**).

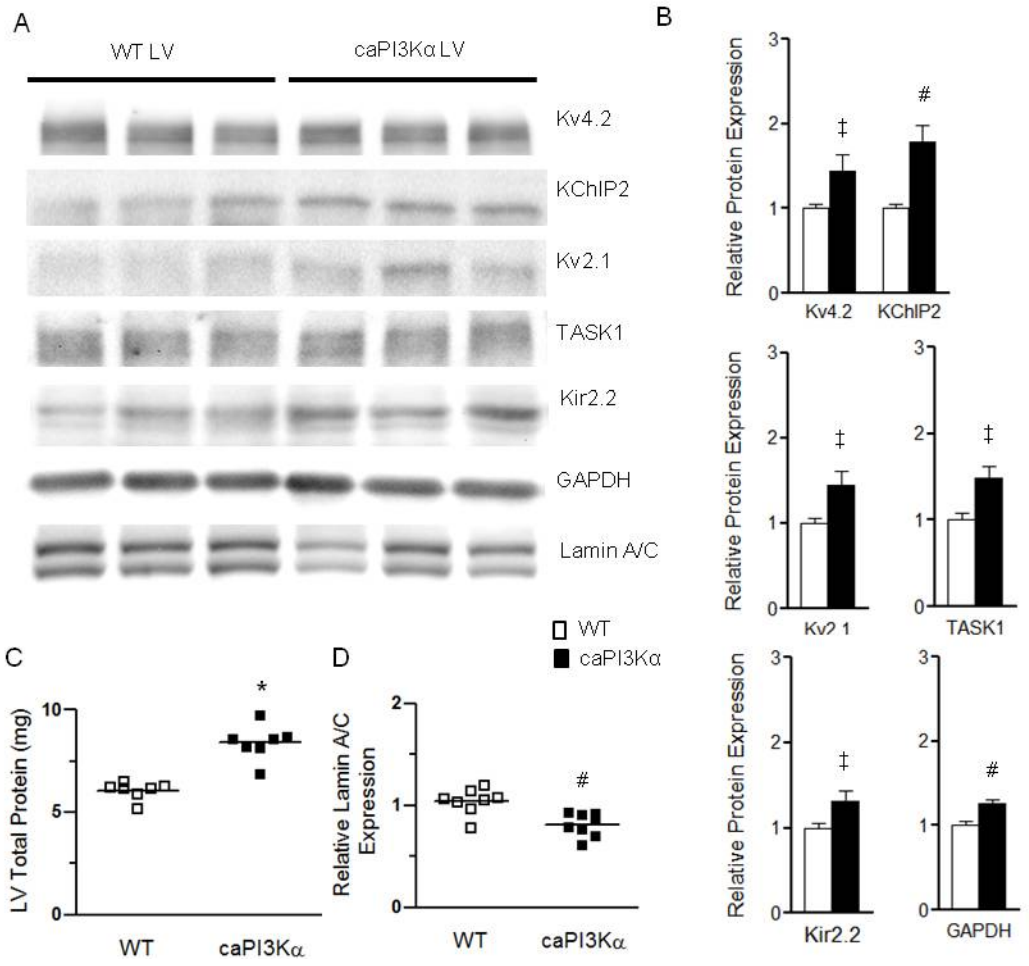

Figure 3. 7 Expression levels of K^+ channel subunit proteins are also increased in caPI3Kα LV.

(A) Individual and mean ± SEM (*P<0.001) protein content are higher in caPI3Kα (n=8), than in WT (n=8), LV. (B) Representative Western blots of fractionated ventricular proteins probed with anti-K^+ channel subunit-specific antibodies, as well as with anti-GAPDH and anti-lamin A/C. (C) Mean ± SEM (n=8) K^+ channel subunit (and GAPDH) expression levels are significantly (‡P<0.05, $^{\#}$P<0.01) higher in caPI3Kα, than in WT, LV.

Additional electrophysiological experiments revealed no significant differences in resting membrane potentials, action potential waveforms, or ECG parameters in WT and caPI3Kα cells/animals (data not illustrated). Exploiting the same strategy as used in the analyses of the LV of swim-trained mice, biochemical experiments were conducted to examine K^+ channel subunit protein expression levels in the LV of caPI3Kα, compared with WT, mice. As illustrated in **Figure 3.7**, these experiments revealed that the protein expression levels of the $I_{to,f}$ channel subunits (Kv4.2 and KChIP2), the $I_{K,slow2}$ channel subunit (Kv2.1), the I_{K1} channel subunit (Kir2.2), and the putative I_{ss} K2P channel subunit (TASK1) (normalized to lamin A/C) are all increased significantly (P<0.05) in caPI3Kα, compared with WT, LV (**Figure 3.7A and 3.7B**). Consistent with the marked hypertrophy in caPI3Kα hearts, total LV protein content is higher than in control LV (P<0.001**; Figure 3.7C**). Normalization of the channel subunit protein expression levels to the total protein measured in the same sample revealed that the observed increases in ion channel subunit protein expression are proportional to the global increase in total protein expression in caPI3Kα LV (**Supplemental Figure 3.2A**). Similar to the observations in swim-trained animals, cardiac specific expression of caPI3Kα is also associated with marked increases in the expression levels of the transcripts encoding repolarizing K^+ (as well as a number of other ion) channel subunits (**Figure 3.8A and 3.8E**) and in total RNA (**Figure 3.8C**), whereas ANF expression is unaffected in the caPI3Kα LV (**Figure 3.8B**). The observed increases in channel subunit transcript expression levels in caPI3Kα LV also parallel the increase in total cellular RNA (**Supplemental Figure 3.2B**).

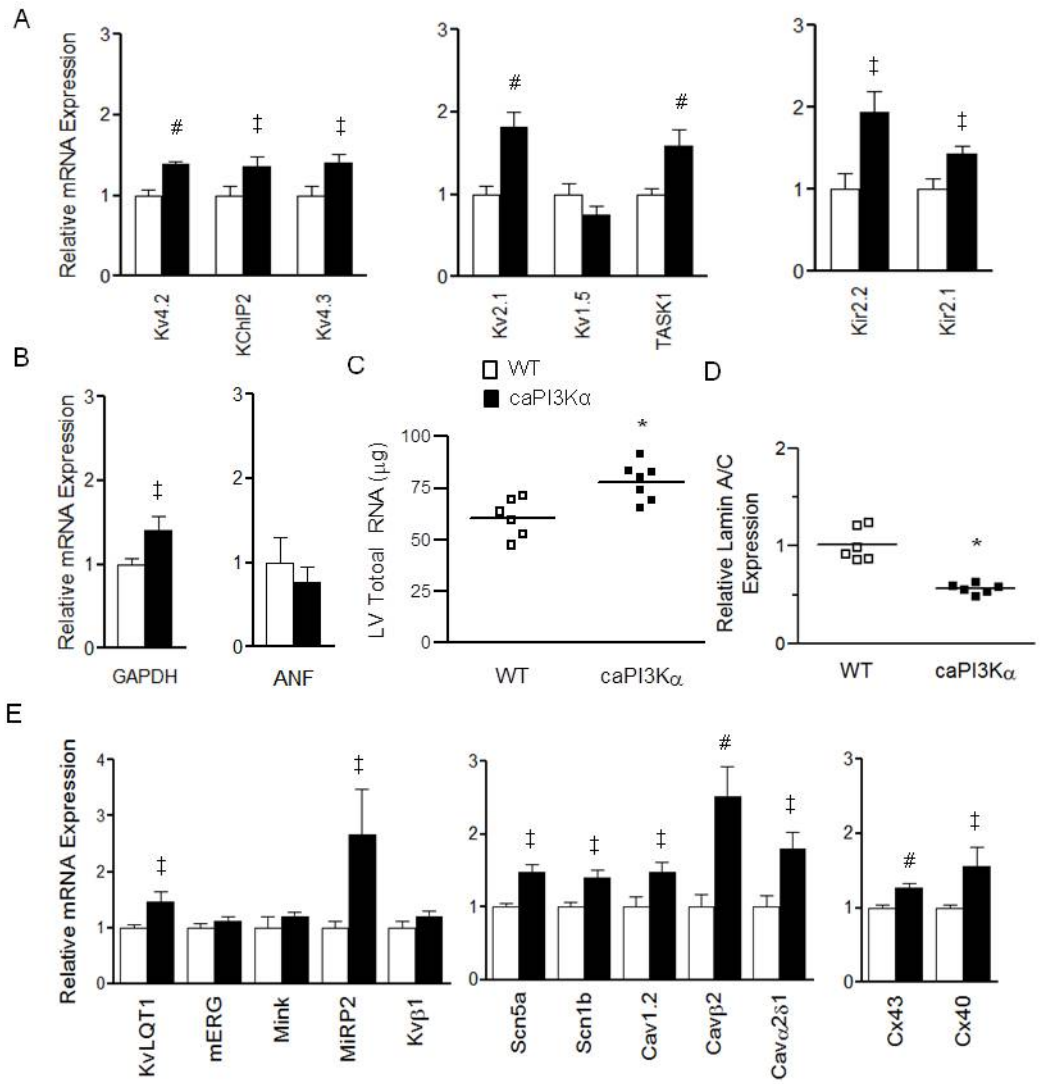

Figure 3. 8 Expression levels of transcripts encoding channel subunits are also increased in caPI3Kα LV.

(A) Individual and mean ± SEM (*P*<0.001) total RNA levels are higher in caPI3Kα (n=6), compared with WT (n=6), LV. The mean ± SEM relative transcript expression level of GAPDH, but not ANF, is higher in caPI3Kα than in WT LV (B). Expression levels of several K^+ channel subunits (C,D), as well as other voltage-gated and gap junction channel subunits (E) are significantly ($^{‡}P<0.05$, $^{\#}P<0.01$) higher in caPI3Kα, compared with WT, LV.

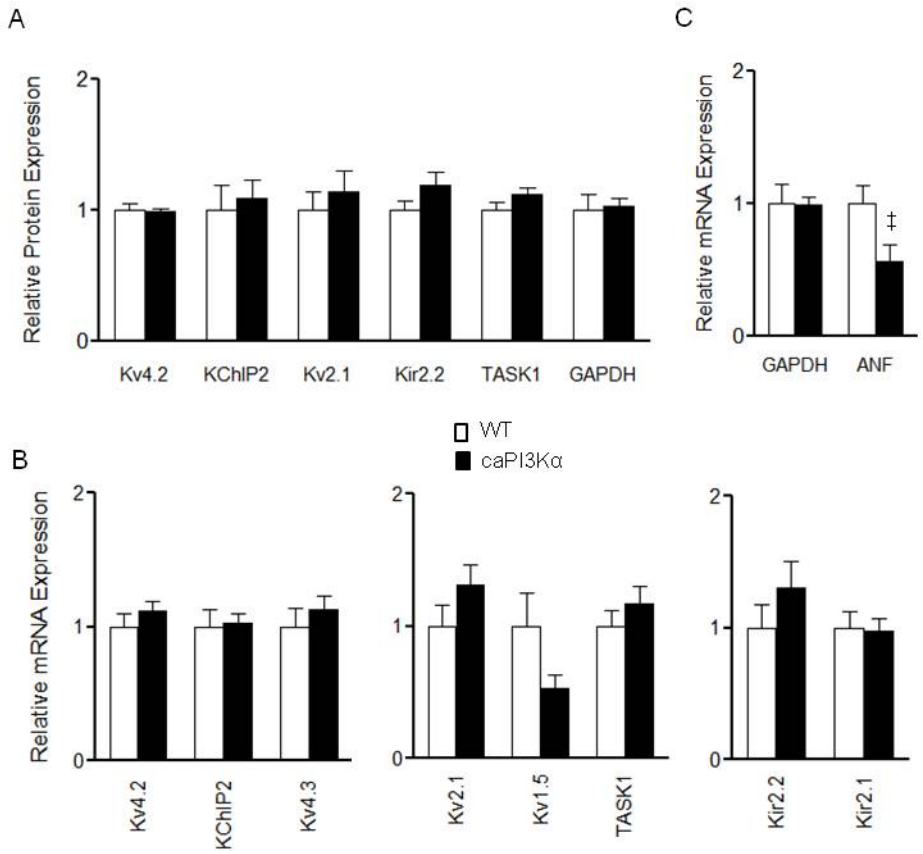

Supplemental Figure 3. 2 Myocardial K^+ channel subunit protein and transcript expression levels in LV samples from caPI3Kα and WT animals increases in parallel with total cellular protein/RNA.

Protein (A) and transcript (B) expression levels of K+ channel subunits were measured in LV samples from caPI3Kα and WT LV, and normalized to the total protein or total RNA respectively determined in the same sample. Values measured in caPI3Kα LV were then expressed relative to WT. Mean ± SEM protein (A) and transcript (B) expression levels are plotted.

3.3.5 Voltage-gated Ca^{2+} currents are also upregulated with physiological hypertrophy

The observation that the expression of repolarizing K^+ currents is upregulated in physiological hypertrophy without altering action potential waveform and ECG parameters suggests that the amplitudes of (depolarizing) inward currents likely are also upregulated to maintain ventricular myocyte excitability. As noted above, RT-PCR analysis revealed that the transcripts encoding voltage-gated Na^+ and Ca^{2+} channel pore-forming and accessory subunits are increased in caPI3Kα (**Figure 3.8E**), as well as

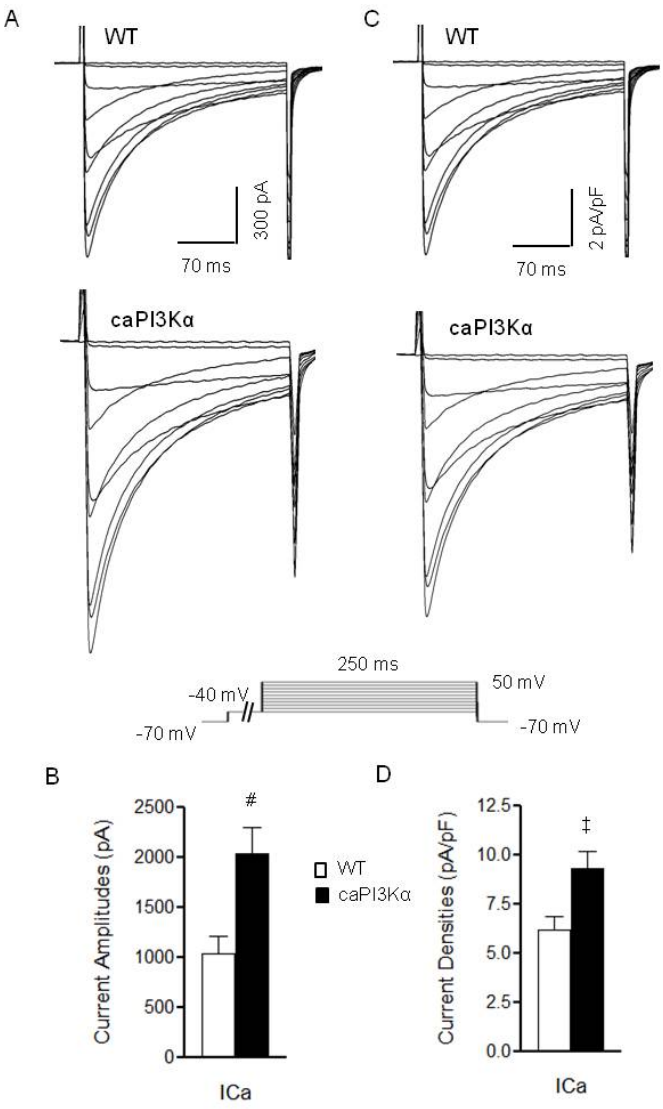

Figure 3. 9 Depolarizing $Ca2^{+}$ (ICa) current amplitudes are increased in LV myocytes from adult caPI3Kα mice.

(A) Representative whole-cell Ca^{2+} currents recorded from myocytes isolated from the LV apex of WT and caPI3Kα mice. Currents were evoked in response to (250 ms) voltage steps to test potentials between -30 and +50 mV from a prepulse potential of -40 mV (used to inactivate Na^{+} currents); the paradigm is illustrated below the records. Mean ± SEM Ca^{2+} current amplitudes (at +10 mV) are significantly higher in caPI3Kα, compared with WT, LV myocytes (B). Current amplitudes were normalized for differences in cell size, and representative (C) and mean ± SEM (D) I_{Ca} densities are illustrated. Values indicated are significantly ($^{‡}P<0.05$, $^{\#}P<0.01$) different in caPI3Kα and WT LV myocytes.

in swim-trained LV (**Figure 3.5E**). Additional voltage-clamp experiments revealed that the peak voltage-gated inward Ca^{2+} current (I_{Ca}) amplitudes are significantly (*P<0.01*) higher in caPI3Kα, than in WT, LV myocytes (**Figure 3.9 A,B**). Normalization of I_{Ca} amplitudes to myocyte size (C_m) revealed that inward Ca^{2+} current densities are also significantly (*P*<0.05) increased in caPI3Kα, compared with WT, LV myocytes (**Figure 3.9 C,D**).

3.3.6 Repolarizing K^+ currents are upregulated in Akt1$^{-/-}$ LV with chronic swim training

The results here demonstrate that chronic exercise (swim training)-induced physiological hypertrophy, which results in increased PI3Kα activation, leads to the upregulation of repolarizing ventricular K^+ and Ca^{2+} currents in parallel with the increase in myocyte size. The critical downstream effector of PI3Kα-mediated physiological hypertrophy in response to exercise training has been demonstrated to be the serine-threonine kinase Akt1 (DeBosch *et al.*, 2006b). Indeed, animals lacking Akt1 (Akt1$^{-/-}$)(Cho *et al.*, 2001b; DeBosch *et al.*, 2006b) failed to display ventricular hypertrophy with exercise training (DeBosch *et al.*, 2006b).

To test the hypothesis that Akt1 is also required for exercise (PI3Kα)-induced electrical remodeling, adult (8-10 week) Akt1$^{-/-}$ mice were subjected to chronic swim training for 4 weeks. Previous studies have demonstrated that Akt1$^{-/-}$ mice are fertile and have a normal life span (Cho *et al.*, 2001a) and that Akt2 and Akt3 expression levels in adult Akt1$^{-/-}$ mouse hearts (DeBosch *et al.*, 2006b) are indistinguishable from WT hearts. Following swim training, mean ± SEM citrate synthase activity in the gastrocnemius muscles was increased significantly (P<0.01) to 1.01±0.12 μmol/mg protein/min (n=4), compared with 0.53±0.07 μmol/mg protein/min (n=4) in muscles from untrained Akt1$^{-/-}$ animals (**Figure 3.10A**), indicating the adequacy of exercise training (Allen *et al.*, 2001). Consistent with previous suggestions that Akt1 is required for exercise training-induced physiological hypertrophy (DeBosch *et al.*, 2006b), however, the LVW/TL ratio (**Figure 3.10B**), as well as the mean ± SEM whole-cell membrane capacitance (C_m), a measurement of cell size, of isolated LV myocytes (Figure 1C), were similar in swim-trained and untrained Akt1$^{-/-}$ animals.

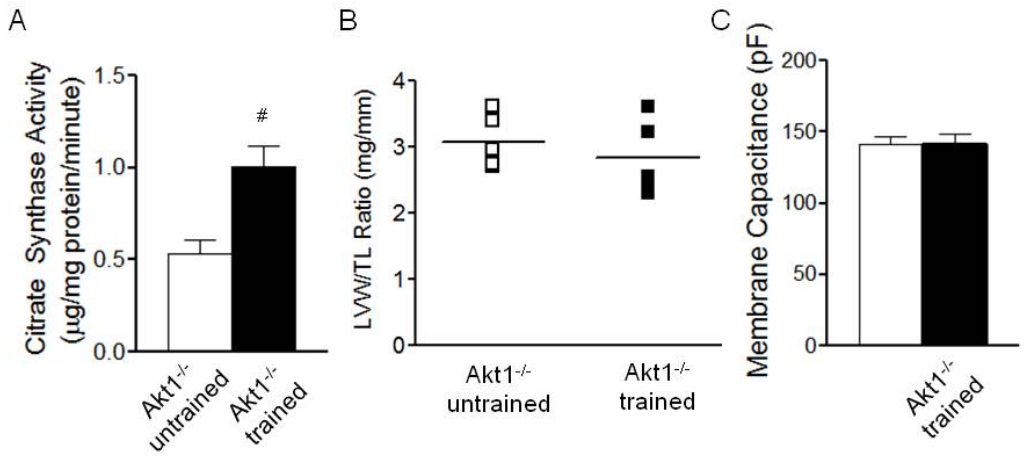

Figure 3. 10 Chronic swim training did not result in cardiac hypertrophy in Akt1$^{-/-}$ animals

(A) Citrate synthase activity was increased significantly (*P*<0.01) in gastrocnemius muscles from swim-trained, compared with untrained, Akt1$^{-/-}$ animals (n=4 in each group), indicating the adequacy of exercise training.(Allen *et al*., 2001) (B) LV mass/tibia length (LVM/TL) ratios were determined in swim trained and untrained Akt1$^{-/-}$ animals (n=6 in each group); individual and mean ± SEM values are plotted. (C) Mean ± SEM whole-cell membrane capacitances (C_m) were similar in LV myocytes isolated from swim-trained and untrained Akt1$^{-/-}$ animals, consistent with the absence of hypertrophic growth in response to exercise training.

Whole-cell voltage-clamp experiments were performed on LV myocytes isolated from swim-trained and untrained Akt1$^{-/-}$ mice. As illustrated in **Figure 3.11**, these experiments revealed that the amplitudes of the peak ($I_{K,peak}$) outward voltage-gated (Kv) and inwardly rectifying (Kir) K^+ currents were significantly higher in the LV myocytes from swim-trained, compared with untrained, Akt1$^{-/-}$ animals (*P*<0.05; **Figure 3.11A,B,D**). Kinetic analyses of the decay phases of the outward K^+ currents revealed that the amplitudes of the individual Kv current components, $I_{to,f}$ and I_{ss}, were higher in swim-trained Akt1$^{-/-}$ LV myocytes (**Figure 3.11D**). The amplitudes of $I_{K,slow}$ were also increased in Akt1$^{-/-}$ LV myocytes with swim training, although the increase did not reach statistical significance. There were no measurable differences in the time- or the voltage-dependent properties of the Kv currents in LV cells from Akt1$^{-/-}$ mice with and without swim training (**Figure 3.11B** and **Table 3.2**).

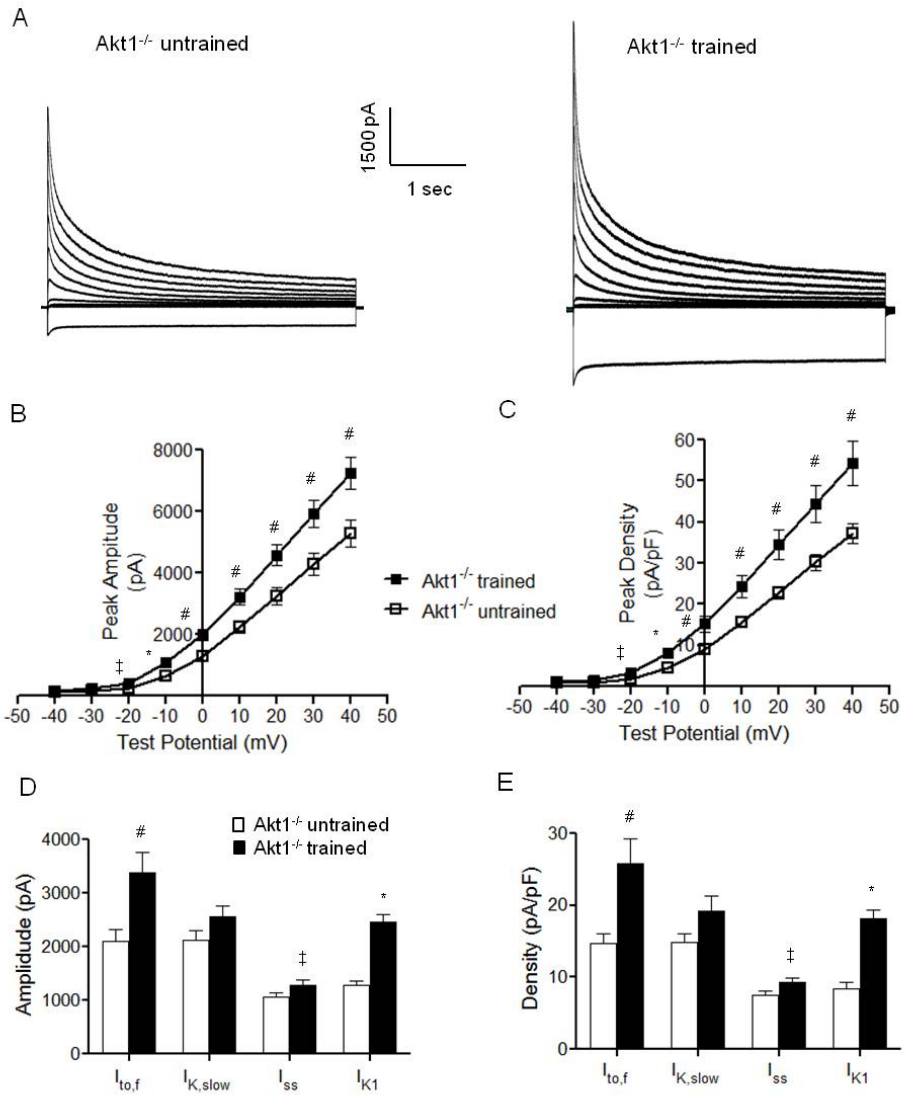

Figure 3. 11 Repolarizing K+ current amplitudes and densities were increased in LV myocytes isolated from swim-trained Akt1-/- animals

(A) Representative whole-cell K^+ currents recorded from myocytes isolated from the LV apex of swim-trained and untrained Akt1$^{-/-}$ mice. Currents were evoked in response to (4.5 s) voltage steps to test potentials between -120 and +40 mV from a holding potential (HP) of -70 mV. (B) The mean ± SEM amplitudes of the peak outward K^+ currents ($I_{K,peak}$) were significantly ($^{‡}P$<0.05, $^{\#}P$<0.01,$^{*}P$<0.001) higher in swim-trained, compared with untrained, Akt1$^{-/-}$ LV myocytes. (D) Normalizing current amplitudes to cell size (C_m) revealed that mean ± SEM $I_{K,peak}$ densities were also significantly higher in LV myocytes from swim-trained, compared with untrained, Akt1$^{-/-}$ LV myocytes. The amplitudes of the individual Kv current components, $I_{to,f}$, $I_{K,slow}$, and I_{ss}, as well as I_{K1}, were also measured (see Methods). Mean ± SEM $I_{to,f}$ and I_{ss} (at +40 mV) and I_{K1} (at -120 mV) current amplitudes (D) and densities (E) were significantly ($^{‡}P$<0.05, $^{\#}P$<0.01, $^{*}P$<0.001) higher in LV apex myocytes from swim-trained, compared with untrained, Akt1$^{-/-}$ animals.

Normalization of the measured K^+ current amplitudes in individual cells to the whole cell capacitance (myocyte size) in the same cell revealed that similar to the current amplitudes, mean ± SEM repolarizing K^+ current ($I_{K,peak}$, $I_{to,f}$, I_{ss} and I_{K1}) densities were significantly (P<0.05) higher in Akt1$^{-/-}$ LV myocytes following swim training (**Figure 3.11C,E**).

Table 3. 2 Kv and Kir Currents in Swim-trained and Untrained Akt1-/-, WT+Vehicle, icaPI3Kα+Vehicle and icaPI3Kα+TCN LV Myocytes.*

LV Cells		C_m (pF)	$I_{K,peak}$	$I_{to,f}$	$I_{K,slow}$	I_{ss}	I_{K1}
Akt1$^{-/-}$ untrained		141 ± 6					
(n=23)	τ (ms)		—	89 ± 6	1597 ± 112	—	—
	Amplitude (pA)		5289 ± 436	2103 ± 225	2118 ± 194	1067 ± 68	-1276 ± 80
	Density (pA/pF)		37.2 ± 2.5	14.7 ± 1.4	14.9 ± 1.1	7.6 ± 0.5	-8.4 ± 0.9
Akt1$^{-/-}$ trained		141 ±7					
(n=20)			—	75 ± 6	1303 ± 61	—	—
	Amplitude (pA)		7235 ± 523$^{\#}$	3387 ± 385$^{\#}$	2557 ± 198	1291 ± 91‡	-2471 ± 139*
	Density (pA/pF)		54.3 ± 5.4$^{\#}$	25.9 ± 3.4$^{\#}$	19.2 ± 2.1	9.3 ± 0.6‡	-12.5 ± 0.6*
WT+Vehicle		181 ± 9					
(n=33)	τ (ms)		—	121 ± 9	1097 ± 95	—	—
	Amplitude (pA)		11485 ± 659	4159 ± 314	5399 ± 391	1599 ± 91	-2677 ± 173
	Density (pA/pF)		67.2 ± 4.0	24.8 ± 2.1	31.1 ± 2.0	9.1 ± 0.4	-14.9 ± 1.0
icaPI3Kα+Vehicle		177 ± 9					
(n=24)	τ (ms)		—	109 ± 55	981 ± 55	—	—
	Amplitude (pA)		16087 ± 1139*	6424 ± 734$^{\#}$	6780 ± 471‡	1837 ± 104	-3457 ± 284‡
	Density (pA/pF)		92.2 ± 5.9$^{\#}$	38.8 ± 4.4$^{\#}$	41.2 ± 3.1‡	11.2 ± 0.7	-19.1 ± 1.4‡
icaPI3Kα+TCN		171 ± 6					
(n=21)	τ (ms)		—	90 ± 36	949 ± 30	—	—
	Amplitude (pA)		15394 ± 903*	6199 ± 493*	6563 ± 367‡	1751 ± 94	-3077 ± 188‡
	Density (pA/pF)		96.1 ± 6.0*	35.0 ± 2.5$^{\#}$	37.4 ± 2.1‡	10.0 ± 0.5	-18.8 ± 1.4‡

* All values are means ± SEM. Kv and Kir current amplitudes/densities reported here were determined at +40 mV and -120mV, respectively. Measured K^+ current amplitudes/densities in swim-trained and untrained Akt1$^{-/-}$ LV myocytes were compared and K^+ currents in icaPI3Kα+Vehicle and icaPI3Kα+TCN LV myocytes were both compared to results from WT+Vehicle animals. Values that are significantly (‡ P<0.05, $^{\#}P$<0.01, $^{*}P$<0.001) different are indicated. Kv indicates voltage-gated K^+ currents; Kir, inwardly rectifying K^+ currents; TCN: triciribine; C_m, cell membrane capacitance; τ, time constant of inactivation.

3.3.7 Transcriptional upregulation of ion channel subunits with chornic exercise training does not require Akt1

The studies here demonstrate that the increases in ventricular K^+ current amplitudes with chronic exercise training reflects the upregulation of the transcripts encoding the underlying K^+ channel pore forming and accessory subunits. Subsequent experiments here, therefore, were aimed at determining if the observed increases in K^+ current amplitudes in Akt1$^{-/-}$ LV myocytes with swim training (**Figure 3.11B,C**) also reflect increased expression of the transcripts encoding the K^+ channel subunits.

As illustrated in **Figure 3.12**, quantitative RT-PCR revealed that the expression levels of the transcripts encoding the $I_{to,f}$ channel pore-forming (α) subunit, *Kcnd2* (Kv4.2) (Guo *et al.*, 2005), and the $I_{to,f}$ channel accessory subunit, *Kcnip2* (KChIP2) (Kuo *et al.*, 2001; Guo *et al.*, 2002), were increased significantly (P<0.05) in the LV of swim-trained, compared with untrained Akt1$^{-/-}$, animals (**Figure 3.12A**). The expression levels of *Kcnb1* (Kv2.1), which encodes $I_{K,slow2}$ (Xu *et al.*, 1999a), and of the K2P channel subunit, *Kcnk3* (TASK1), which has been suggested to underlie I_{ss} in rat cardiomyocytes (Putzke *et al.*, 2007), were also increased significantly (P<0.05) in swim-trained Akt1$^{-/-}$ LV (**Figure 3.12B**). Similarly, the expression levels of the I_{K1} channel subunit, *Kcnj12* (Kir2.2) (Zaritsky *et al.*, 2001), as well as of *Kcnh2* (mERG) (Sanguinetti *et al.*, 1996), the α subunits encoding the rapid cardiac delayed rectifiers, I_{Kr}, in large mammals, were also elevated in Akt1$^{-/-}$ LV following swim training (**Figure 3.12C,D**). In addition, the transcripts encoding depolarizing voltage-gated Na^+ and Ca^{2+} channel pore-forming and accessory subunits were also significantly (P<0.05) increased in swim-trained, compared with untrained, Akt1$^{-/-}$ LV. These results, which are similar to the results observed in WT animals, demonstrate that chronic exercise training leads to the transcriptional upregulation of both repolarizing and depolarizing cardiac ion channel subunits,

independent of cellular hypertrophy and Akt1. Also similar to above findings in WT mice, this parallel upregulation of the subunits encoding depolarizing and repolarizing myocardial ion channels in response to exercise training results in the maintenance of normal myocardial excitability: ECG waveforms in swim-trained and untrained Akt1$^{-/-}$ animals were indistinguishable (**Figure 3.12F, G**).

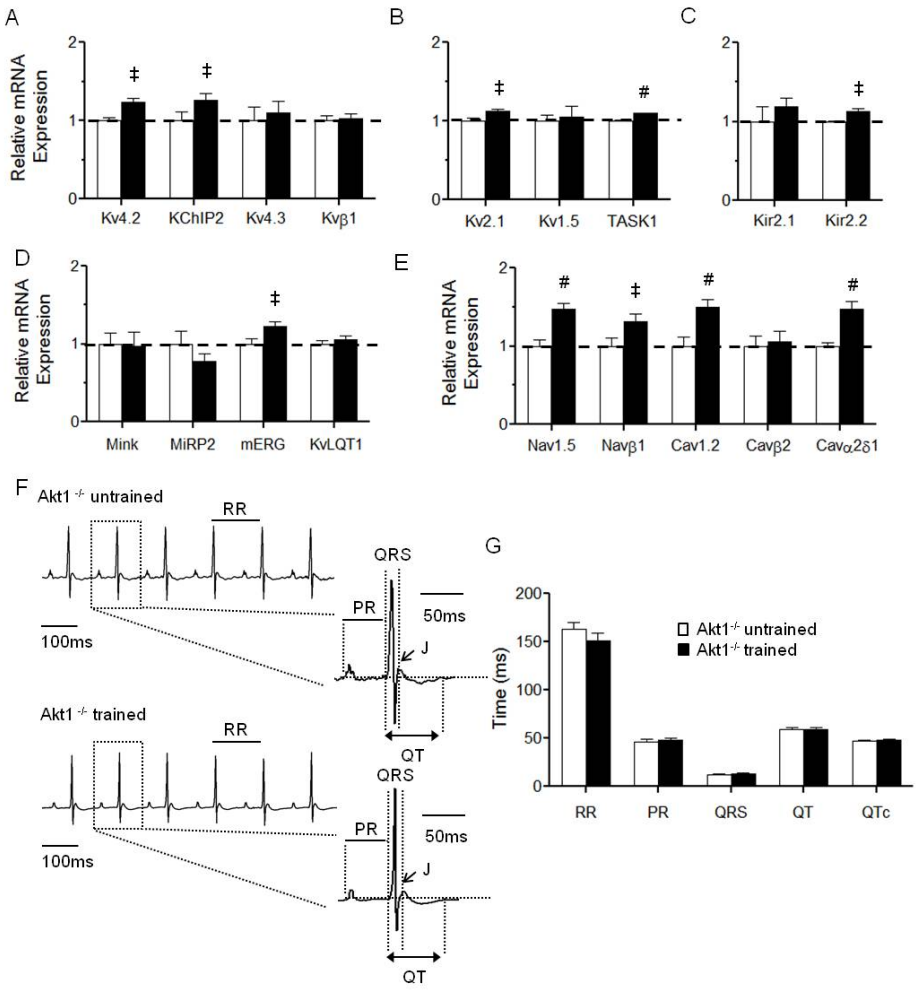

Figure 3. 12 Transcriptional upregulation of ion channel subunits with chronic exercise training maintains electrical functioning in animals lacking Akt1

Expression levels of transcripts encoding repolarizing K^+ (A-D), as well as depolarizing Na^+ and Ca^{2+} (E) channel subunits were measured in individual LV samples from swim-trained (n=6) and untrained (n=6) Akt1$^{-/-}$ LV, normalized to *Hprt* and subsequently to the mean value of the untrained Akt1$^{-/-}$ LV samples. The mean ± SEM relative expression levels of many ion channel subunit transcripts were significantly ($^{‡}P$<0.05, $^{\#}P$<0.01,$^{*}P$<0.001) higher in swim-trained, than in untrained, Akt1$^{-/-}$ LV. (F) Representative ECG (lead II) waveforms from anesthetized adult Akt1$^{-/-}$ mice, with and without swim-training, are illustrated. (G) Mean ± SEM RR, PR, QRS, QT and QTc intervals in Akt1$^{-/-}$ animals with and without swim-training were not significantly different.

3.3.8 Short-term activation of cardiac PI3Kα signaling upregulates repolarizing K^+ currents independent of Akt

The results here have shown that cardiac specific expression of constitutively active PI3Kα (caPI3Kα) mimicks the effects of exercise training, increasing repolarizing ventricular K^+ current amplitudes and normalizing K^+ current densities to the increase in myocyte size (hypertrophy). Also similar to exercise training, cardiac-specific expression of caPI3Kα results in transcriptional upregulation of the subunits encoding repolarizing K^+ and depolarizing (Na^+/Ca^{2+}) currents. Additional experiments here, therefore, were designed to test the hypothesis that Akt activation is required for the upregulation of ventricular K^+ currents and ion channel subunits in response to increased PI3Kα signaling.

For these experiments, a mouse model previously developed and described by Yano and colleagues (Yano *et al.*, 2008) with tetracycline transactivator (tet-off) controlled, cardiac-specific expression of caPI3Kα (icaPI3Kα), was utilized. In this transgenic mouse line, cardiac PI3Kα activity and Akt phosphorylation are significantly increased with transgene induction following the removal of dietary doxycycline for 2 weeks. Short-term (2-8 weeks), but not chronic (>8 weeks), activation of cadiac PI3Kα in this mouse model does not produce significant cardiac hypertrophy, despite the marked increases in PI3Kα signaling activities (Yano *et al.*, 2008). Using the protocol schematized in **Figure 3.13A**, expression of the caPI3Kα transgene was induced in adult (8-10 weeks) icaPI3Kα animals by removing the Dox containing diet. Similar to the findings reported in the original description of the icaPI3Kα animals (Yano *et al.*, 2008), removal of the Dox diet for 4 weeks and the resultant expression of the caPI3Kα transgene in the adult mouse heart did not produce measurable cardiac hypertrophy (**Figure 3.13B**). Significantly (P<0.001) increased PI3Kα signaling, however, was evident in the ~3 fold

increase in pAkt and in the pAkt/Akt ratio in icaPI3Kα, compared with WT, LV (**Figure 3.13C,D**).

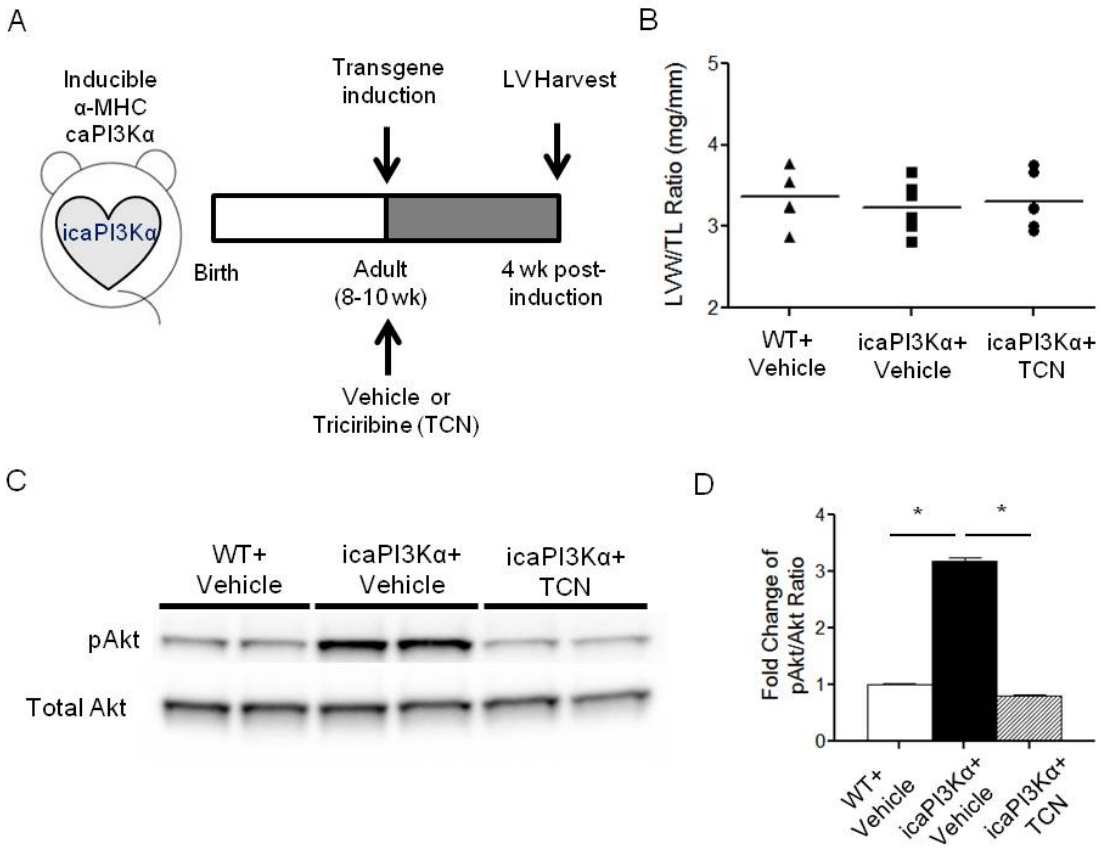

Figure 3. 13 Administration of triciribine (TCN) in icaPI3Kα animals blocked the hyperphorysphorylation of cardiac Akt.

(A) Schematic illustration of the caPI3Kα transgene induction and the pan-Akt inhibitor triciribine (TCN) injection protocol in icaPI3Kα animals. (B) LVW/TL ratios were similar in WT+Vehicle, icaPI3Kα+Vehicle and icaPI3Kα+TCN animals. (C) Representative Western blots of fractionated LV proteins from WT+Vehicle, icaPI3Kα+Vehicle and icaPI3Kα+TCN animals (n=4 in each group) probed with anti-pAkt and anti-total Akt antibodies. The expression level of pAkt in each lane on each blot was measured and normalized to the expression of total-Akt in the same lane on the same blot. Mean pAkt/Akt ratios in the LV from icaPI3Kα animals, vehicle- or TCN-treated, were expressed relative to the mean value in the control (WT+Vehicle) LV samples. (D) Mean ± SEM pAkt/Akt ratio is significantly (*P<0.001) higher in icaPI3Kα+Vehicle, compared with WT+Vehicle, LV. In addition, 4 week administration of TCN significantly (*P<0.001) reduced the phosphorylation of Akt in icaPI3Kα LV (see text).

Voltage-clamp recordings revealed that the amplitudes of $I_{K,peak}$ and I_{K1}, as well as of the Kv current components, $I_{to,f}$ and $I_{K,slow}$, were increased significantly (P<0.05) in icaPI3Kα, compared with WT, LV myocytes (**Figure 3.14A, B**); the mean ± SEM amplitude of I_{ss} was also higher in icaPI3Kα LV myocytes, although this increase was not statistically significant. Although the amplitudes were increased, the time- and voltage-dependent properties of $I_{to,f}$ and $I_{K,slow}$ in icaPI3Kα and WT cells were not significantly different (**Table 3.2**). Interestingly, the mean C_m (**Figure 3.14C**) values determined in icaPI3Kα and WT LV myocytes were similar, revealing that cellular hypertrophy is not evident following 4 weeks of induced caPI3Kα expression. These observations are consistent with the absence of LV hypertrophy in icaPI3Kα animals (**Figure 3.13B**). The increased K^+ current amplitudes (**Figure 3.14B**) in icaPI3Kα LV myocytes, therefore, translate directly into increased K^+ current densities (**Figure 3.14D**). With the exception of I_{ss}, repolarizing K^+ current densities were increased significantly in icaPI3Kα, than in WT, LV cells (**Figure 3.14D**).

To block Akt activation (hyperphosphorylation) in parallel with the induction of caPI3Kα transgene expression, a pan-Akt inhibitor triciribine (TCN) was administered (0.5 mg/kg/day, i.p.) daily to icaPI3Kα animals simultaneous with the removal of Dox diet (**Figure 3.13A**) for four weeks. The hyperphosphorylation of Akt in icaPI3Kα LV was completely abrogated with 4 weeks of TCN treatment (**Figure 3.13C, D**), indicating the successful blockade of Akt activation. As illustrated in Figure 5, however, the amplitudes of the repolarizing K^+ currents, $I_{to,f}$, $I_{K,slow}$, and I_{K1} were *increased* significantly (P<0.05) in LV myocytes isolated from icaPI3Kα+TCN animals (**Figure 3.14A, B**). Normalizing the current amplitudes to measured C_m revealed that mean ± SEM $I_{K,peak}$, $I_{to,f}$, $I_{K,slow}$ and I_{K1} densities were also *higher* (**Figure 3.14D**) in icaPI3Kα+TCN, compared to WT, cells.

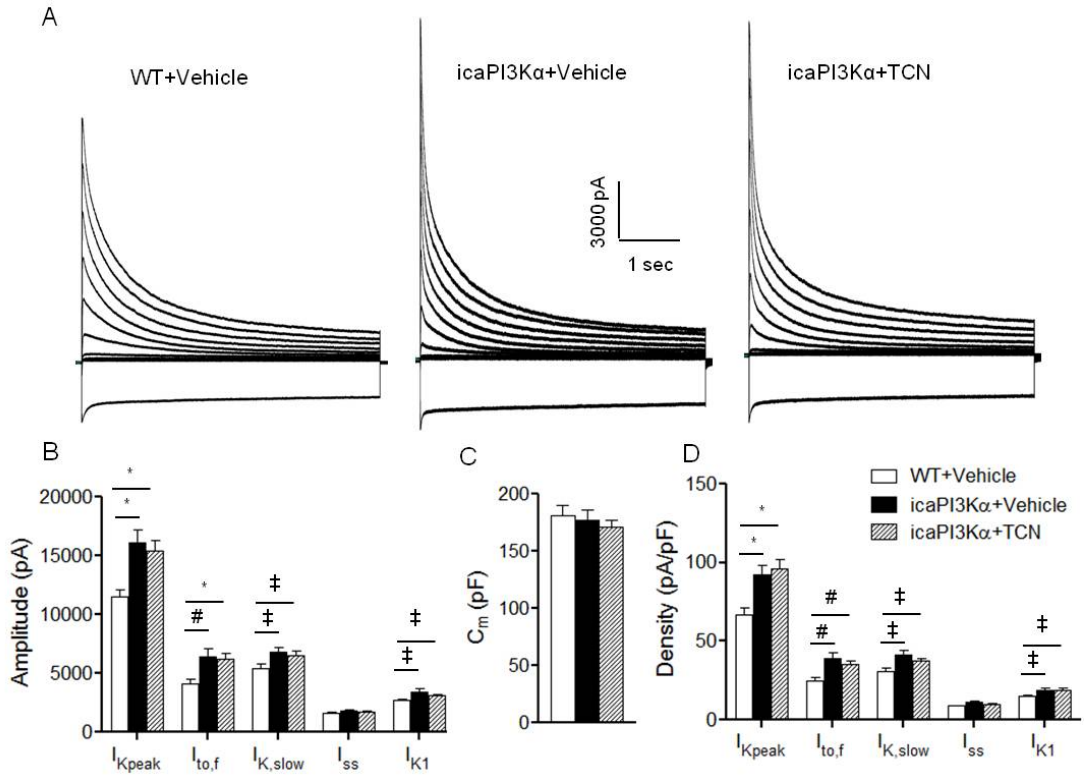

Figure 3. 14 Short-term activation of cardiac PI3Kα signaling upregulates repolarizing K+ currents in an Akt-independent manner.

(A) Representative whole-cell K^+ currents were recorded from LV myocytes isolated from WT+Vehicle, icaPI3Kα+Vehicle and icaPI3Kα+TCN animals. (B) Mean ± SEM $I_{K,peak}$, $I_{to,f}$ and $I_{K,slow}$ amplitudes in icaPI3Kα+Vehicle (n=24) were markedly increased compared with WT+Vehicle (n=33) LV myocytes; the increases in K^+ current amplitudes ($I_{K,peak}$, $I_{to,f}$, $I_{K,slow}$ and I_{K1}) in icaPI3Kα LV myocytes persisted with TCN treatment (n=21). (C) Mean ± SEM C_m values were similar in WT+Vehicle, icaPI3Kα+Vehicle and icaPI3Kα+TCN LV myocytes. (D) Normalization of current amplitudes for differences in cell size (C_m) revealed that mean ± SEM $I_{K,peak}$, $I_{to,f}$, $I_{K,slow}$ and I_{K1} densities were significantly ($^{‡}P<0.05$, $^{\#}P<0.01$, $^{*}P<0.001$) higher in icaPI3Kα+vehicle, than in WT+Vehicle, LV myocytes. The repolarizing K^+ current densities in icaPI3Kα LV myocytes remained increased despite the inhibition of Akt activation.

3.4 Transcriptional Upregulation of Ion Channel Subunits by Enhanced PI3Kα Signaling is Akt-Independent

Quantitative RT-PCR experiments were conducted to examine ion channel subunit expression levels in the LV of WT+Vehicle, icaPI3Kα+Vehicle and icaPI3Kα+TCN mice. Consistent with the observed increases in K^+ current amplitudes, the expression levels of the $I_{to,f}$ channel subunit, Kv4.2, the $I_{K,slow1}$ pore-forming subunit Kv1.5, the putative I_{ss} subunit, TASK1, and the I_{K1} channel subunit, Kir2.1, were also higher in icaPI3Kα+Vehicle, compared to WT+Vehicle, LV (**Figures 3.15A-C**). In addition, the transcript expression of voltage-gated Na^+ and Ca^{2+} channel subunits was increased in the LV of icaPI3Kα+Vehicle, than in WT+Vehicle, animals (Figure **3.15D**). The transcriptional upregulation of these ion channel subunits by enhanced PI3Kα signaling, however, was not affected by TCN treatment, revealing that PI3Kα-mediated transcriptional upregulatioin of ion channel subunits is independent of Akt activation.

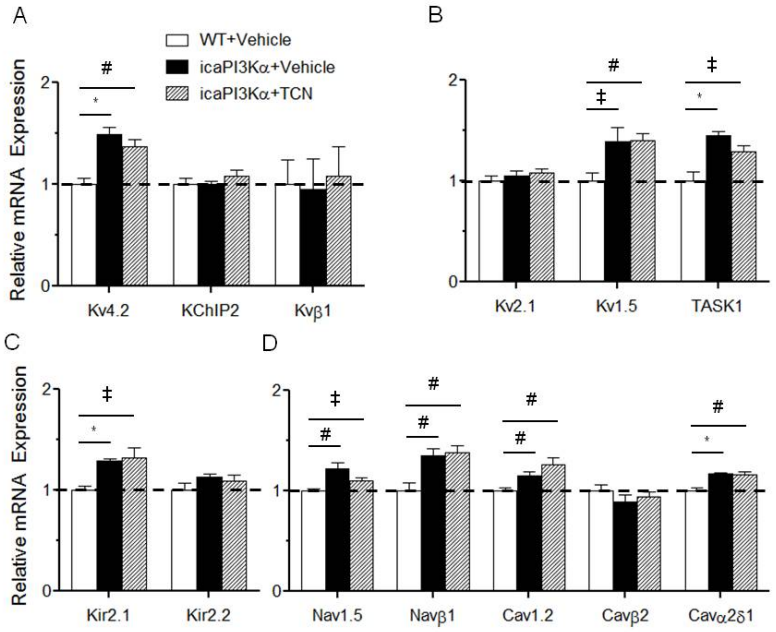

Figure 3.15 Transcriptional upregulation of ion channel subunits with activation of PI3Kα signaling is independent of Akt.

Channel subunit transcript expression levels were measured in individual LV samples from WT+Vehicle, icaPI3Kα+Vehicle and icaPI3Kα+TCN LV (n=6 in each group), normalized to *Hprt* in the same sample and to the mean value of the WT+Vehicle control LV samples. The expression levels of the transcripts encoding several K^+ (A,B,C), as well as Na^+ and Ca^{2+} (D), channel subunits were increased significantly ($^{‡}P<0.05$, $^{*}P<0.001$) in icaPI3Kα+Vehicle, compared with WT+Vehicle, LV. In addition, the increases in the expression of the channel subunit transcripts with PI3Kα induction were not affected by inhibition of Akt.

3.4 Discussion

Aerobic exercise training helps to preserve cardiac function, reducing detrimental ventricular remodeling and improving survival in animal models of heart failure (McMullen *et al.*, 2007) and pressure/volume overload-induced LV hypertrophy (McMullen *et al.*, 2003; Lachance *et al.*, 2009). Several mechanisms have been proposed to account for the beneficial effects of exercise, including increased myocardial perfusion (Hambrecht *et al.*, 2000b), balanced autonomic nervous input (Coats *et al.*, 1992), improved myocardial energy metabolism (O'Neill *et al.*, 2007), reduced myocardial fibrosis (McMullen *et al.*, 2003), and/or calcium handling (Medeiros *et al.*, 2008). The results here demonstrate that exercise training, as well as the resulting increased PI3Kα signaling, also maintain normal electrical function through the transcriptional upregulation of ion channels in proportion to the increase in myocyte size.

The phosphoinositide-3-kinases (PI3Ks) are a family of enzymes with both protein and lipid kinase activity that are known to be involved in many cellular processes (Cantley, 2002). PI3Kα is a heterodimeric lipid kinase with a 110 kDa catalytic subunit (p110α) and an 85 kDa regulatory subunit (p85) (Cantley, 2002) that is activated upon stimulation of insulin or growth factor receptor-coupled tyrosine kinases (Cantley, 2002). Activation of PI3Kα catalyzes the conversion of the membrane lipid PIP2 to PIP3, which in turn, recruits and activates downstream signaling cascades, most notably those involving Akt which link PI3Kα to myocyte growth, hypertrophy, proliferation, survival, metabolism, aging and regeneration (Sussman *et al.*, 2011). The results of the experiments detailed here, however, surprisingly revealed that Akt, despite its ubiquitous importance across a wide range of cellular processes, is not required for PI3Kα-mediated myocardial electrical remodeling.

3.4.1 Physiological ventricular hypertrophy in swim-trained and caPI3Kα mice

Ventricular hypertrophy is clearly evident in swim-trained and in caPI3Kα mice. Consistent with the increase in left ventricular mass, membrane capacitance measurements demonstrated that LV myocytes from swim-trained and caPI3Kα animals are significantly (P<0.001) larger than control LV myocytes. Direct histological examination revealed increased LV myocyte cross-sectional area in swim-trained, compared with control, animals without interstitial fibrosis (**Figure 1B**). The expression of ANF, a molecular marker of pathological hypertrophy (McMullen & Jennings, 2007), is not increased in swim-trained or caPI3Kα LV. Consistent with previous reports (McMullen *et al.*, 2003; McMullen *et al.*, 2007), therefore, swim-training and cardiac-specific activation of PI3Kα signaling result in physiological hypertrophy.

3.4.2 Upregulation of ionic currents in swim-trained and caPI3Kα LV myocytes

The amplitudes of the repolarizing Kv ($I_{to,f}$, $I_{K,slow}$ and I_{ss}) and Kir (I_{K1}) currents are markedly increased in LV myocytes from both swim-trained and caPI3Kα mice. Importantly, the time and voltage-dependent properties of the currents are indistinguishable from control LV myocytes, suggesting that the higher amplitudes of the K^+ currents in swim-trained and caPI3Kα LV myocytes reflect increases in the numbers of functional K^+ channels, rather than changes in channel properties. The increases in K^+ current amplitudes are sufficient to compensate for the cellular hypertrophy, normalizing K^+ current densities in swim-trained and caPI3Kα myocytes to levels similar to controls. In fact, I_{ss} and I_{K1} densities are actually higher in LV myocytes from both swim-trained and caPI3Kα animals. In caPI3Kα LV myocytes, $I_{K,slow}$ densities are also higher than in WT cells. The results here clearly suggest that the observed upregulation of K^+ currents with exercise training is directly related to the activation of PI3Kα signaling pathways. Establishment of this direct link warrants further investigation and would be of direct

interest to the development of therapeutic strategies aimed at normalizing/increasing K^+ channel expression in pathological hypertrophy.

Although increased outward K^+ current densities can lead to abbreviated myocardial action potential durations and shortened QT intervals (Brugada *et al.*, 2004; Priori *et al.*, 2005), no differences in action potential durations or QT intervals were observed in swim-trained or caPI3Kα, compared with control myocytes/animals. The normalization of action potential waveform and QT intervals likely reflects the fact that inward Ca^{2+} current densities are also increased in physiological hypertrophy, in parallel with the increases in repolarizing K^+ currents.

3.4.3 Molecular mechanisms underlying the homeostatic regulation of myocardial excitability

The results presented here demonstrate that the observed increases in myocardial membrane currents in physiological hypertrophy primarily reflect increased expression of the transcripts encoding the underlying ion channel subunits. One exception to this generality is *Kcna5*, which encodes Kv1.5, and underlies mouse ventricular $I_{K,slow1}$ (London *et al.*, 2001b); *Kcna5* transcript expression was not measurably increased in swim-trained or caPI3Kα LV. It is possible that increased expression of Kv2.1, which underlies $I_{K,slow2}$ (Xu *et al.*, 1999a), alone is sufficient to account for the increase in $I_{K,slow}$ amplitudes in swim-trained and caPI3Kα LV myocytes. It is also possible that Kv1.5 protein expression is increased by post-transcriptional mechanisms and contributes to the observed increases in $I_{K,slow}$ amplitudes. The lack of a reliable anti-Kv1.5 specific antibody precludes a direct test of this hypothesis. Finally, additional post-transcriptional as well as post-translational mechanisms may contribute to the observed increases in

functional channel expression (i.e., increases in current amplitudes and densities) with physiological hypertrophy.

3.4.4 Exercise training-induced electrical remodeling is independent of cellular hypertrophy and Akt1

As reported previously, the results here demonstrate that genetic deletion of Akt1 disrupts hypertrophic growth in response to chronic exercise training (**Figure 3.10B,C**). The observation that repolarizing K^+ current amplitudes and the expression of multiple ion channel subunits are upregulated in swim-trained Akt1$^{-/-}$ animals suggests that the "electrical remodeling" induced by exercise training does not require the presence of Akt1 and is, therefore, also completely disconnected from cellular hypertrophy. The disconnection between electrical remodeling and the global increases in RNA synthesis accompanying exercise training-induced hypertrophy (Hannan *et al.*, 2003) implies a unique regulatory mechanism coordinating myocardial ion channel gene expression, independent of the general transcriptional machinery that is robustly activated in response to hypertrophic stimuli such as exercise training.

Although it would certainly be of interest to utilize a similar experimental strategy to determine if Akt2, the only other Akt robustly expressed in the myocardium (Muslin & DeBosch, 2006), is required for exercise training-induced ion channel upregulation, it has been reported previously that adult Akt2$^{-/-}$ animals have severe hyperglycemia(Cho *et al.*, 2001a) and evidence of diabetic cardiomyopathy (Etzion *et al.*, 2010). Several previous studies have demonstrated alterations in ionic currents and ion channel subunit expression levels in rodent models of diabetic cardiomyopathy (Qin *et al.*, 2001; Marionneau *et al.*, 2008a). The diabetic phenotype of the Akt2$^{-/-}$ mice, therefore, seems likely to complicate the quantification of ionic currents and ion channel subunit

expression levels at baseline and with exercises, compromising the interpretation of experimental results. As an alternative approach, we examined the effects of an inhibitor, triciribine (TCN), which blocks both Akt1 and Akt2 in parallel with increased expression of PI3Kα.

3.4.5 Increased PI3Kα activities upregulates K^+ current and ion channel subunit expression independent of Akt signaling

The experiments conducted using the tet-off inducible caPI3Kα mouse model demonstrate that short-term activation of cardiac PI3Kα signaling also upregulates K^+ currents and the expression of ion channel subunit transcripts. Inhibition of cardiac Akt (both Akt1 and Akt2) activation in the context of enhanced PI3Kα signaling did not prevent the upregulation of myocardial K^+ currents and ion channel subunit transcripts, suggesting that the impact of PI3Kα signaling on myocardial "electrical remodeling" is independent of Akt signaling. These results extend the findings obtained in the $Akt1^{-/-}$ exercise training experiments and suggest that both Akt1 and Akt2 are dispensable for PI3Kα-mediated electrical remodeling. The pharmacological approach of simultaneously blocking both Akt1 and Akt2 avoids several potential caveats in the interpretation of data obtained from animals lacking Akt1 or Akt2. First, this approach ruled out the role of Akt2 in PI3Kα-mediated electrical remodeling without using $Akt2^{-/-}$ animals, for which, as discussed above, the quantification of ionic currents and channel subunit expression might be complicated by the presence of the diabetic phenotype. Secondly, the interpretation of negative results obtained from either $Akt1^{-/-}$ or $Akt2^{-/-}$ animals requires taking into consideration the potential functional redundancy between Akt1 and Akt2. Theoretically, using animals lacking both Akt1 and Akt2 ($Akt1^{-/-}/Akt2^{-/-}$) might solve this issue. This, however, is not feasible as mice lacking both Akt1 and Akt2 die shortly after birth (Peng *et al.*, 2003).

Interestingly, it has been shown that PI3Kα activation is also critical in mediating myocardial metabolic remodeling in physiological hypertrophy, including increased capacity to oxidize fatty acids/glucose and increased mitochondrial biogenesis, and that this metabolic remodeling mediated by PI3Kα is also Akt-independent (O'Neill *et al.*, 2007). Taken together, these results demonstrate that PI3Kα signaling exerts distinct biological effects on the myocardium through divergent downstream pathways: Akt1-dependent physiological cardiac growth, Akt2-dependent insulin-sensitization and cellular survival, as well as Akt-independent effects on metabolic and electrical remodeling. The signaling mechanisms linking PI3Kα to metabolic and electrical remodeling have not been defined, although it has been suggested that PKCλ/ζ could be the potential downstream mediator that is required for PI3Kα-dependent metabolic remodeling (O'Neill *et al.*, 2007). Interestingly, PI3Kα has also been shown previously to modulate the activities of a number of transcription factors, such as FOXO (Philip-Couderc *et al.*, 2008) or NFκB (Brunet *et al.*, 1999; Panama *et al.*, 2011), that could potentially affect cardiac ion channel expression. Further studies are required to explore these hypotheses directly and to identify the downstream signaling effectors that mediate myocardial electrical remodeling in response to PI3Kα activation.

3.4.6 Conclusions

Taken together, the results presented here demonstrate that physiological cardiac hypertrophy, induced by exercise-training or transgenic activation of PI3Kα (a critical regulator of exercise-induced heart growth) signaling, is associated with increased expression of myocardial ion channel subunits in proportion to increased myocyte size and the global increases in RNA and protein expression. The resulting homeostatic regulation of myocardial electrical excitability clearly distinguishes physiological from pathological cardiac hypertrophy, which is associated with marked reductions in the

densities of repolarizing K^+ currents, action potential prolongation and increased risk of arrhythmias (McIntyre & Fry, 1997; Haider *et al.*, 1998; Marionneau *et al.*, 2008b). The experiments here also demonstrate that the transcriptional upregulation of ion channel subunits (the “electrical remodeling”) induced by enhanced PI3Kα signaling, unlike hypertrophic growth or insulin sensitization, is Akt-independent. These observations suggest a multifaceted role of PI3Kα signaling in regulating myocardial functioning through distinct downstream signaling mediators. In addition, the studies here suggest that activating PI3Kα signaling pathways might be a useful therapeutic strategy to normalize the expression of K^+ currents in pathological cardiac hypertrophy and in other cardiac diseases associated with reduced K^+ current densities and impaired repolarization, thereby reducing the risk of life-threatening arrhythmias. Additional studies are needed to explore directly the hypothesis that activation of PI3Kα signaling pathways will impact the incidence of arrhythmias and the risk of sudden cardiac death in pathological hypertrophy.

Chapter 4: Enhanced Cardiac PI3Kα Signaling Mitigates Arrhythmogenic Electrical Remodeling in Pathological Hypertrophy and Heart Failure

4.1 Abstract

Aims: Cardiac hypertrophy and heart failure are associated with QT prolongation and lethal ventricular arrhythmias, resulting from decreased K^+ current densities and impaired repolarization. Recent studies in mouse models of physiological cardiac hypertrophy revealed that increased phosphoinositide-3-kinase-α (PI3Kα) signaling results in the upregulation of K^+ channels and the normalization of ventricular repolarization. The experiments here were undertaken to test the hypothesis that increased PI3Kα signaling will counteract the adverse electrophysiological remodeling associated with pathological hypertrophy and heart failure.

Methods and Results: In contrast to wild-type mice, left ventricular (LV) hypertrophy, induced by transverse aortic constriction (TAC), did not result in prolongation of ventricular action potentials or QT intervals in mice with cardiac-specific expression of constitutively active PI3Kα (caPI3Kα). Indeed, repolarizing K^+ currents and K^+ channel subunit transcripts were *increased* in caPI3Kα+TAC LV myocytes in proportion to the TAC-induced cellular hypertrophy. Congestive heart failure in a transgenic model of dilated cardiomyopathy model is accompanied by prolonged QT intervals and ventricular action potentials, reduced K^+ currents and K^+ channel transcripts. Increased PI3Kα signaling, but not renin-angiotensin system blockade, in this model also results in increased K^+ currents and improved ventricular repolarization.

Conclusion: In the setting of pathological hypertrophy or heart failure, enhanced PI3Kα signaling results in the upregulation of K^+ channel subunits, normalization of K^+ current densities and preserved ventricular function. Augmentation of PI3Kα signaling, therefore, may be a useful and unique strategy to protect against the increased risk of ventricular arrhythmias and sudden death associated with cardiomyopathy.

4.2 Introduction

Left ventricular (LV) dysfunction is associated with increased risk of life-threatening arrhythmias (Tomaselli *et al.*, 1994; Haider *et al.*, 1998). Sudden cardiac death, presumably due to lethal ventricular arrhythmias, accounts for approximately 50% of deaths in individuals with heart failure (Tomaselli *et al.*, 1994). Electrical remodeling in cardiac hypertrophy (Mayet *et al.*, 1996; McIntyre & Fry, 1997) and heart failure (Beuckelmann *et al.*, 1993) results, at least in part, from reductions in the densities of repolarizing K^+ currents (Beuckelmann *et al.*, 1993; Marionneau *et al.*, 2008b), which can lead to action potential prolongation and increased dispersion of repolarization, both of which are arrhythmogenic. Despite advances in pharmacological and device therapies for LV dysfunction, none purposefully targets fundamental arrhythmia mechanisms at the level of ion channel remodeling (Jessup & Brozena, 2003).

It was recently demonstrated that physiological hypertrophy, induced by exercise training or by cardiac-specific expression of constitutively active PI3Kα (caPI3Kα), is associated with transcriptional upregulation of the subunits encoding repolarizing K^+ channels (Yang *et al.*, 2010). This upregulation results in increased repolarizing K^+ current amplitudes in proportion to the cellular hypertrophy, thereby normalizing ventricular K^+ current densities, action potential waveforms, and QT intervals. These observations suggest that activating the PI3Kα signaling pathway could be a therapeutic strategy in pathological cardiac hypertrophy and heart failure to maintain K^+ current densities and reduce the risk of life-threatening ventricular arrhythmias.

To test this hypothesis, the impact of increased PI3Kα signaling was examined in: (1) a mouse model of non-failing, pressure overload-induced pathological left ventricular hypertrophy (LVH), produced by transverse aortic constriction (TAC) (Marionneau *et al.*,

2008b); and, (2) a transgenic mouse model (TG9) of dilated cardiomyopathy and consequent congestive heart failure (Buerger *et al.*, 2006; McMullen *et al.*, 2007). These experiments revealed that enhanced PI3Kα signaling results in transcriptional upregulation of repolarizing K^+ channel subunits, leading to increased K^+ current amplitudes, thereby normalizing ventricular K^+ current densities, action potential waveforms and functioning.

4.3 Results

4.3.1 Increased PI3Kα signaling prevents the ECG changes associated with pressure-overload induced LVH

Similar to wild-type (WT) mice (Marionneau *et al.*, 2008b), TAC produced LVH in caPI3Kα mice (McMullen *et al.*, 2007). The mean ± SEM left ventricular mass to tibia length ratio (LVM/TL), for example, was significantly (P<0.001) higher (by 29 ± 6 %) in caPI3Kα+TAC, than in control caPI3Kα (**Figure 4.1A**), animals. In addition, expression of ANF, a marker of pathological hypertrophy, was increased significantly (P<0.01) in caPI3Kα+TAC, compared with control caPI3Kα, LV (**Figure 4.1B**). Interestingly, ECG recordings (**Figure 4.1C**) revealed that the morphologies of the QRS complexes, P, J and T waves (**Figure 4.1C**), as well as the durations of the RR, PR, QRS, QT and corrected QT (QTc) intervals (**Figure 4.1D**), were indistinguishable in caPI3Kα control and caPI3Kα+TAC animals. These observations contrast markedly with the ECG abnormalities (prolonged QTc intervals and flattened J waves) observed in WT mice with TAC-induced LVH (**Figure 4.1 inset** (Marionneau *et al.*, 2008b)). In spite of the marked increases in LV mass and ANF expression, the ECG changes were not observed in caPI3Kα animals with TAC (**Figure 4.1 C,D**).

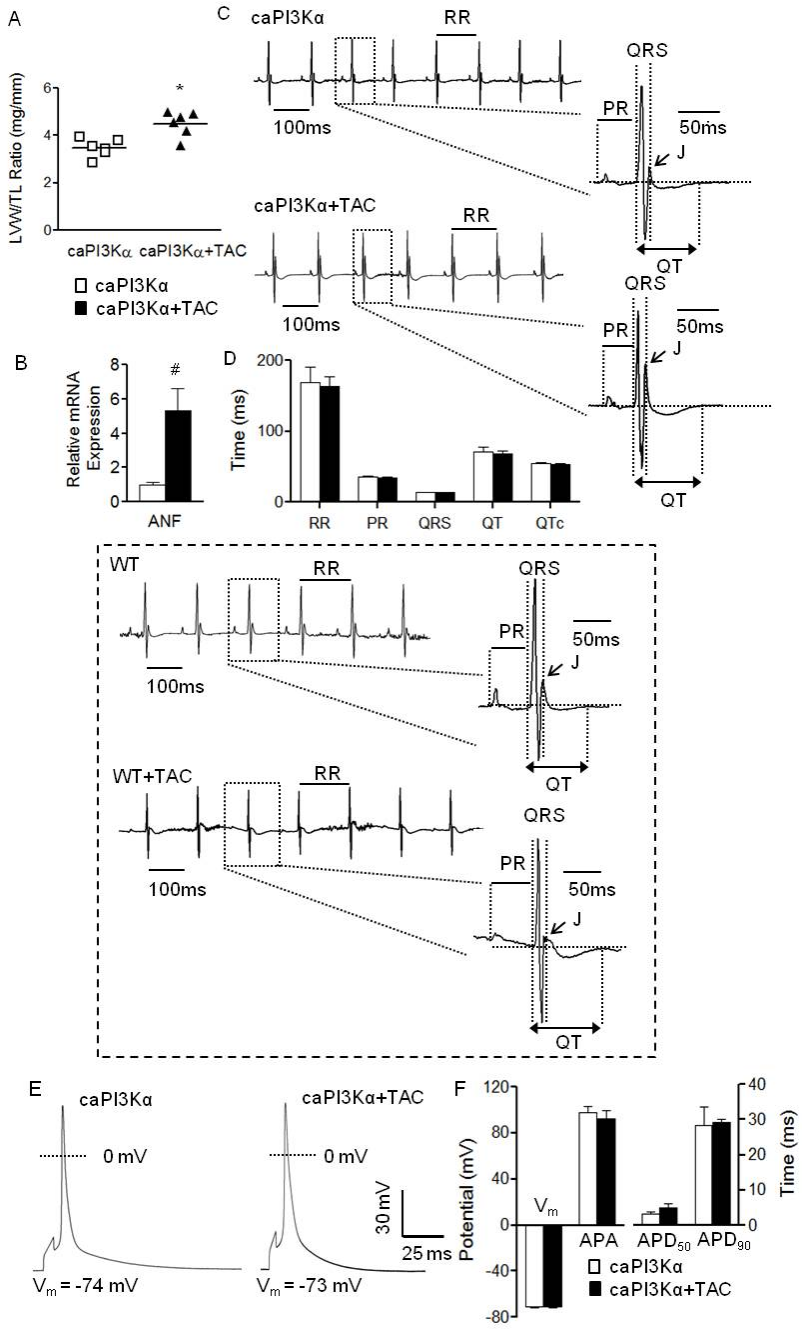

Figure 4. 1 Increased PI3Kα signaling prevents ECG and action potential waveform abnormalities associated with pressure overload-induced LVH following transverse aortic constriction (TAC).

(A) LV mass/tibia length (LVM/TL) ratios were determined in caPI3Kα control (n=6) and caPI3Kα+TAC (n=6) animals; individual and mean ± SEM values ($^{*}P$<0.001) are plotted. (B) Mean ± SEM (n=6) relative transcript expression level of atrial natriuretic factor (ANF) is significantly ($^{\#}P$<0.01) higher in caPI3Kα+TAC than in caPI3Kα control LV. (C) Representative ECG (lead II) waveforms from caPI3Kα mice with and without TAC are illustrated; individual beats are shown on an expanded timescale on the right in each panel. (D) Mean ± SEM RR, PR, QRS, QT and QTc intervals measured in caPI3Kα+TAC (n=6) and caPI3Kα control (n=6) animals were not significantly different. Inset: In contrast to the findings in caPI3Kα animals, and as reported previously,(Marionneau *et al.*, 2008b) TAC in WT animals results in J point suppression and QT prolongation. (E) Action potential waveforms in LV myocytes from caPI3Kα control and caPI3Kα+TAC animals are indistinguishable. (F) No significant differences in mean ± SEM resting membrane potentials (V_m), action potential amplitudes (APA) or action potential durations at 50% (APD_{50}) and 90% (APD_{90}) repolarization were observed in caPI3Kα control (n=10) and caPI3Kα+TAC (n=9) LV myocytes.

4.3.2 Increased PI3Kα signaling prevents TAC-induced action potential prolongation

In WT mice, TAC-induced LVH results in impaired repolarization and prolonged action potential durations (Marionneau *et al.*, 2008b). The observation that ECG waveforms in caPI3Kα animals were not measurably affected by TAC (**Figure 4.1 C,D**) suggests that augmented PI3Kα signaling abrogates the detrimental effects of pressure overload-induced LVH on ventricular repolarization. To test this hypothesis directly, current clamp recordings were obtained from LV myocytes isolated from caPI3Kα+TAC and caPI3Kα control animals. As shown in **Figure 4.1E**, action potential waveforms in caPI3Kα+TAC and caPI3Kα control LV myocytes were indistinguishable. Additionally, no significant differences in mean resting membrane potentials, action potential amplitudes or action potential durations at 50% (APD_{50}) and 90% (APD_{90}) repolarization in caPI3Kα+TAC and caPI3Kα control LV myocytes were observed (**Figure 4.1F**).

4.3.3 Repolarizing K^+ current amplitudes are increased in caPI3Kα+TAC LV myocytes

Studies conducted on experimental models of pressure overload-induced LVH have consistently reported reductions in repolarizing LV K^+ current densities (Volk *et al.*, 2001b; Marionneau *et al.*, 2008b), resulting in impaired repolarization (prolonged ventricular APDs and QT/QTc intervals) (Marionneau *et al.*, 2008b) and predisposing to life-threatening ventricular arrhythmias (McIntyre & Fry, 1997). The finding that no electrical abnormalities were evident in caPI3Kα animals with pressure overload-induced LVH suggests that increased PI3Kα signaling results in upregulation of K^+ currents, in parallel with the increase in myocyte size, and the normalization of K^+ current densities. To explore this hypothesis, voltage-clamp recordings were obtained from LV apex myocytes isolated from caPI3Kα control and caPI3Kα+TAC animals. As illustrated in

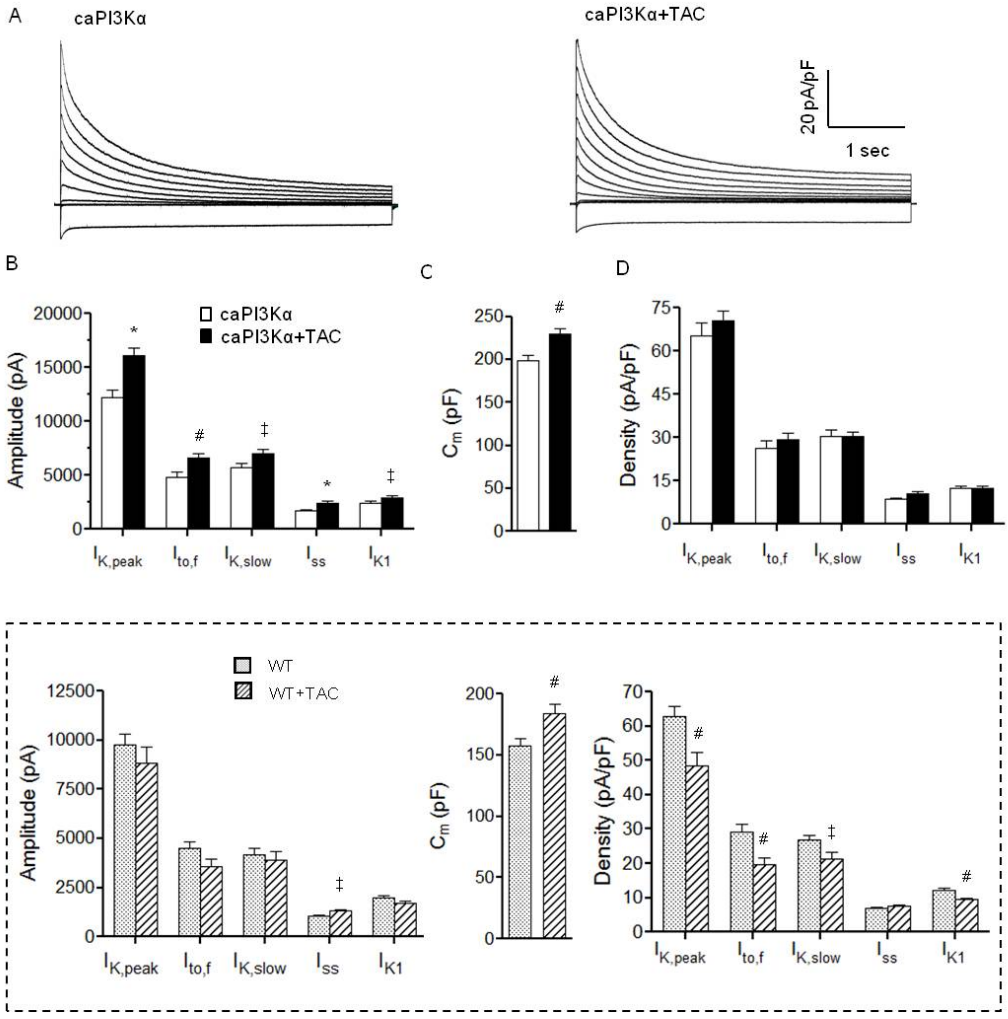

Figure 4. 2 Repolarizing K^+ current amplitudes are increased and K^+ current densities are normalized in caPI3Kα+TAC LV myocytes.

(A) Representative whole-cell K^+ currents recorded from myocytes isolated from the LV apex of caPI3Kα control and caPI3Kα+TAC mice. Currents were evoked in response to (4.5 s) voltage steps to test potentials between -120 and +40 mV from a holding potential (HP) of -70 mV. (B) The mean ± SEM amplitudes of the K^+ currents are significantly ($^{‡}P$<0.05, $^{\#}P$<0.01,$^{*}P$<0.001) higher in caPI3Kα+TAC, compared with caPI3Kα control, LV myocytes. (C) A significant ($^{\#}P$<0.01) increase in mean ± SEM whole-cell membrane capacitance (C_m), consistent with cellular hypertrophy, is also evident in caPI3K+TAC LV myocytes. (D) Normalizing current amplitudes for differences in cell size (C_m) revealed that mean ± SEM K^+ current densities in LV myocytes from caPI3Kα+TAC and caPI3Kα control animals are indistinguishable. Inset: As reported previously,(Marionneau *et al.*, 2008b) $I_{K,peak}$, $I_{to,f}$, $I_{K,slow}$ and I_{K1}amplitudes are not increased in WT LV myocytes with TAC and current densities are decreased significantly ($^{‡}P$<0.05, $^{\#}P$<0.01).

Supplemental Figure 4. 1 Kv and Kir Currents in caPI3Kα, caPI3Kα+TAC, WT and WT+TAC LV Myocytes.

LV Cells		C_m (pF)	$I_{K,peak}$	$I_{to,f}$	$I_{K,slow}$	I_{ss}	I_{K1}
caPI3Kα		198 ± 7					
(n=31)	τ_d (ms)		—	115 ± 12	1067 ± 41	—	—
	Amplitude (pA)		12261 ± 668	4841 ± 434	5746 ± 359	1674 ± 122	-2428 ± 152
	Density (pA/pF)		65.3 ± 4.5	26.2 ± 2.6	30.5 ± 2.3	8.6 ± 0.6	-12.4 ± 0.8
caPI3Kα +TAC		230 ± 6$^{\#}$					
(n=45)	τ_d (ms)		—	106 ± 10	1003 ± 30	—	—
	Amplitude (pA)		16165 ± 681*	6611 ± 422$^{\#}$	7035 ± 379‡	2458 ± 125*	-2936 ± 160‡
	Density (pA/pF)		70.6 ± 3.2	29.4 ± 2.1	30.4 ± 1.7	10.7 ± 0.6	-12.5 ± 0.6
WT		158 ± 6					
(n=26)	τ_d (ms)		—	76 ± 6	996 ± 29	—	—
	Amplitude (pA)		9782 ± 534	4524 ± 304	4202 ± 278	1056 ± 70	-1959 ± 111
	Density (pA/pF)		63 ± 3.1	29.3 ± 2.0	26.8 ± 1.4	6.8 ± 0.4	-12.2 ± 0.6
WT+TAC		184 ± 8$^{\#}$					
(n=18)	τ_d (ms)		—	94 ± 9	1087 ± 47	—	—
	Amplitude (pA)		8842 ± 794	3549 ± 424	3922 ± 407	1307 ± 58‡	-1717 ± 97
	Density (pA/pF)		48.5 ± 4.0$^{\#}$	19.6 ± 2.3$^{\#}$	21.3 ± 2.0‡	7.6 ± 0.5	-9.4 ± 0.5$^{\#}$

* All values are means ± SEM. Kv and Kir current amplitudes/densities reported here were determined at +40 mV and -120mV, respectively. Measured current amplitudes/densities in caPI3Kα+TAC and control caPI3Kα LV myocytes or WT and WT+TAC LV myocytes were compared. For each of these comparisons, values that are significantly (‡ P<0.05, $^{\#}$$P$<0.01, *$P$<0.001) different are indicated. Kv indicates voltage-gated K^+ currents; Kir, inwardly rectifying K^+ currents; TAC, transverse aortic constriction; C_m, cell membrane capacitance.

Figure 4.2, these experiments revealed that the amplitudes of the peak ($I_{K,peak}$) outward voltage-gated (Kv) and the inwardly rectifying (Kir) K^+ currents were significantly higher in caPI3Kα+TAC, compared with caPI3Kα control, LV myocytes (P<0.05; **Figure 4.2B**). Kinetic analyses of the decay phases of the outward K^+ currents revealed that the amplitudes of the individual Kv current components, $I_{to,f}$, $I_{K,slow}$ and I_{ss}, were higher in caPI3Kα+TAC LV myocytes (**Figure 4.2B**). There were no measurable differences in the time- or the voltage-dependent properties of the Kv currents in cells from caPI3Kα control and caPI3Kα+TAC mice (**Supplementary Table 4.1**). Consistent with TAC-induced LVH, cellular hypertrophy was clearly evident in caPI3Kα+TAC LV myocytes (**Figure 4.2C**); the mean whole-cell membrane capacitance (C_m) was significantly (P<0.01) higher in caPI3Kα+TAC, than in caPI3Kα control, LV cells (**Figure 4.2C**). Normalization of the Kv and Kir (I_{K1}) current amplitudes (**Figure 4.2 B**) to the measured

C_m values (in the same cell) revealed that repolarizing K^+ current densities in caPI3Kα+TAC and caPI3Kα control LV cells were indistinguishable (**Figure 4.2 A,D**). These results are in striking contrast to observations in WT animals with TAC-induced LVH (Marionneau *et al.*, 2008b). Indeed, the amplitudes of the individual K^+ currents (except for I_{ss}) were not increased in WT cells in response to TAC and, when normalized to the increase in cell size (C_m), repolarizing K^+ current densities were actually decreased significantly in WT LV cells with TAC (**Figure 4.2** inset and **Supplementary Table 4.1**).

4.3.4 Transcriptional upregulation of K^+ channel subunits in caPI3Kα+TAC LV

Recent studies demonstrated that the increase in ventricular K^+ current amplitudes with enhanced myocardial PI3Kα signaling reflects the upregulation of the transcripts encoding the underlying K^+ channel subunits (Yang *et al.*, 2010). Subsequent experiments here, therefore, were aimed at determining if the observed increases in K^+ current amplitudes in caPI3Kα LV myocytes with TAC (**Figure 4.2B**) might also reflect increased expression of the transcripts encoding the various repolarizing K^+ channel subunits. As illustrated in **Figure 4.3**, quantitative RT-PCR revealed that the expression levels of the transcripts encoding $I_{to,f}$ channel pore-forming (α) subunits, *Kcnd2* (Kv4.2) (Guo *et al.*, 2005) and *Kcnd3* (Kv4.3) (Guo *et al.*, 2002), as well as the $I_{to,f}$ channel accessory subunit, *Kcnip2* (KChIP2) (Kuo *et al.*, 2001; Guo *et al.*, 2002), were increased significantly (P<0.05) in caPI3Kα+TAC, compared with caPI3Kα control, LV (**Figure 4.3A**). The expression levels of *Kcna5* (Kv1.5) and *Kcnb1* (Kv2.1), which encode $I_{K,slow1}$ (London *et al.*, 2001b) and $I_{K,slow2}$ (Xu *et al.*, 1999a), respectively, as well as of the K2P channel subunit *Kcnk3* (TASK1), which has been suggested to underlie I_{ss} in rat cardiomyocytes (Putzke *et al.*, 2007), were also increased significantly (P<0.05) in caPI3Kα+TAC LV (**Figure 4.3A**).

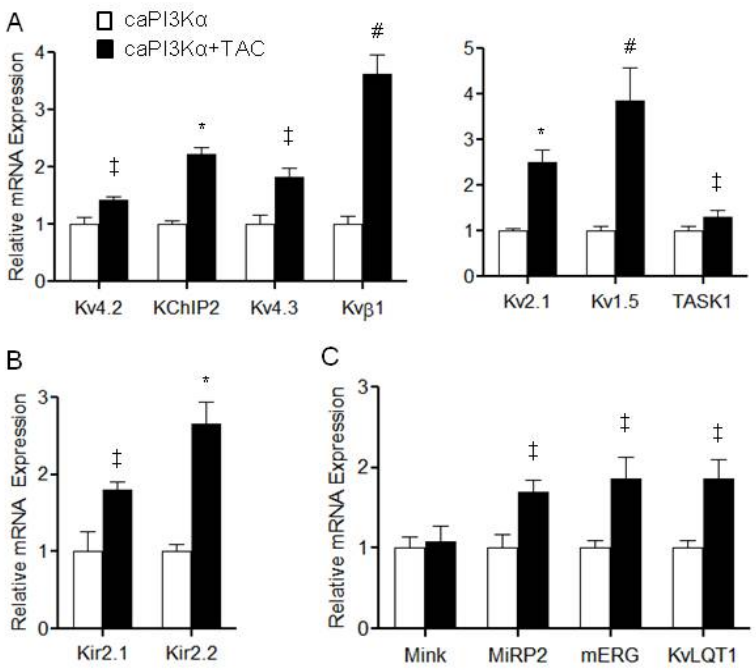

Figure 4. 3 Transcriptional upregulation of K+ channel subunits with TAC-induced LVH in caPI3Kα LV.

K^+ channel subunit transcript expression levels were measured in individual LV samples from caPI3Kα+TAC (n=6) and caPI3Kα control (n=6) LV, normalized to lamin A/C and subsequently to the mean value of the caPI3Kα control LV samples (A-C). The mean ± SEM relative expression levels of most of the K^+ channel subunit transcripts are significantly ($^{‡}P<0.05$,$^{\#}P<0.01$,$^{*}P<0.001$) higher in caPI3Kα+TAC, than in caPI3Kα control, LV.

Similarly, expression of the I_{K1} channel subunits *Kcnj2* (Kir2.1) and *Kcnj12* (Kir2.2) (Zaritsky *et al.*, 2001), as well as of *Kcnh2* (mERG) (Sanguinetti *et al.*, 1995) and *Kcnq1* (KvLQT1) (Sanguinetti *et al.*, 1996), the α subunits encoding the rapid and slow cardiac delayed rectifiers, I_{Kr} and I_{Ks}, in large mammals, were also increased in caPI3Kα+TAC LV (**Figure 4.3B,C**). In contrast with WT animals (Marionneau *et al.*, 2008b), therefore, the expression levels of a number of K^+ channel subunits were actually *upregulated* in caPI3Kα ventricles with TAC (see **4.4 Discussion**).

4.3.5 Increased PI3Kα signaling attenuates ECG and action potential abnormalities in a mouse model of dilated cardiomyopathy

To test the hypothesis that increased PI3Kα signaling might also ameliorate the electrical abnormalities in failing hearts, additional experiments were conducted using a transgenic mouse model of dilated cardiomyopathy (TG9) (Buerger *et al.*, 2006).

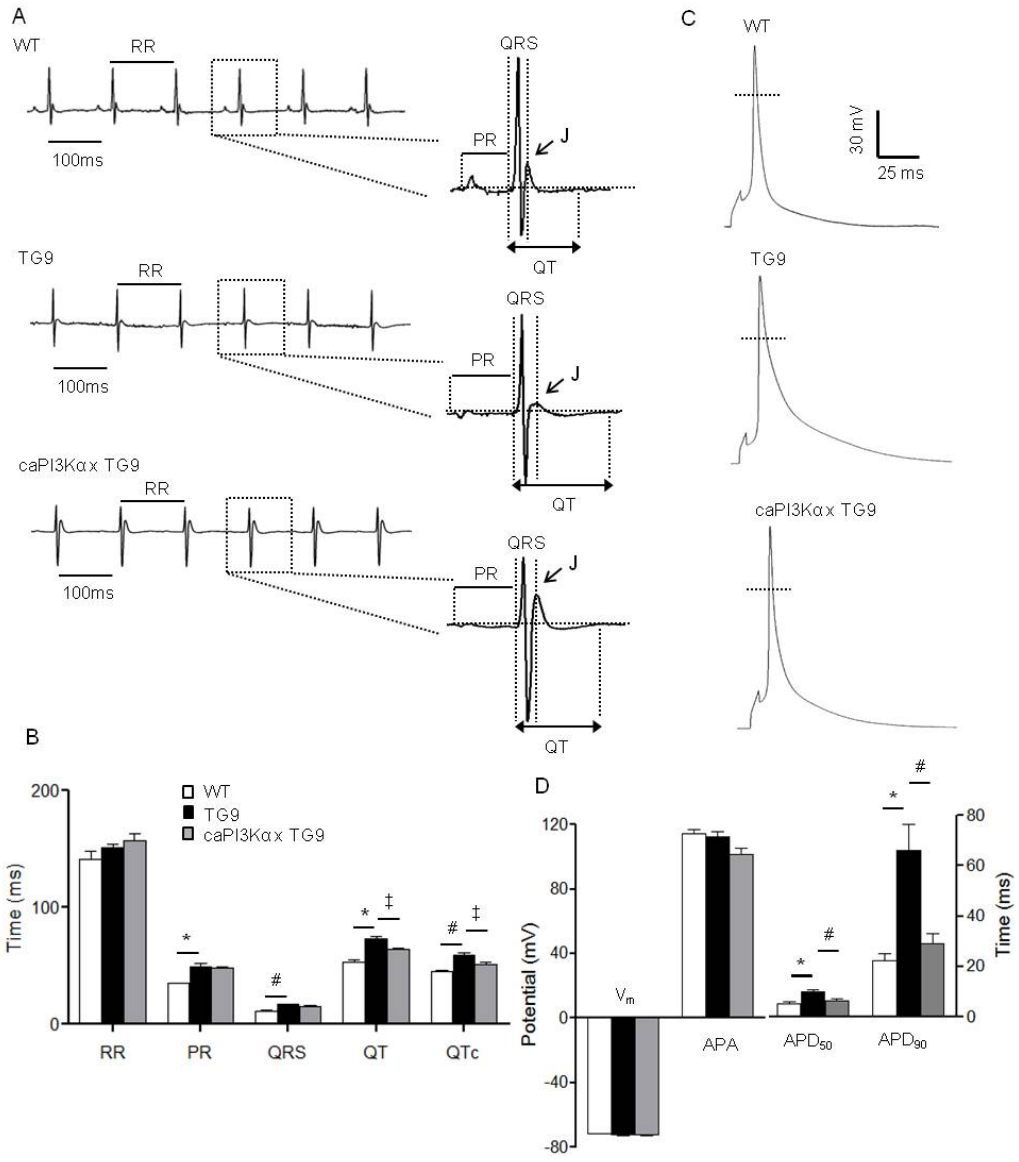

Figure 4. 4 Increased cardiac PI3Kα signaling attenuates the ECG and action potential abnormalities in a transgenic mouse model (TG9) of heart failure.

(A) Representative ECG waveforms from WT, TG9, and caPI3KαxTG9 mice. (B) Mean ± SEM PR, QRS, QT and QTc intervals are significantly ($^{\#}P$<0.01, $^{*}P$<0.001) prolonged in TG9 (n=6), compared with WT (n=6), animals. Interestingly, mean QT and QTc intervals in caPI3KαxTG9 mice are significantly ($^{\ddagger}P$<0.05) shorter than in TG9 mice. (C) Representative action potential waveforms recorded from LV myocytes isolated from WT, TG9 and caPI3KαxTG9 animals are shown. (D) Mean ± SEM APD_{50} and APD_{90} were significantly ($^{*}P$<0.001) longer in TG9 (n=10) than in WT (n=16) LV myocytes. Increased PI3Kα signaling significantly ($^{\#}P$<0.01) attenuates the APD prolongation (C,D) seen in TG9 LV myocytes.

As reported previously (Buerger *et al.*, 2006), TG9 mice develop progressive dilated cardiomyopathy, beginning at 6 weeks of age, and die of overt heart failure at 11-13 weeks. Surface ECG recordings revealed that QT and QTc intervals were significantly (*P*<0.001) prolonged in (10 week) TG9, compared with WT, mice (**Figure 4.4A,B**), indicating impaired ventricular repolarization, reminiscent of the electrical abnormalities observed in heart failure patients (Barr *et al.*, 1994) and in animal models of heart failure (Adamson & Vanoli, 2001; Rose *et al.*, 2005). Interestingly, PR and QRS intervals were prolonged in TG9, compared with WT, animals (**Figure 4.4A,B**) suggesting the presence of conduction abnormalities, which are also prevalent in patients with advanced heart failure (Akar & Tomaselli, 2005). To determine the impact of increased PI3Kα signaling on electrical function in heart failure, TG9 and caPI3Kα mice were crossed (caPI3KαxTG9). Surface ECG recordings from (10 week) caPI3KαxTG9 mice revealed that mean ± SEM QT and QTc intervals were abbreviated significantly (P<0.05) compared with TG9 mice (**Figure 4.4A,B**), albeit not identical to WT. In contrast, PR and QRS intervals were prolonged similarly in caPI3KαxTG9 and TG9 animals. (see **4.4 Discussion**). Consistent with the prolonged QT/QTc intervals (**Figure 4.4A,B**), current clamp recordings from LV apex myocytes isolated from TG9 animals revealed significantly (*P*<0.001) prolonged action potential durations (APD_{50} and APD_{90}), compared with recordings from WT LV apex myocytes (**Figure 4.4C,D**). The action potential prolongation evident in TG9 myocytes (**Figure 4.4C,D**), however, was attenuated significantly (*P*<0.01) in LV cells isolated from (caPI3KαxTG9) animals with increased caPI3Kα expression.

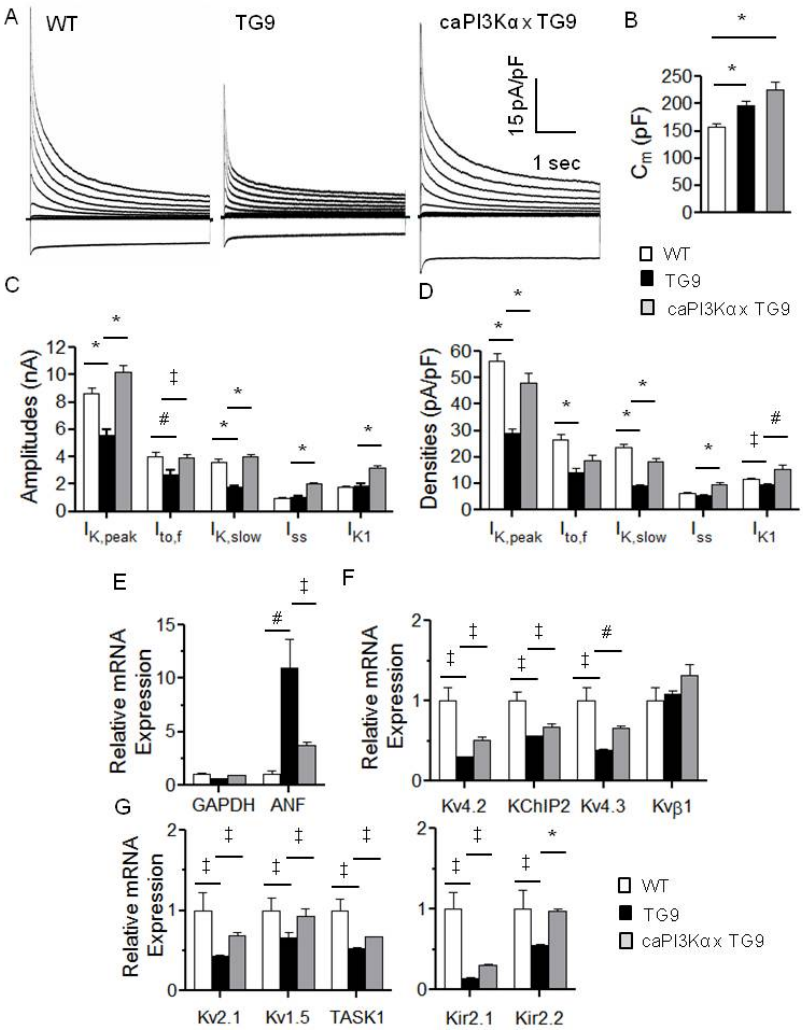

Figure 4. 5 Increased cardiac PI3Kα signaling in heart failure upregulates repolarizing K+ currents and the underlying K+ channel subunit transcripts.

(A) Representative whole-cell K^+ currents were recorded from LV myocytes isolated from WT, TG9 and caPI3KαxTG9 mice. (B) Mean ± SEM C_m values are significantly (P<0.001) higher in TG9 (n=21) and in caPI3KαxTG9 (n=32), than in WT (n=22), LV myocytes. (C) Mean ± SEM $I_{K,peak}$, $I_{to,f}$ and $I_{K,slow}$ amplitudes in TG9 (n=21) are markedly reduced compared with WT (n=22) LV myocytes, whereas mean ± SEM K^+ current amplitudes ($I_{K,peak}$, $I_{to,f}$, $I_{K,slow}$, I_{ss} and I_{K1}) are higher in caPI3KαxTG9, than in TG9, cells. (D) Normalization for differences in cell size (C_m) revealed that mean ± SEM $I_{K,peak}$, $I_{to,f}$, $I_{K,slow}$ and I_{K1} densities are significantly ($^{‡}P$<0.05, $^{*}P$<0.001) lower in TG9 (n=21), than in WT (n=22), LV myocytes, and that increasing PI3Kα signaling in TG9 myocytes results in significant ($^{\#}P$<0.01,$^{*}P$<0.001) increases in $I_{K,peak}$, $I_{K,slow}$, I_{ss} and I_{K1} densities. Atrial natriuretic factor (ANF) and K^+ channel subunit transcript expression levels were determined in individual LV samples from WT, TG9 and caPI3KαxTG9 LV, normalized to lamin A/C in the same sample and to the mean value of the WT control LV samples. As reported previously (Buerger *et al.*, 2006), ANF expression is increased ~10 fold in TG9 LV. The increase in ANF expression is blunted in the LV of caPI3KαxTG9 animals (E). The expression levels of the transcripts encoding several K^+ channel subunits (F,G) are reduced significantly ($^{‡}P$<0.05) in TG9, compared with WT, LV; the expression levels of many of these K^+ channel subunits, however, are increased ($^{‡}P$<0.05, $^{\#}P$<0.01,$^{*}P$<0.001) in caPI3KαxTG9, compared with TG9, LV.

4.3.6 Augmentation of PI3Kα signaling results in increased repolarizing K^+ currents in failing hearts

As might be expected based on observations in humans (Beuckelmann *et al.*, 1993) and in animal models of heart failure (Rose *et al.*, 2005; Petkova-Kirova *et al.*, 2006), voltage-clamp recordings revealed that $I_{K,peak}$ amplitudes were significantly (P<0.001) lower in TG9, compared with WT, LV myocytes (**Figure 4.5C**). The amplitudes of $I_{to,f}$ and $I_{K,slow}$ were also lower (P<0.001) in TG9 myocytes (**Figure 4.5C**); the time- and voltage-dependent properties of the ($I_{to,f}$ and $I_{K,slow}$) currents in TG9 and WT cells, however, were similar (**Supplemental Table 4.2**). The higher mean C_m (**Figure 4.5B**) is consistent with marked cellular hypertrophy in TG9, compared with WT, LV cells. Normalization of the K^+ current amplitudes (**Figure 4.5C**) to myocyte size (**Figure 4.5B**) revealed that repolarizing K^+ current densities, with the exception of I_{ss}, were significantly lower in TG9, than in WT, LV cells (**Figure 4.5A,D**). As also illustrated in **Figure 4.5C**, however, increased PI3Kα signaling resulted in significant (P<0.05) increases in the amplitudes of all of the repolarizing K^+ currents, $I_{to,f}$, $I_{K,slow}$, I_{ss} and I_{K1}, in TG9 LV myocytes. Normalizing the current amplitudes to measured C_m revealed that mean ± SEM $I_{K,peak}$, $I_{K,slow}$, I_{ss} and I_{K1} densities were actually *increased* (**Figure 4.5A,D**) in caPI3KαxTG9, compared to TG9, cells.

Additional experiments were carried out in TG9 animals treated with the ACE inhibitor, captopril, which has been shown to improve the cardiac function/survival in heart failure patients (Pfeffer *et al.*, 1992), as well as the survival of TG9 animals (Buerger *et al.*, 2006). These experiments, however, did not reveal measurable effects of renin-angiotensin system blockade on K^+ current densities or action potential waveforms (**Supplemental Figure 4.1**) in TG9 LV myocytes (see **4.4 Discussion**).

Supplemental Table 4. 1 Kv and Kir Currents in WT, TG9, caPI3Kα x TG9 and swim-trained TG9 LV Myocytes.*

LV Cells		C_m (pF)	$I_{K,peak}$	$I_{to,f}$	$I_{K,slow}$	I_{ss}	I_{K1}
WT		157 ± 7					
(n=22)	τ_d (ms)		—	74 ± 8	1010 ± 31	—	—
	Amplitude (pA)		8651 ± 430	4052 ± 292	3637 ± 214	962 ± 79	-1801 ± 94
	Density (pA/pF)		56.1 ± 3.3	26.5 ± 2.3	23.5 ± 1.4	6.2 ± 0.4	-11.5 ± 0.7
TG9		197 ± 8*					
(n=21)	τ_d (ms)		—	81 ± 8	1466 ± 56	—	—
	Amplitude (pA)		5596 ± 357*	2733 ± 319#	1787 ± 86*	1076 ± 63	-1897 ± 132
	Density (pA/pF)		28.9 ± 1.8*	14.1 ± 1.6*	9.3 ± 0.5*	5.5 ± 0.2	-9.5 ± 0.6‡
caPI3Kα x TG9		226 ± 13					
(n=32)	τ_d (ms)		—	85 ± 5	1175 ± 39	—	—
	Amplitude (pA)		10174 ± 557*	3892 ± 333‡	4028 ± 164*	2011 ± 112*	-3176 ± 156
	Density (pA/pF)		48.1 ± 3.9*	18.5 ± 2.2	18.3 ± 1.2*	9.6 ± 0.8*	-15.5 ± 1.4#
TG9 with swim training		184 ± 11					
(n=15)	τ_d (ms)		—	75 ±12	1563 ± 127	—	—
	Amplitude (pA)		9031 ± 960*	3568 ± 820	2477 ± 219#	2986 ± 198*	-3395 ± 294
	Density (pA/pF)		53.5 ± 4.7*	20.6 ± 4.5	14.8 ± 1.1#	18.1 ± 1.3*	-20.3 ± 1.7*

* All values are means ± SEM. Kv and Kir current amplitudes/densities reported here were determined at +40 mV and -120mV, respectively. Measured current amplitudes/densities in WT and TG9 LV myocytes, TG9 and caPI3Kα x TG9 LV myocytes or TG9 and swim-trained TG9 LV myocytes, were compared. For each of these comparisons, values that are significantly (‡ $P<0.05$, # $P<0.01$, * $P<0.001$) different are indicated. Kv indicates voltage-gated K^+ currents; Kir, inwardly rectifying K^+ currents; C_m, cell membrane capacitance.

Quantitative RT-PCR experiments were also conducted to examine K^+ channel subunit and ANF transcript expression levels in the LV of WT, TG9 and caPI3KαxTG9 mice. ANF expression was significantly ($P<0.01$) increased in TG9, compared to WT, LV, but this increase was attenuated in caPI3KαxTG9 LV (**Figure 4.5E**). Consistent with the observed decreases in K^+ current amplitudes, the expression levels of $I_{to,f}$ subunits, Kv4.2, Kv4.3 and KChIP2, $I_{K,slow}$ subunits Kv1.5 and Kv2.1, the putative I_{ss} subunit, TASK1, and both Kir2.1 and Kir2.2 (I_{K1} subunits) were also lower in TG9, compared to WT, (**Figures 4.5F,G**) LV. Increased PI3Kα signaling in TG9 LV, however, resulted in marked increases in the expression levels of all of these K^+ channel subunit transcripts (**Figure 4.5F,G**).

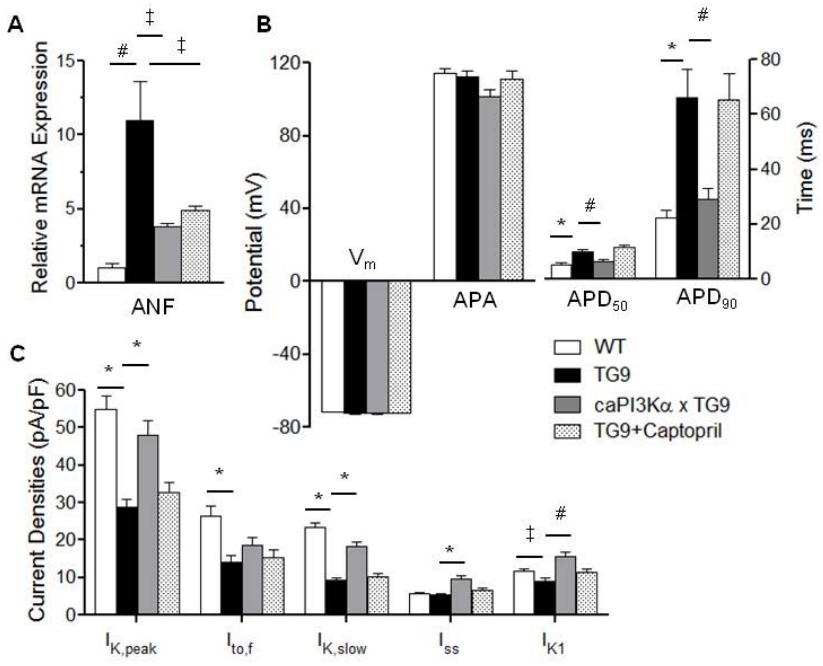

Supplemental Figure 4. 2 Captopril treatment does not measurably affect action potential waveforms or ventricular K+ currents in heart failure.

Four weeks of captopril treatment (Sigma, 50mg/L in drinking water from 6 weeks of age), which has been reported to improve the survival of TG9 animals,(Buerger *et al.*, 2006) attenuated the increase of ANF expression in the TG9 LV (A), suggesting delayed deterioration of cardiac function. Mean ± SEM APD_{50} and APD_{90}, however, were prolonged similarly in TG9 animals with (n=15) and without (n=10) captopril treatment (B). In contrast to the finding that repolarizing K^+ current densities are increased in TG9 LV with enhanced PI3Kα activity (C), K^+ current densities were not increased in LV myocytes from TG9 animals treated with captopril; indeed, K^+ current densities in LV myocytes from TG9 animals with (n=25) and without (n=21) captopril treatment were not significantly different.

4.3.7 Exercise training also upregulates repolarizing K^+ currents in heart failure

It was recently demonstrated that chronic exercise (swim training)-induced physiological hypertrophy, which results in increased PI3Kα activation (McMullen *et al.*, 2003; Yang *et al.*, 2010), leads to the upregulation of repolarizing ventricular K^+ currents in parallel with the cellular hypertrophy (increase in myocyte size) (Yang *et al.*, 2010). Additional experiments here, therefore, were designed to determine if chronic exercise training also results in K^+ current upregulation in the context of heart failure.

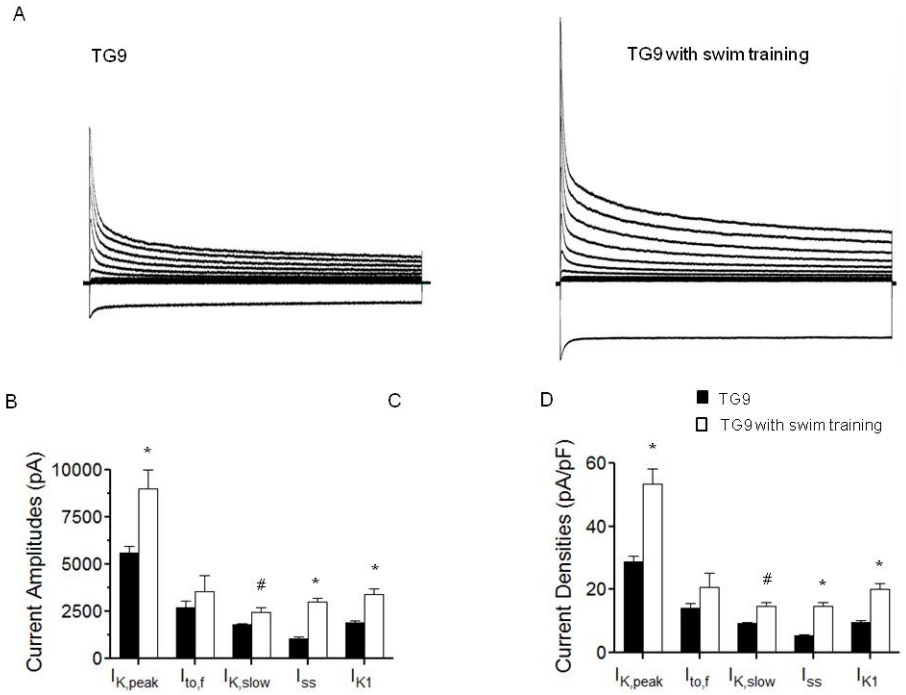

Figure 4. 6 Exercise training also results in K^+ current upregulation in heart failure.

(A) Representative whole-cell K^+ currents in myocytes isolated from the LV of TG9 mice with and without swim training are illustrated. (B-D) Mean ± SEM $I_{K,peak}$, $I_{K,slow}$, I_{ss} and I_{K1} amplitudes and densities are significantly ($^{\#}P$<0.01, $^{*}P$<0.001) higher in LV myocytes from swim-trained (n=15), compared with untrained (n=21), TG9 animals. Although mean $I_{to,f}$ amplitudes/densities are also higher in swim-trained TG9 LV myocytes, the differences did not reach statistical significance.

Following 4 week chronic swim training, voltage-clamp experiments were performed on LV myocytes isolated from (10 week) trained and untrained TG9 mice. Mean ± SEM citrate synthase activity was increased significantly (P<0.05) in the gastrocnemius muscles from swim-trained (0.92±0.11 µmol/mg protein/min; n=4), compared with untrained (0.49±0.09 µmol/mg protein/min; n=4), TG9 animals, indicating the robustness of aerobic exercise training (Allen *et al.*, 2001). The amplitudes of $I_{K,peak}$ and I_{K1} (P<0.001), as well as of the Kv current components, $I_{K,slow}$ (P<0.01) and I_{ss} (P<0.001), were significantly higher in TG9 LV myocytes from the swim-trained, compared with the untrained, TG9 animals (**Figure 4.6B**). The mean ± SEM C_m determined in LV myocytes from trained and untrained animals were similar (**Figure 4.6C**). Repolarizing K^+ current

($I_{K,peak}$, $I_{K,slow}$, I_{ss} and I_{K1}) densities, therefore, were significantly (P<0.01) higher in TG9 LV myocytes following swim training (**Figure 4.6A,D**). Indeed $I_{K,peak}$ and I_{K1} densities were normalized to the levels found in WT cells (compare values in **Supplemental Table 4.2**).

4.4 Discussion

The increased incidence of life-threatening ventricular arrhythmias in patients with LV dysfunction is a consequence of complex pathological remodeling in cardiac structural (Akar *et al.*, 2004), neurohumoral (Vaseghi & Shivkumar, 2008) and electrophysiological properties (Beuckelmann *et al.*, 1993; Marionneau *et al.*, 2008b). Advances in the clinical management of heart failure, specifically pharmacologic (Kober *et al.*, 1995; Pitt *et al.*, 1999) and device therapies (Moss *et al.*, 2009) which are aimed at treating neurohumoral and structural abnormalities, have improved patient outcomes (Kober *et al.*, 1995; Pitt *et al.*, 1999; Moss *et al.*, 2009). Targeting the electrophysiological derangements using anti-arrhythmic agents has proven to be much more problematic and, indeed, has been associated with increased, rather than decreased, mortality (CAST, 1989). The results presented here demonstrate that increased PI3Kα signaling in pathological hypertrophy and heart failure helps to normalize ventricular repolarization and maintain electrical functioning through the transcriptional upregulation of repolarizing K^+ channels, a mechanism of action distinct from classic heart failure therapeutics.

Interestingly, PI3Kα signaling has been shown to modulate a number of transcription factors that could potentially affect the expression of cardiac K^+ channels. The Forkhead (FOXO) family of transcriptional factors, for example, which are direct targets of the downstream target of PI3Kα, Akt, has been shown to regulate the promoter activity of several K^+ channel genes such as *Kcnj8* (Kir6.1), *Kcnj11* (Kir6.2) and *Abcc8* (SUR1)

(Philip-Couderc *et al.*, 2008). Promoter analyses (using web-based program rVista 2.0, http://rvista.decode.org) (Loots & Ovcharenko, 2004) also reveal multiple FOXO transcription factor binding sites in *Kcnd2* (Kv4.2), *Kcnip2* (KChIP2), *Kcnb1* (Kv2.1) and *Kcnk3* (TASK1). Glycogen synthase kinase 3 beta (GSK3β), another important downstream target of PI3Kα, also modulates the activity of several transcriptional factors, including NFAT, GATA4, myocardin, c-Myc, c-Jun and β-catenin, many of which have putative binding sites in the promoter regions of several K^+ channel subunit genes and could potentially contribute to the transcriptional regulation of K^+ channel expression mediated by increased PI3Kα. Further experiments are needed to explore these hypotheses and delineate PI3Kα-mediated transcriptional regulatory mechanisms directly.

4.4.1 Increased PI3Kα signaling mitigates impaired repolarization in hypertrophied and failing hearts

Chronic cardiac-specific increases in PI3Kα signaling produce physiological hypertrophy characterized by normal electrical and mechanical function (Shioi *et al.*, 2000; McMullen *et al.*, 2003; Yang *et al.*, 2010). The results here demonstrate that increased myocardial PI3Kα signaling also eliminates the effects of pressure overload-induced LV (pathological) hypertrophy on ventricular action potential durations. In addition, in caPI3Kα+TAC LV myocytes, the transcripts encoding the subunits that underlie the generation of several repolarizing K^+ channels were *increased* significantly and in parallel with the TAC-induced increase in myocyte size, resulting in normalized K^+ current densities. These results contrast strikingly with the effects of TAC-induced LVH in WT animals, in which K^+ channel subunit expression levels are not increased in parallel with the cellular hypertrophy, resulting in decreased K^+ current densities and

impaired repolarization (Marionneau *et al.*, 2008b). Augmented PI3Kα signaling, therefore, has a clear beneficial effect in the context of pathological LVH.

The experiments here also demonstrated that repolarizing K^+ channel subunit transcript expression levels are upregulated and K^+ current amplitudes are increased in failing TG9 hearts with increased PI3Kα signaling. Although the treatment with the ACE inhibitor captopril also improves the survival of TG9 animals (Buerger *et al.*, 2006), there were no detectable effects of captopril treatment on ventricular K^+ currents or action potentials in TG9 hearts (**Supplemental Figure 4.1**). Enhanced PI3Kα signaling in the setting of heart failure, therefore, has unique beneficial effects on electrical functioning that are not observed with renin-angiotensin system blockade.

QRS complexes were widened in TG9, compared with WT, mice, suggesting the presence of intracardiac conduction slowing, which is also commonly observed in heart failure patients (Hombach, 2002) and in animal models of non-ischemic dilated cardiomyopathy (Akar *et al.*, 2004). In contrast with the effects on QT intervals, however, increased PI3Kα activity does not normalize the widened QRS complexes in TG9 mice. These observations may reflect low expression of the caPI3Kα transgene in the specialized conduction system, as previous reports suggest that transgenes driven by the α-MHC promoter may not be expressed consistently in nodal and His-Purkinje tissues (Dobrzynski *et al.*, 2006). It is also possible, however, that increased PI3Kα signaling is not sufficient to reverse the structural and molecular changes that underlie the abnormal conduction. Further experiments focused on the conduction system directly are needed to explore these possibilities directly.

4.4.2 Chronic Swim-Training Normalizes K^+ Current Densities in Heart Failure

The observation that increased PI3Kα signaling in failing hearts provides beneficial effects in maintaining physiological K^+ current expression levels suggests an attractive strategy for alleviating arrhythmogenic electrical remodeling in heart failure (Beuckelmann *et al.*, 1993). A simple and practical approach to increasing cardiac PI3Kα signaling is aerobic exercise training (McMullen *et al.*, 2003; Yang *et al.*, 2010). Indeed, aerobic exercise training has been shown to improve LV function and prolong survival in heart failure patients (Coats, 2011), as well as in animal models of heart failure (McMullen *et al.*, 2007; Lachance *et al.*, 2009). Various mechanisms have been proposed to explain the beneficial effects of exercise, including improved endothelial function (Hambrecht *et al.*, 2000a), reduced myocardial fibrosis (McMullen *et al.*, 2007), and balanced sympathovagal input (Coats *et al.*, 1992). The results here demonstrate that chronic exercise training also upregulates repolarizing K^+ currents in the setting of heart failure, an effect that normalizes ventricular repolarizing K^+ current densities and action potential durations and reduce arrhythmia susceptibility. In spite of the benefits of exercise, however, it is also clear that adherence to, or compliance with, prescribed exercise regimens can be very difficult for heart failure patients (O'Connor *et al.*, 2009). Importantly, the results here suggests the potential of a therapeutic strategy focused on enhancing PI3Kα signaling directly.

4.4.3 Conclusion

In summary, enhanced cardiac PI3Kα activity is associated with increased expression of myocardial K^+ channel subunits in pressure overload-induced LVH and heart failure. The transcriptional upregulation of K^+ channel subunits produced by increased PI3Kα activity leads to increased K^+ current amplitudes in proportion to the increase in cell size, thereby normalizing K^+ current densities, action potential waveforms, and QT intervals.

The experiments here also demonstrate that chronic exercise training, a physiological means to enhance PI3Kα signaling leads to K^+ channel upregulation in the failing heart, whereas the ACE inhibitor captopril does not. These observations suggest that increased PI3Kα signaling, either by exercise or by direct pharmacological intervention, could directly address the electrophysiological basis of life-threatening arrhythmias associated with pathological LVH and heart failure. These results argue for further research focused on developing practical methods to activate PI3Kα signaling in the human heart, as well as on detailing the effects of these manipulations on arrhythmia vulnerability and sudden cardiac death.

Chapter 5: Combined Deep microRNA and mRNA Sequencing Identifies Protective Transcriptomal Signature of Enhanced PI3Kα Signaling in Cardiac Hypertrophy

5.1 Abstract

Rationale: The perturbation of myocardial transcriptome homeostasis is the hallmark of pathological hypertrophy, underlying the maladaptive structural and functional remodeling of the heart in response to pathological stresses. Classic and novel therapeutics that provide beneficial effects against pathological remodeling likely impact myocardial transcriptome architecture, including miRNA and mRNA expression profiles. Microarray and PCR-based technologies, although employed extensively, cannot provide adequate sequence coverage or quantitative accuracy to test this hypothesis directly.

Objective: To develop and exploit next-generation sequencing approaches for comprehensive and quantitative analyses of myocardial miRNAs and mRNAs to test the hypothesis that augmented phosphoinositide-3-kinase-p110α (PI3Kα) signaling in the setting of pathological hypertrophy provides beneficial effects through remodeling of the myocardial transcriptome signature.

Methods and Results: A molecular and bioinformatic pipeline permitting comprehensive analysis and quantification of myocardial miRNA and mRNA expression with next-generation sequencing was developed and the impact of enhanced PI3Kα signaling on the myocardial transcriptome signature of pressure overload-induced pathological hypertrophy was explored. These analyses identified multiple miRNAs and mRNAs that were abnormally expressed in pathological hypertrophy and partially or completely normalized with increased PI3Kα signaling. Additionally, several novel miRNAs potentially linked to remodeling in cardiac hypertrophy were identified. Additional experiments revealed that increased PI3Kα signaling reduces cardiac fibrosis in pathological hypertrophy through modulating TGF-β signaling and miR-21 expression.

Conclusion: These studies demonstrate that combined deep miRNA- and mRNA-sequencing analyses can be exploited to provide sensitive, accurate and comprehensive

quantification of the cardiac transcriptome, the potential to uncover novel miRNAs, and insights into the molecular mechanisms involved in the pathophysiology of cardiac remodeling.

*** Chapter 5 contains large datasets that can be accessed through the following link:**

Online Table S5.3, S5.4, S5.5, S5.7, S5.8
https://docs.google.com/open?id=0B2YE75Fy4fPpZjViZTYwZjEtNGVmZi00MWMxLThkNzItM2FjYzZkYTFmNmU0

Online Table S5.6
https://docs.google.com/open?id=0B2YE75Fy4fPpZWNhOWM3N2YtYzBiZC00ODdiLWEzMDctNjU5NjBhNWRlZjkz

Online Table S5.9, S5.10, S5.11, S5.12

https://docs.google.com/open?id=0B2YE75Fy4fPpMzA3ZDYwMTYtZjYxZi00ZGRkLWJmNmYtMTVmMDdiZGVlNDM1

5.2 Introduction

Comparative transcriptional profiling has been used extensively to explore disease mechanisms and to improve the accuracy of clinical diagnosis and outcome predictions (Golub *et al.*, 1999; Heidecker *et al.*, 2008). Although standard hybridization technologies (microarrays)- and PCR-based profiling have been employed extensively, the sensitivity and the sequence coverage provided by these assays are quite limited. As high-throughput sequencing technologies have evolved over the past few years, deep sequencing has proven superior to microarray- or PCR-based methods of transcriptional profiling, owing to its capacity to provide comprehensive and quantitative transcript expression data over a wide dynamic range (Marguerat & Bahler, 2010; Matkovich *et al.*, 2010). The high sensitivity of deep sequencing is particularly useful in miRNA research because of the wide range over which miRNAs are expressed, from tens of thousands of copies to a single copy per cell (Matkovich *et al.*, 2010; van Rooij, 2011). Moreover, deep sequencing, unlike microarrays, is not limited by the number of probes, allowing the discovery of novel miRNAs. With the evolution of next-generation sequencing technologies, the amount and speed of data output have reached unprecedented levels, yet the overall cost is decreasing. Despite the potential and the decreasing costs, there have to date, been remarkably few studies applying deep sequencing in cardiovascular miRNA research (Rao *et al.*, 2009), likely reflecting the considerable bioinformatic challenges involved in the analyses of such large datasets. Here, we developed a molecular and bioinformatic pipeline using state-of-the-art next-generation sequencing to provide a comprehensive miRNA and mRNA expression profiling in the mouse heart, and used this approach to study remodeling in pathological and physiological cardiac hypertrophy.

Pathological cardiac hypertrophy, a maladaptive response of the myocardium to increased biomechanical stresses, is associated with increased propensity to develop interstitial fibrosis, heart failure, life-threatening arrhythmias and sudden cardiac death (Levy *et al.*, 1990; McMullen & Jennings, 2007). Physiological hypertrophy in response to exercise training, in contrast, is characterized by normal cardiac structure and maintained cardiac function, and is not associated with increased risk of heart failure, arrhythmias or sudden cardiac death (McMullen *et al.*, 2003; McMullen & Jennings, 2007). Two distinct signaling mechanisms, G-protein coupled receptor (GPCR) signaling (D'Angelo *et al.*, 1997; Mende *et al.*, 1998; McMullen & Jennings, 2007) and phosphoinositide-3-kinase-p110α (PI3Kα) signaling (McMullen *et al.*, 2003), have been linked to the development of pathological and physiological hypertrophy, respectively. In addition, it has been demonstrated that augmentation of PI3Kα signaling is beneficial in the setting of pathological hypertrophy and heart failure (McMullen *et al.*, 2007; Yang *et al.*, 2012), resulting in improved cardiac function and survival. The mechanisms through which enhanced PI3Kα signaling is protective, however, have not been delineated.

A hallmark of pathological hypertrophy is that the myocardial transcriptome landscape, including mRNAs, miRNAs, long noncoding RNAs and other RNA species, is dramatically altered (Matkovich *et al.*, 2010; Lee *et al.*, 2011), suggesting that perturbation of transcriptome homeostasis is critically coupled to the disease process. We hypothesized that augmented PI3Kα signaling provides protective effects by preventing or reversing the changes in myocardial miRNA and mRNA expression associated with pathological hypertrophy. Exploiting a molecular and bioinformatic pipeline optimized for transcriptome profiling with next-generation high-throughput sequencing, we examined directly the impact of increased PI3Kα signaling on myocardial transcriptome structure in the setting of pathological hypertrophy. The results

presented here demonstrate that combining miRNA- and mRNA-Seq analyses allows quantitative in-depth profiling of myocardial miRNA and mRNA expression, identification of novel miRNA species, and the potential to explore the detailed molecular mechanisms contributing both to the pathophysiology associated with cardiac hypertrophy and the beneficial effects of potential therapeutic interventions.

5.3 Results

5.3.1 Enhanced PI3Kα signaling mitigates pressure overload-induced pathological remodeling

Transverse aortic constriction (TAC) in WT animals, as expected, resulted in marked pressure overload-induced LV hypertrophy, evident in the ~30% increase in LVW/TL ratio (**Figure 5.1A** and **Supplemental Table 5.1**) and a significantly (~12 fold, P<0.001) increased expression (**Figure 5.1B**) in ANF, a molecular marker of pathological hypertrophy (McMullen & Jennings, 2007). Although cardiac specific expression of constitutively active PI3Kα (caPI3Kα) also produces marked LV hypertrophy (**Figure 5.1A** and **Supplemental Table 5.1**), in this case, without increased ANF expression (**Figure 5.1B**), consistent with the development of physiological hypertrophy (Shioi *et al.*, 2000).

Supplemental Table 5. 1 Demographic and echocardiographic measurements in experimental animals

Data Measure	WT Sham (n=6)	WT+TAC (n=6)	caPI3Kα Sham (n=6)	caPI3Kα+TAC (n=6)
Body weight (g)	27.9±0.4	26.6±0.4	29.7±1.1	30.0±0.9
Tibia length (mm)	21.9±0.2	21.6±0.2	21.7±0.2	21.6±0.1
Heart weight (g)	122.5±3.8	145.9±2.7*	149.1±4.5	169.1±9.3‡
LV weight (g)	68.1±2.6	85.8±3.4$^{\#}$	84.7±2.9	98.3±4.8‡
LVW/TL ratio (mg/mm)	3.1±0.1	4.1±0.2*	3.9±0.1	4.5±0.2‡
Fractional shortening (%)	55.7±1.5	54.0±7.1	51.1±3.1	53.1±2.9
VTI ratio (Ao/LVOT)	0.9±0.1	5.8±0.4*	0.9±0.0	5.9±0.8$^{\#}$

LVMI: LV mass index; VTI: velocity time integral; Ao: aorta; LVOT: LV outflow tract; all values are means ± SEM. Values in WT+TAC or in caPI3Kα+TAC that are significantly ($^{‡}P$<0.05, $^{\#}P$<0.01 , $^{*}P$<0.001) different from the values in WT sham or caPI3Kα sham animals, respectively, are indicated.

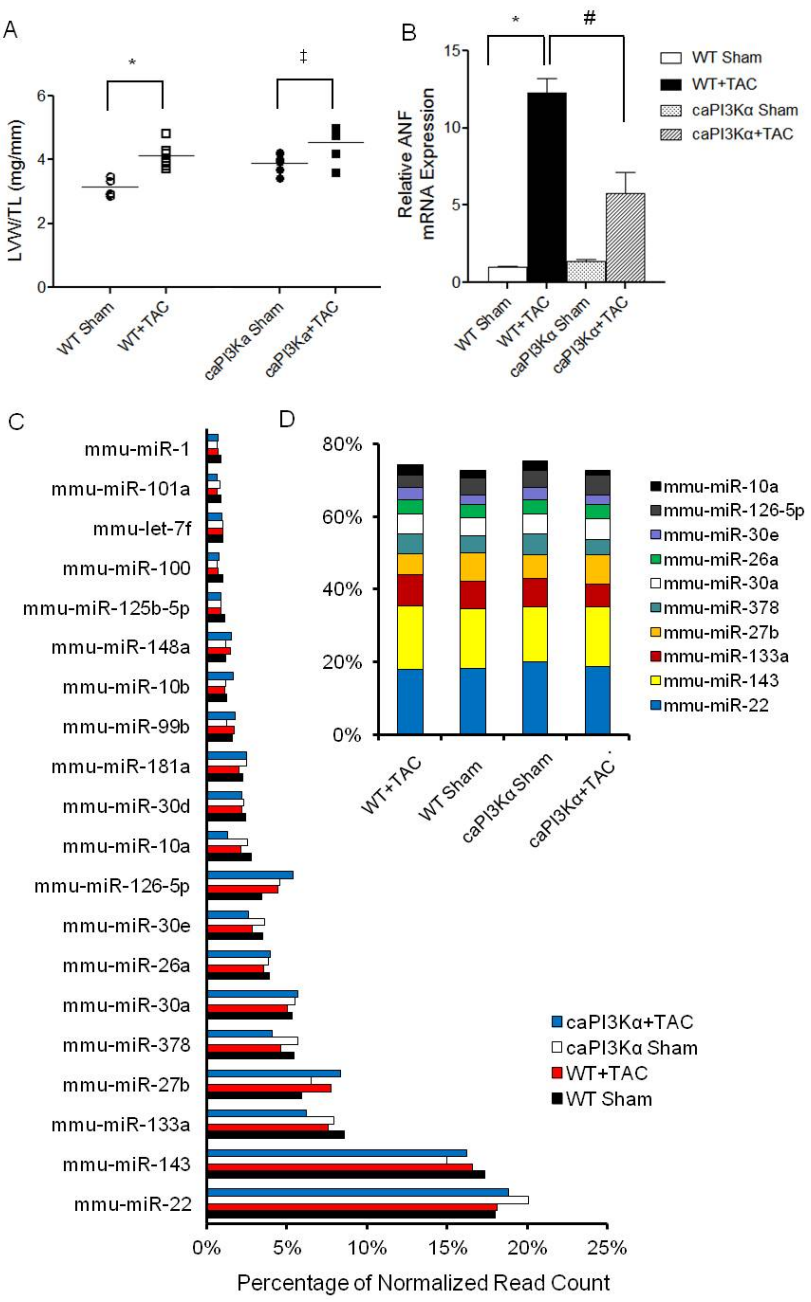

Figure 5. 1 Functional impact of enhanced PI3Kα signaling on pressure overload-induced LVH and the LV miRNA abundance.

(A) LV weight/tibia length (LVW/TL) ratios were determined in WT sham, WT+TAC, caPI3Kα sham and caPI3Kα+TAC (n=6 in each group) animals; individual and mean ± SEM values ($^{*}P$<0.001, $^{‡}P$<0.05) are plotted. (B) Transcript expression of ANF, the molecular marker of pathological hypertrophy is increased ~12 fold with TAC in WT LV. The increase in ANF expression in response to TAC is significantly (P<0.01) blunted in the LV of caPI3Kα animals. (C) Expression of the 20 most abundant miRNAs in WT sham, WT+TAC, caPI3Kα sham and caPI3Kα+TAC LV are compared. The abundances of the individual miRNAs were expressed as percentages of individual miRNA read counts contributing to the total read counts of known miRNAs in a cDNA library. (D)The 10 most abundant miRNAs account for >70% of the total miRNA reads in mouse LV.

Enhanced PI3Kα signaling, however, significantly (P<0.001) attenuated the TAC-induced increase in ANF expression (~5 fold, **Figure 5.1B**), consistent with previous

reports suggesting that enhanced PI3Kα signaling is protective and mitigates the maladaptive, pathological myocardial remodeling secondary to pressure overload (McMullen *et al.*, 2007; Yang *et al.*, 2012).

5.3.2 Deep sequencing of microRNAs in Sham-operated and TAC- WT and caPI3Kα LV

Using the 15 barcoded small RNA libraries prepared from the (4 WT sham, 5 WT+TAC, 3 caPI3Kα sham and 3 caPI3Kα+TAC) mouse LV samples, a total of 165,496,374 reads were generated from 2 flow cell lanes on the HiSeq2000 sequencer (**Table 5.1**), on average producing >10 million reads per library. The read lengths obtained from the libraries showed a Gaussian distribution with a peak at 22 nucleotides (**Supplemental Figure 5.1**), consistent with the enrichment of miRNAs. More than 152 million of the sequence reads (92.2%) were aligned to the mouse genome (mm9), ~88 million (53.3%) mapped to known miRNAs, and ~11 million (6.7%) to RNA species other than miRNA. Approximately 53 million (32.3%) of the remaining reads mapped to unannotated genomic regions, and ~10 million of these were subsequently re-classified to be putative miRNAs (see below). In each sample, the read counts of each of the known miRNAs were then normalized to the total counts of sequences mapped to the miRbase v.18 database and presented as PMMR (sequences per million mapped reads). Scatter plots of the normalized read counts of all known miRNAs showed high degrees of correlation (β=0.95, R^2=0.99, **Supplemental Figure 5.2A**) between biological replicates, indicating high levels of reproducibility for these miRNA-Seq experiments. The expression levels of several of the miRNAs identified in WT sham LV were also examined with qRT-PCR and the relative abundances (in C_T) of the individual miRNAs were found to be well correlated with the results from miRNA-Seq (**Supplemental Figure 5.2B**).

Table 5. 1 Summary of miRNA- and mRNA-Seq read counts and mapping results

miRNA-Seq Read Counts	WT Sham (n=4)	WT TAC (n=5)	caPI3Kα Sham (n=3)	caPI3Kα TAC (n=3)	Total
Total	45901044	49701319	37441052	32452959	165496374
Mapped	41986529 (91.5)	45593199 (91.7%)	34304088 (91.6%)	30735651 (94.7%)	152619467 (92.2%)
Unmapped	3914515 (8.5%)	4108120 (8.3%)	3136964 (8.4%)	1717308 (5.3%)	12876907 (7.8%)
Known miRNAs	22981918 (50.1%)	27443912 (55.2%)	18360999 (49.0%)	19354436 (59.6%)	88141265 (53.3%)
Putative miRNAs	2514756 (5.5%)	2564454 (5.2%)	2696651 (7.2%)	2444635 (7.5%)	10220496 (6.2%)
Mapped to other RNA species	2968104 (6.5%)	2942701 (5.9%)	2950463 (7.9%)	2282158 (7.0%)	11143426 (6.7%)
Mapped to genome, unannotated	13521751 (29.5%)	12642132 (25.4%)	10295975 (27.5%)	6654422 (20.5%)	43114280 (26.1%)
mRNA-Seq Read Counts	WT Sham (n=4)	WT+TAC (n=3)	caPI3Kα Sham (n=2)	caPI3Kα+TAC (n=2)	Total
Total	47913934	45178741	84373729	65384703	242851107
Mapped	40884751 (85.3%)	38297928 (84.8%)	70954141 (84.1%)	55108361 (84.3%)	205245181 (84.5%)
Unmapped	7029183 (14.7%)	6880813 (15.2%)	13419588 (15.9%)	10276342 (15.7%)	37605926 (15.5%)
Mapped to exon regions	26279745 (54.8%)	26838716 (59.4%)	48917894 (58.0%)	37761525 (57.8%)	139797880 (57.6%)

TAC: trans-thoracic aortic constriction

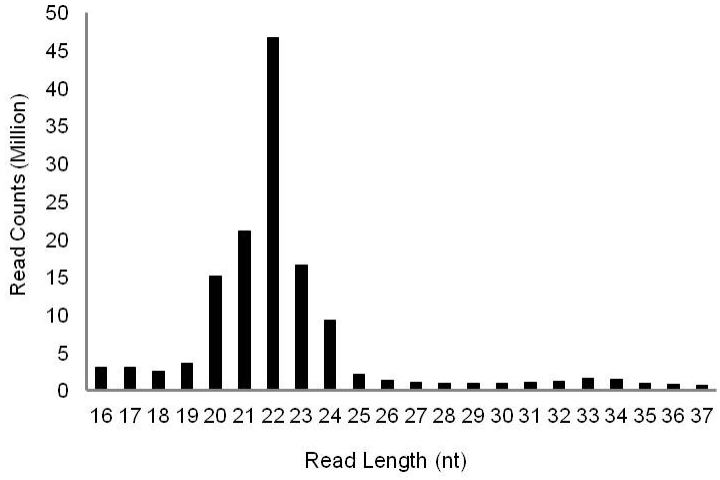

Supplemental Figure 5. 1 Read length distribution of miRNA sequencing experiments.

The read lengths obtained from the small RNA libraries showed a Gaussian pattern distribution with a peak at a length of 22 nucleotides (ranging from 16 to 37 nt), consistent with the expected miRNA lengths and the enrichment of miRNAs in the libraries

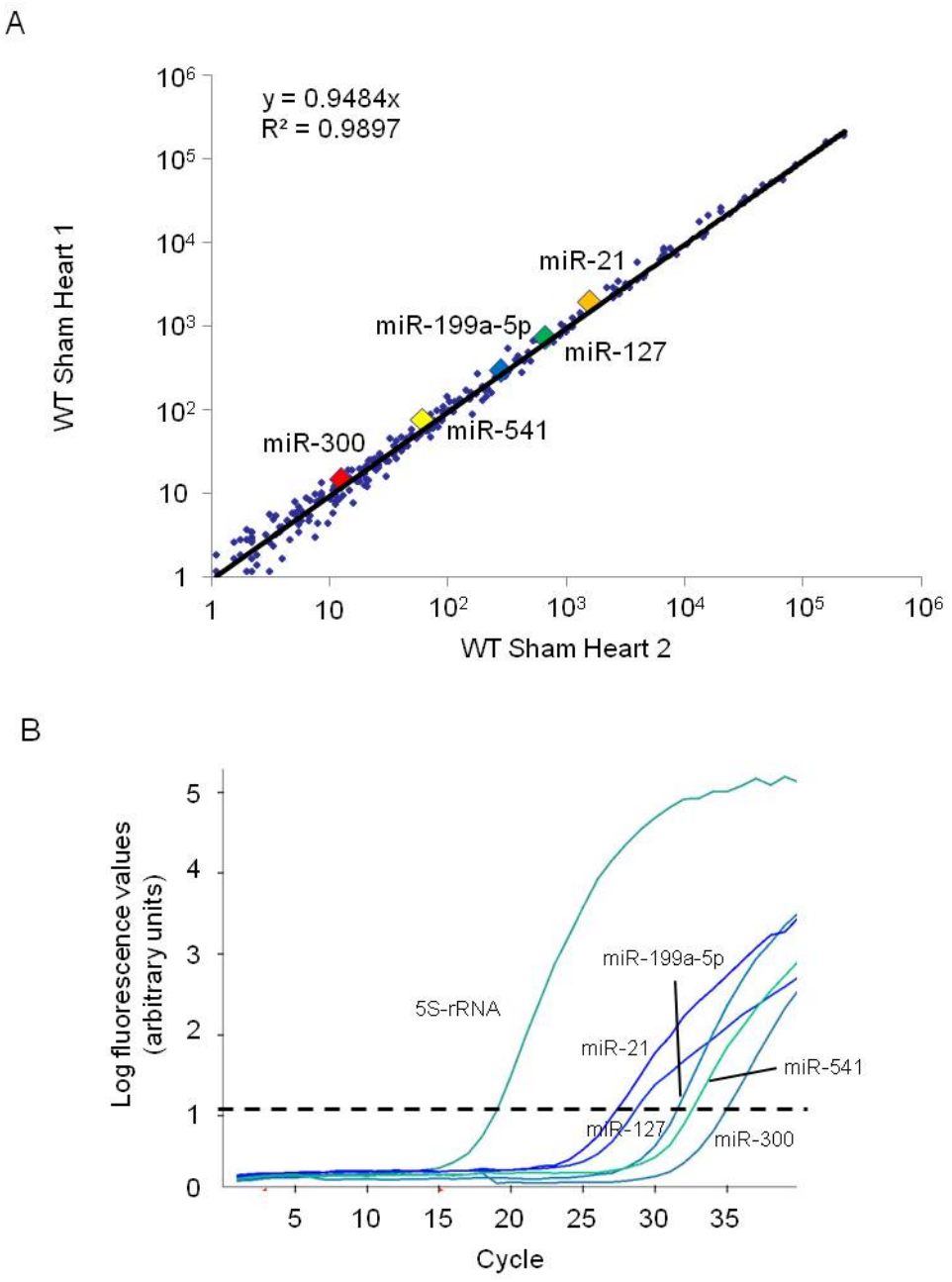

Supplemental Figure 5. 2 Scatter plot of normalized read counts between biological replicates and correlation with qPCR results confirms the reproducibility and accuracy of miRNA-Seq experiments

(A) Scatter plot of the normalized read counts of all known miRNAs shows high degree of correlation (β=0.95, R^2=0.99) between biological replicates (WT sham heart 1 and 2), documenting the reproducibility of the miRNA-Seq experiments. (B) Representative qRT-PCR amplication plots of selected miRs (indicated with colored squares in Supplemental Figure 2A) in WT sham LV. The relative abundances (C_T values) of the individual miRs were accurately reflected in the results of miRNA-seq experiments.

Using the criterion that a miRNA sequence must be detected in at least 2 small RNA libraries, the sequence reads were mapped to 393 mature miRNAs reported in miRbase v.18 (**Online Supplemental Table S5.3**). A wide range of miRNA expression levels, ranging from 0.1 to 222655.7 PMMR, was observed. MiR-22 was the most abundant mature miRNA expressed in mouse LV, corresponding to 18-20% of all of the miRNA sequence reads. The relative expression levels of the 20 most abundant mature miRNAs are shown in **Figure 5.1C**. Interestingly, 13 out of these 20 miRNAs, including muscle-specific miR-1 and miR-133a (Rao *et al.*, 2006), and endothelial cell-specific miR-126-5p (Wang *et al.*, 2008), have been reported previously to be highly abundant in the mouse heart (Rao *et al.*, 2009). The 10 most abundant miRNAs accounted for >70% of all miRNA sequence reads in all LV samples (**Figure 5.1D**). In addition to known mature miRNAs, 13 novel miRNA* (mature-star miRNA, mature miRNAs derived from the less-expressed, opposite arm) sequences were identified for known miRNA genes without prior annotation in miRBase v.18 (**Table 5.2 and Online Supplemental Table S5.4**).

Table 5. 2 Novel miRNA* identified in mouse LV

Novel miRNA*	WT Sham Mean PMMR	WT TAC/ WT Sham	caPI3Kα Sham/ WT Sham	caPI3Kα TAC/ WT Sham
mmu-mir-145*	287.96	0.75	0.87	0.67
mmu-mir-322*	54.41	1.16	0.90	0.91
mmu-mir-425*	5.97	1.72	1.36	1.7
mmu-mir-1960*	1.55	0.94	1.03	0.81
mmu-mir-503*	1.31	1.36	0.79	1.94
mmu-mir-28*	1.26	1.46	1.12	0.53
mmu-mir-30d*	1.18	0.13	0.50	0.14
mmu-mir-382*	0.81	1.73	1.00	1.45
mmu-mir-153*	0.39	0.14	0.61	1.74
mmu-mir-3068*	0.22	0.97	0.48	0.00
mmu-mir-486*	0.20	0.00	3.96	0.69
mmu-mir-455*	0.19	1.23	0.00	0.00
mmu-mir-140*	0.08	3.26	2.87	0.00
mmu-mir-143*	0.00	N.A.	N.A.	N.A.

Comparative analyses revealed that 78 miRNAs were differentially expressed in the 4 sets of LV samples analyzed (P<0.01 at a false-discovery rate of 0.05). A complete list of the differentially expressed miRNAs, with mean PMMR values, fold differences (compared to WT sham LV) and *P* values, is presented in **Online Supplemental Table S5.5**. Consistent with previous studies demonstrating normal cardiac structure and function in the caPI3Kα mouse model of physiological hypertrophy (Shioi *et al.*, 2000), unsupervised hierarchical clustering analyses revealed that the miRNA expression profiles in WT sham and caPI3Kα sham LV samples were similar (**Supplemental Figure 5.3**).

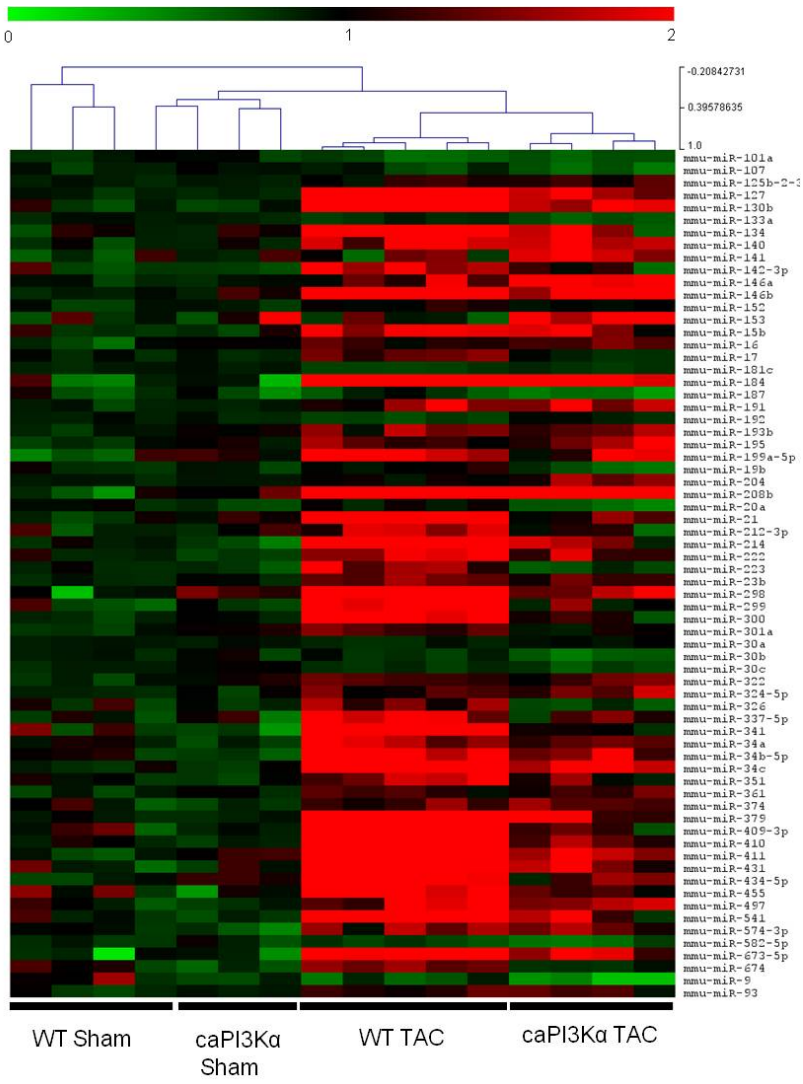

Supplemental Figure 5. 3 Differentially regulated miRNAs in WT sham, WT+TAC, caPI3Kα sham and caPI3Kα+TAC LV.

Heat map and hierarchical clustering of the differentially regulated miRNAs in WT sham, WT+TAC, caPI3Kα sham and caPI3Kα+TAC LV samples. The miRNA expression signatures of WT sham and caPI3Kα sham LV were similar. The WT+TAC LV miRNA expression profile, however, was distinct; increased PI3Kα signaling attenuated the abnormal miRNA expression pattern observed in response with TAC.

In contrast, the miRNA expression signature of WT+TAC LV was dramatically different from both WT sham and caPI3Kα sham LV, segregating the WT+TAC from the WT sham and caPI3Kα sham LV samples (**Supplemental Figure 5.3**). Consistent with previous miRNA studies in murine models of pressure overload-induced pathological hypertrophy, the expression levels of the miR-146 family (Cheng *et al.*, 2007), as well as miR-199a-5p (van Rooij *et al.*, 2006; Sayed *et al.*, 2007), miR-21 (van Rooij *et al.*, 2006; Cheng *et al.*, 2007; Sayed *et al.*, 2007), miR-212 (Jentzsch *et al.*, 2011) and miR-214 (van Rooij *et al.*, 2006; Cheng *et al.*, 2007; Sayed *et al.*, 2007) were upregulated, whereas miR-133a (van Rooij *et al.*, 2006; Cheng *et al.*, 2007) was downregulated in WT+TAC, compared with WT sham, LV. Interestingly, when comparing the miRNA expression profiles of WT+TAC and caPI3Kα+TAC LV, it is clear that the aberrant expression pattern of miRNAs observed with TAC-induced LVH was blunted substantially with increased PI3Kα signaling (**Supplemental Figure 5.3 and Online Supplemental Table S5.5**).

To identify miRNAs that were abnormally expressed in pathological hypertrophy but partially or completely normalized with increased PI3Kα signaling, an unsupervised, self-organized tree analysis for the differentially expressed miRNAs (in **Online Supplemental Table S5.5**) was conducted (**Supplemental Figure 5.4**). A total of 23 miRNAs fitting this “protective PI3Kα microRNome” expression pattern were identified and clustered (**Figure 5.2**). Most of these miRNAs were upregulated ≥ 2 fold in WT+TAC, compared with WT sham, LV, and were normalized or markedly reduced with increased PI3Kα signaling. A number of the miRNAs identified in the “protective PI3Kα microRNome” have been shown to cause or to contribute to various myocardial pathologies, including cardiac hypertrophy (miR-146b, miR199a-5p, miR-21, miR-212, miR-214), heart failure (miR-146b, miR199a-5p, miR-21, miR-212, miR-214), myocardial

ischemia (miR-134, miR-199a-5p, miR-21, miR-214, miR-379), cardiac fibrosis (miR-21) and fetal gene program activation (miR-21, miR-212). A complete list of the 23 miRNAs identified and references to the identified cardiac and extra-cardiac functions of these miRNAs is provided in **Online Supplemental Table S5.6.** Taken together, these data indicate that enhanced PI3Kα signaling ameliorates the adverse effects of pathological stress on multiple disease-linked miRNAs, normalizing their expression in the myocardium.

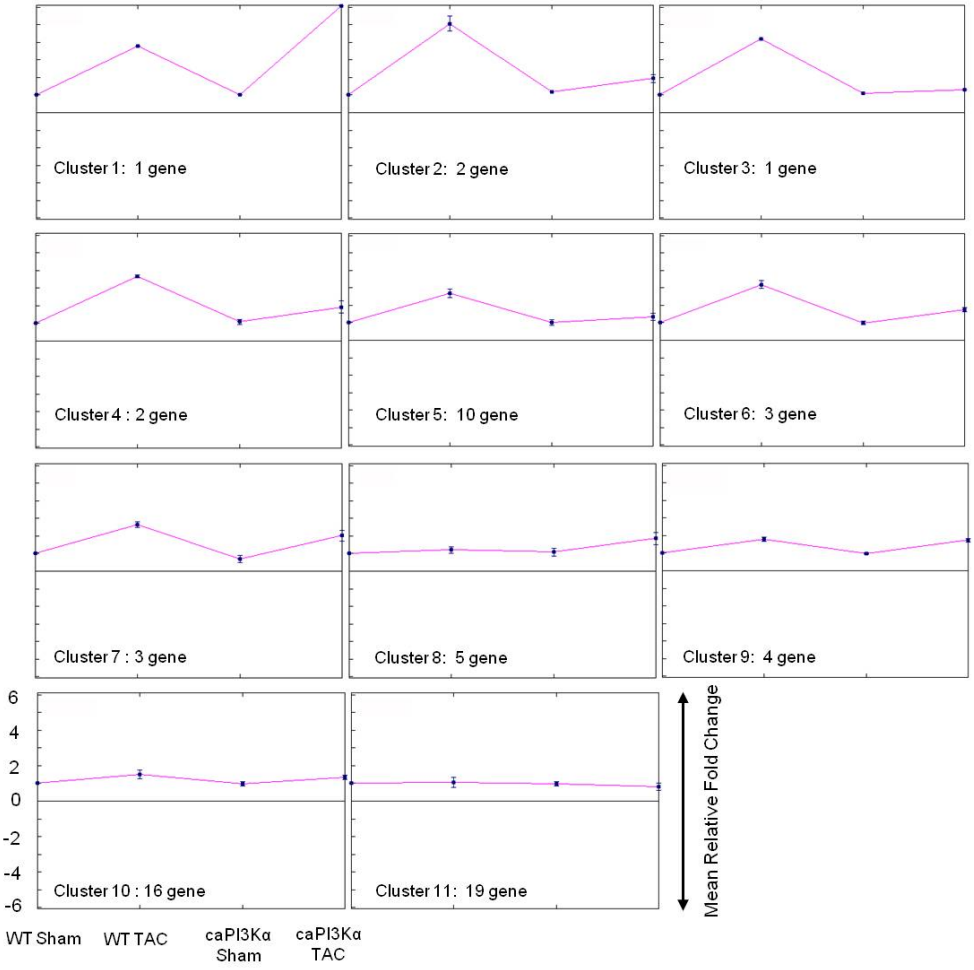

Supplemental Figure 5. 4 miRNA clustering using self organizing tree algorithm.

Differentially regulated miRNAs in the four groups of LV samples were clustered using Self Organizing Tree Algorithm (SOTA). Only the clusters showing aberrant regulation of miRNAs in response to TAC that were also normalized with increased myocardial PI3Kα signaling were selected (cluster 2, 3, 4, 5, 6 and 7). Two additional miRNAs fitting the expected expression pattern were found in cluster 10.

A

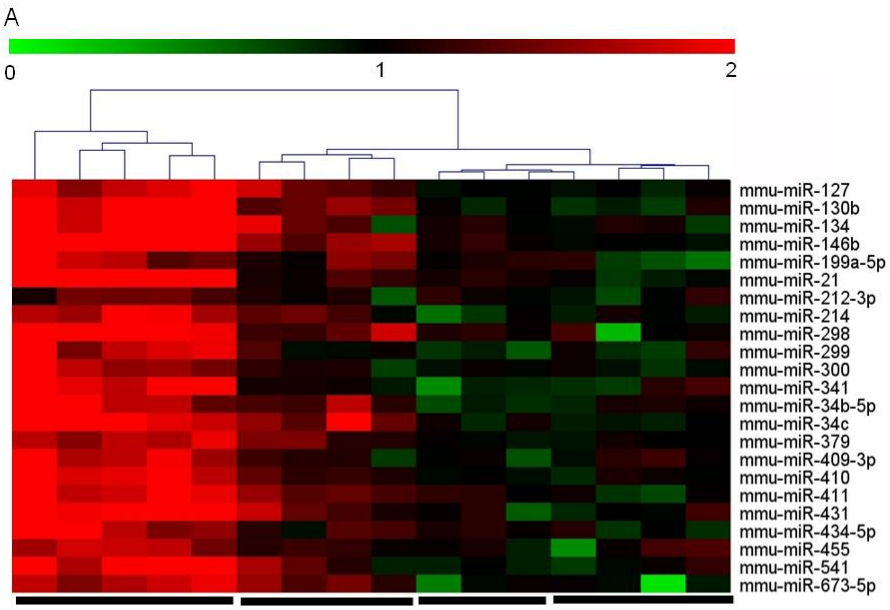

B

miRNA	WT Sham mean PMMR	WT TAC/ WT Sham	caPI3Kα Sham/ WT Sham	caPI3Kα TAC/ WT Sham	*P* value
mmu-mir-21	3792.0	4.21	1.13	1.33	2.03E-05
mmu-mir-127	1051.7	2.64	0.93	1.91	2.30E-05
mmu-mir-199a-5p	578.2	2.35	0.99	1.59	0.004653
mmu-mir-146b	386.5	4.77	1.18	2.1	8.22E-09
mmu-mir-411	125.2	2.87	1.14	1.81	1.33E-06
mmu-mir-541	82.9	3.34	0.98	1.57	3.61E-05
mmu-mir-34c	56.1	3.66	0.95	2.17	2.43E-04
mmu-mir-214	50.0	2.74	0.78	1.54	1.18E-04
mmu-mir-300	32.5	2.43	0.94	1.13	9.89E-05
mmu-mir-410	30.9	2.96	1.03	1.45	1.83E-06
mmu-mir-434-5p	24.2	2.84	1.18	1.38	0.003044
mmu-mir-212-3p	12.0	1.70	1.15	1.05	0.008502
mmu-mir-379	10.7	2.47	1.01	1.65	1.01E-05
mmu-mir-455	7.2	2.38	1.26	1.31	1.85E-04
mmu-mir-409-3p	6.7	2.68	1.19	1.21	2.58E-05
mmu-mir-341	5.9	3.09	0.89	1.1	1.86E-06
mmu-mir-673-5p	4.2	2.49	0.53	1.77	1.12E-05
mmu-mir-431	4.1	3.38	1.12	1.78	1.43E-05
mmu-mir-130b	3.8	3.36	0.89	1.89	8.00E-06
mmu-mir-134	3.7	3.65	1.22	1.73	1.50E-04
mmu-mir-34b-5p	2.8	2.98	0.95	1.72	0.003575
mmu-mir-298	2.6	5.37	1.2	1.84	2.30E-04
mmu-mir-299	2.3	2.65	0.81	1.17	1.77E-05

Figure 5. 2 MicroRNAs aberrantly expressed in pathological hypertrophy are normalized with enhanced PI3Kα signaling.

(A) Heat map and hierarchical clustering of miRNAs found to be aberrantly expressed in TAC-induced pathological hypertrophy and normalized with augmented myocardial PI3Kα signaling. Green denotes low expression; red, high expression. (B)The average PMMR, fold change (compared to WT sham) and *P* values (ANOVA) of each miRNA identified are listed.

5.3.3 Identification of novel miRNAs expressed in mouse ventricular tissue

One advantage of miRNA-Seq is the opportunity to discover novel miRNAs. Using a computational algorithm on the basis of miRNA biogenesis (Hackenberg *et al.*, 2009), we identified ~10 million unannotated mapped sequence reads that share characteristics of microRNAs. These sequence reads generated 896 alignment clusters. Of these, 543 had read counts ≥10 and these clusters were further filtered to exclude contamination from repetitive sequences and mRNA or noncoding RNA degradation products. Clusters with a read depths ≥100 were chosen for further analyses. A total of 246 of these identified clusters were subjected to subsequent analyses for miRNA precursor characteristics, including predicted folding structures and negative ΔG criteria (see Methods). Using the combined read depth and precursor characteristics criteria, we identified 26 putative miRNAs that were not in miRBase v.16. Interestingly, 15 of these putative miRNAs (**Online Supplemental Table S5.7**) were reported in miRBase v.18, which was updated in Nov 2011, validating the analytical approaches used. Among the remaining 11 novel miRNAs (**Online Supplemental Table S5.8**) identified in mouse LV, 3 were differentially regulated in WT+TAC, compared with WT sham, LV (**Figure 5.3A**). The predicted secondary structure and precursor sequence of one of these novel miRNAs (miR-cluster 16) are illustrated in **Figure 5.3B**. The expression of miR-cluster 16 and the two other novel miRNAs in WT sham and WT+TAC LV were also confirmed using qRT-PCR (**Figures 5.3C and 5.3D**).

A

Novel miRNAs that are differentially downregulated in pathological hypertrophy

Cluster ID	Strand	Mature sequence	WT Sham Mean PMMR	WT TAC/ WT Sham	P value
16	+	CACGGCGGCTGGAATTCCC	247.4	0.34	0.026
4	+	ACCATCTGTGGGATTATGACTGAACG	825.2	0.29	0.005
54	+	GGGGGCGTGGAATTATCGGGT	66.4	0.12	0.015

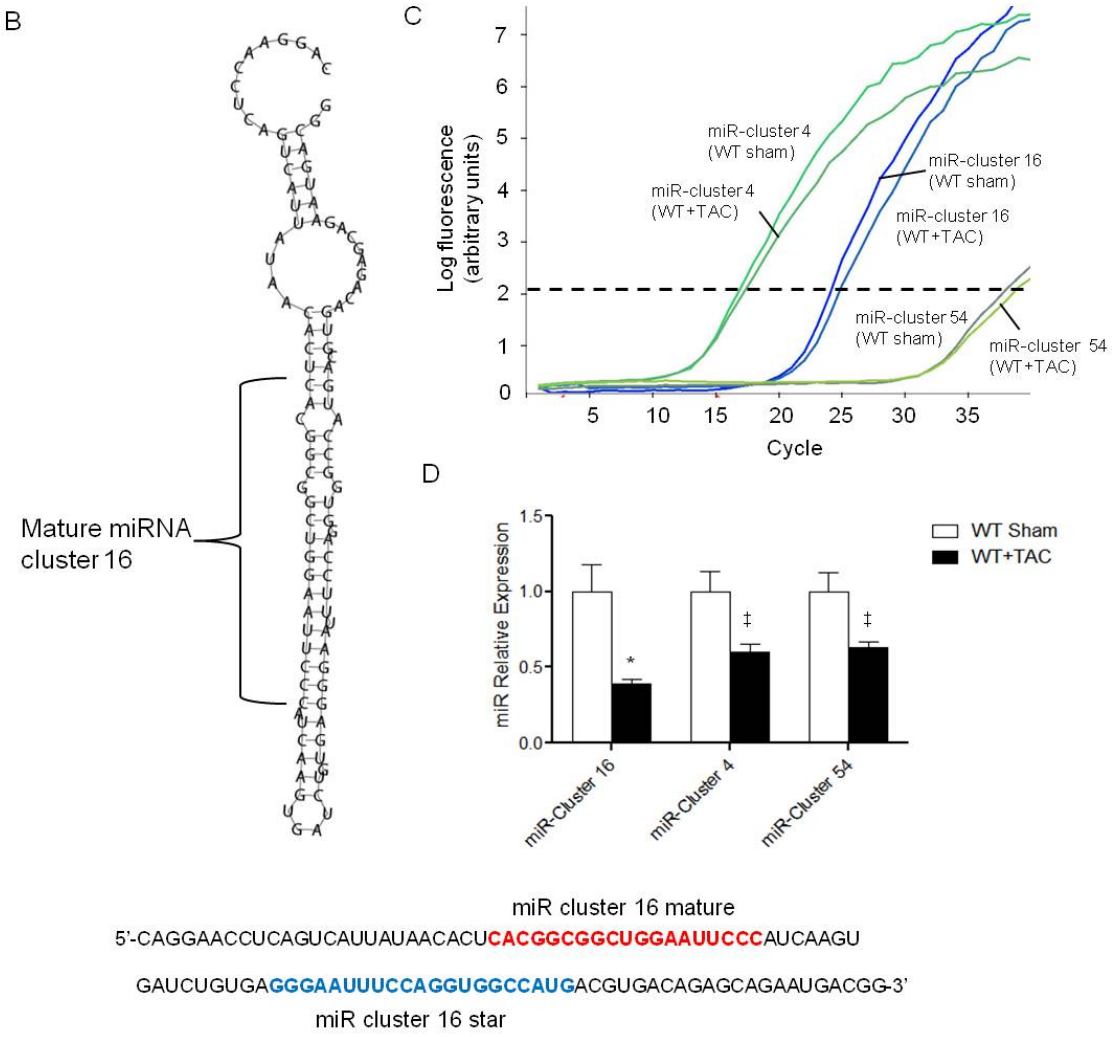

Figure 5. 3 Novel miRNAs identified in mouse ventricles are differentially expressed.

(A) Three novel miRNAs (miR-cluster 16, 4 and 54), identified by miRNA-seq, were differentially expressed in WT+TAC, compared with WT sham, LV. (B) Sequence and predicted secondary structure of the miR-cluster 16 precursor. The linear sequence with the mature miRNA sequence in red and miRNA star sequence in blue is also illustrated. (C) Representative qRT-PCR amplication plots for miR-cluster 16, 4 and 54 in WT sham and WT+TAC LV. Dotted line indicates fluorescence threshold for determining C_T values. (D) qRT-PCR confirmed the differential expression of miR-cluster 16, 4 and 54 in WT sham (n=6) and WT+TAC (n=6) LV. ($^{*}P<0.001$, $^{\ddagger}P<0.05$)

5.3.4 Parallel messenger RNA expression profiling in mouse LV with mRNA sequencing

To complete the functional transcriptome profiling, mRNA sequencing (mRNA-Seq) experiments were conducted in parallel to the miRNA-Seq. Eleven barcoded mRNA libraries were prepared from mouse LV samples (4 WT sham, 3 WT+TAC, 2 caPI3Kα sham and 2 caPI3Kα+TAC). A total of 242,851,107 sequence reads were generated from 2 HiSeq2000 flow cell lanes (**Table 5.1**), with an average sequencing depth of > 22 million reads per library. Among the 242 million sequence reads obtained, 84.5% (~205 million reads) were aligned to mm9 mouse genome, among which ~140 million reads (57.6% of total reads) were mapped within exon regions (**Table 5.1**). Read counts mapped to different isoforms of individual genes were pooled together to calculate the RPKM (reads per kilobase of exon per million mapped reads) value of each gene. These mRNA-Seq experiments were highly reproducible among biological replicates (**Supplemental Figure 5.5**).

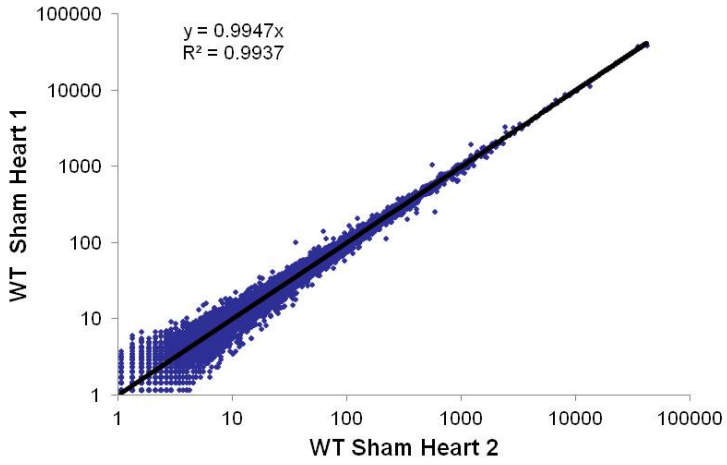

Supplemental Figure 5. 5 Scatter plot of normalized read counts between biological replicates reveals the reproducibility of mRNA-Seq experiments.

Scatter plot of the normalized mapped read counts annotated in the RefSeq database showed high degree of correlation (β=0.99, R^2=0.99) between biological replicates (WT sham heart 1 and 2), consistent with high reproducibility of the RNA-Seq experiments.

Using the cutoff value of 3 RPKM, which corresponds to expression level ≈1 copy per cell (Mortazavi *et al.*, 2008), we identified a total of 8989 genes that were expressed at ≥ 3 RPKM in at least one LV sample (**Online Supplemental Table S5.9**); 2638 genes were found to be differentially expressed (P<0.05, FDR of 0.05) among the four groups of LV samples (**Online Supplemental Table S5.10**). As an internal control, the expression level of the *pik3ca* gene was increased by 15-20 fold in every caPI3Kα, compared to WT, LV sample, consistent with the overexpression of the caPI3Kα transgene in these animals. The caPI3Kα sham LV share similar transcriptome signatures with WT sham LV, whereas the transcriptional signature of WT+TAC LV was distinct (**Figure 5.4**) from WT and caPI3Kα sham LV. In WT+TAC LV, for example, the activation of fetal gene program (*nppa, nppb* and *acta1*) (Hoshijima & Chien, 2002; Olson & Schneider, 2003) and increased expression of cardiac fibrosis genes (*col3a1, col5a2, col8a1, col15a1, col6a1*) were evident. Interestingly, consistent with the notion that enhancing PI3Kα signaling in pathological hypertrophy is protective, the expression levels of many of the genes identified as abnormally expressed in (compared with WT sham) WT+TAC LV were attenuated or normalized (in caPI3Kα+TAC LV) with increased myocardial PI3Kα signaling (**Figure 5.4**).

The self-organizing tree algorithm was applied to identify genes that were downregulated or upregulated in pathological hypertrophy, and normalized or reversed with increased PI3Kα signaling, i.e., the “protective PI3Kα mRNome”. These genes are presented in **Online Supplemental Table S5.11 and S5.12**. A total of 249 genes were found to be down-regulated in pathological LVH and normalized with increased PI3Kα signaling (**Figure 5.5A**).

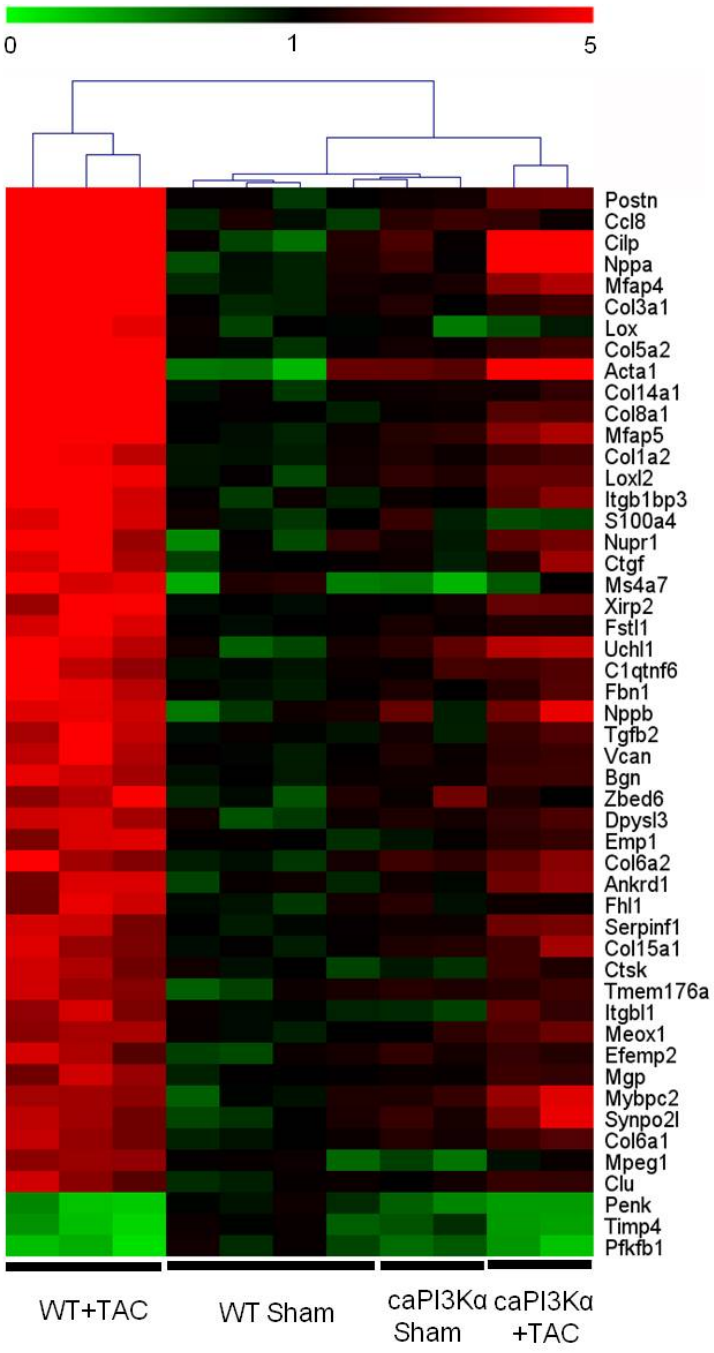

Figure 5. 4 Distinct mRNA expression profiles in pathological and physiological hypertrophy.

Heat map and hierarchical clustering of the top 50 differentially regulated mRNAs (ranked by *P* value) in WT sham, WT+TAC, caPI3Kα sham and caPI3Kα+TAC LV.

Gene ontology analysis of these 249 genes revealed an enrichment in mitochondrial, cellular catabolism, oxidation-reduction and lipid metabolism genes (**Figure 5.5B**), consistent with previous reports suggesting the critical role of PI3Kα signaling in maintaining homeostatic mitochondria biogenesis and lipid metabolism.(O'Neill *et al.*, 2007) The expression levels of 156 other genes, however, were found to be upregulated in WT+TAC LV, and reversed with enhanced PI3Kα signaling (**Figure 5.5C**); in this case, many genes linked to development, stress responses and the extracellular matrix were identified (**Figure 5.5D**), consistent with previous suggestions that PI3Kα signaling attenuates the activation of the fetal gene program and the fibrotic changes associated with pressure overload-induced LVH (McMullen *et al.*, 2007; Yang *et al.*, 2012). Interestingly, a number of genes involved in immune and inflammatory responses including *Il6, Il6st, Nfkb1,Tlr4, Vcam1, Icam2, Tnfrsf1a and Tnfrsf1b*, were also upregulated with TAC-induced pathological hypertrophy (**Supplemental Figure 5.6**), consistent with previous reports linking innate immunity/inflammatory responses and cardiac hypertrophy/LV dysfunction.(Mann, 2011; Valen, 2011; Masiha *et al.*, 2012) Interestingly, the upregulation of these nflammatory markers by TAC was also markedly blunted with increased PI3Kα signaling (**Supplemental Figure 5.6**).

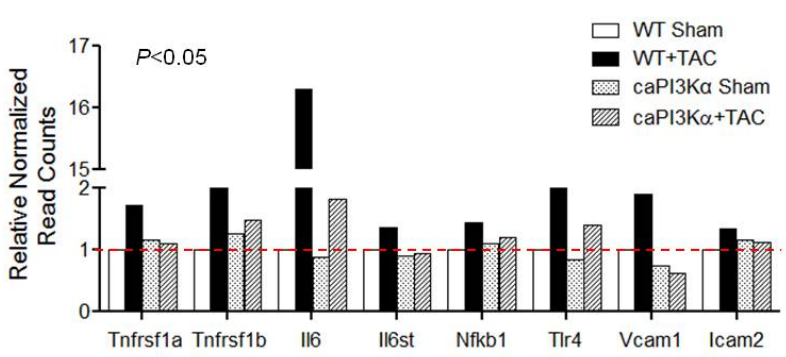

Supplemental Figure 5. 6 Enhanced PI3Kα signaling normalizes inflammatory markers that are increased with TAC-induced pathological hypertrophy.

Averaged normalized read count of genes involved in inflammatory responses (*Il6, Il6st, Nfkb1,Tlr4, Vcam1, Icam2, Tnfrsf1a and Tnfrsf1b*). Normalized read count data were expressed relative to the mean WT sham value.

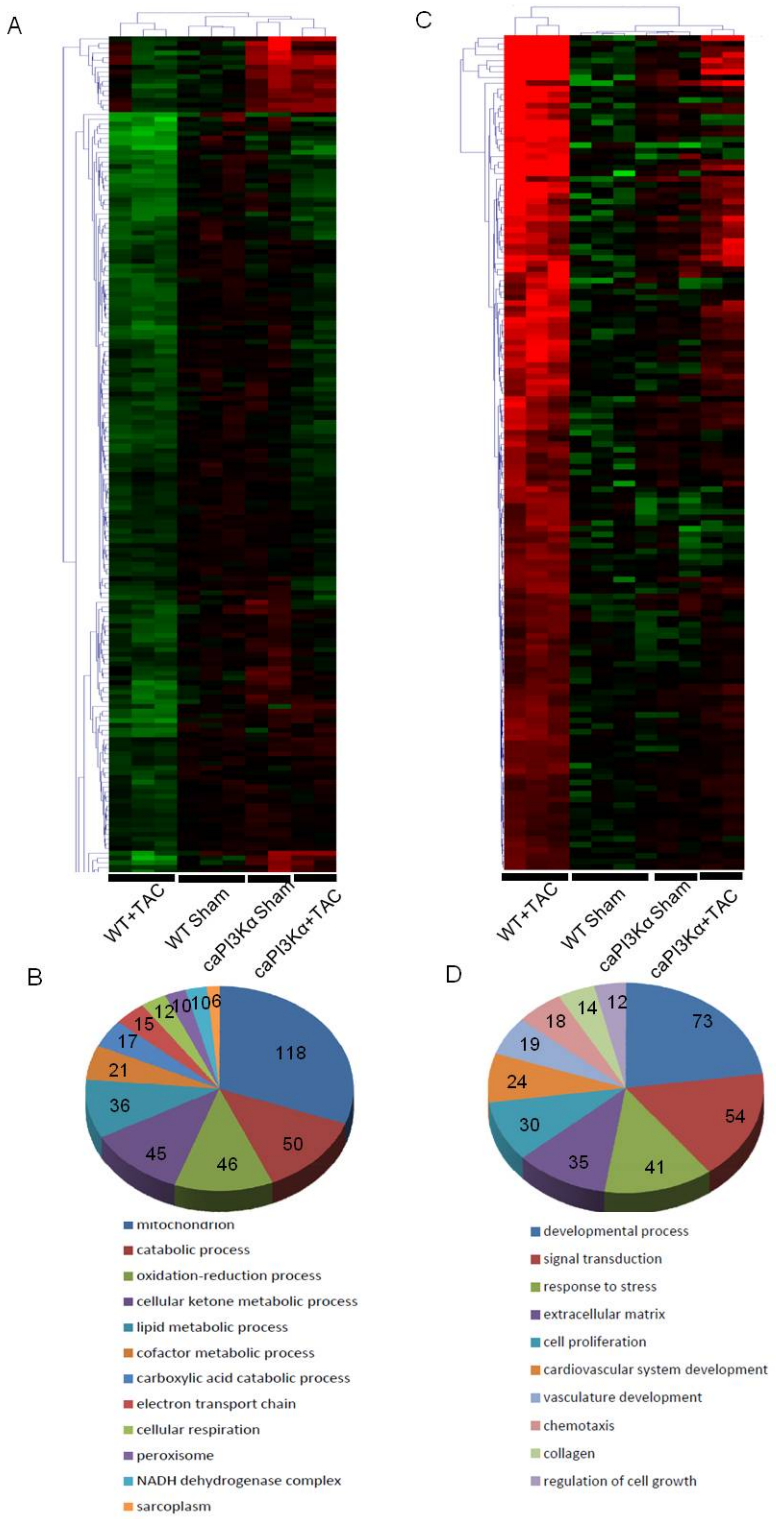

Figure 5. 5 Transcripts increased/decreased with pathological hypertrophy and normalized with enhanced PI3Kα signaling are segregated to distinct functional groups.

(A) Unsupervised hierarchical clustering of the transcripts that were downregulated in pathological hypertrophy and normalized with enhanced PI3Kα signaling. (B)Gene ontology analysis revealed enrichment of genes that are required for normal myocardial functioning, including mitochondrial regulation, cellular catabolism, oxidation/reduction, electron transport, and lipid metabolism. (C) Unsupervised hierarchical clustering of the genes that were upregulated in pathological hypertrophy and normalized with enhanced PI3Kα signaling; gene ontology analysis revealed enrichment of genes involved in maladaptive myocardial responses to pathological stimuli, including genes involved in development, stress responses and extracellular matrix formation (D).

5.3.5 MicroRNA-21 involved in the inhibition of cardiac fibrosis by enhanced PI3Kα signaling

Enhanced PI3Kα signaling has been shown to reduce cardiac fibrosis in pathological LVH induced by pressure overload (McMullen *et al.*, 2007). Indeed, the upregulation of fibrosis genes, including collagens, fibronectin (*fbn1*), fibrillin (*fn1*) and connective tissue growth factor (*ctgf*), in TAC-induced LVH was largely abrogated with enhanced myocardial PI3Kα signaling (**Figure 5.6A**). Interestingly, miR-21, which has been shown to promote tissue fibrosis in pulmonary (Liu *et al.*) and cardiac (Thum *et al.*, 2008) disease, was highly upregulated in response to TAC, and this upregulation was significantly attenuated with increased PI3Kα signaling (**Figure 5.2A,B**). It has been shown that miR-21 promotes cardiac fibrosis through translational suppression of *Sprouty-1*, which inhibits the pro-fibrotic ERK-MAPK signaling pathway (Thum *et al.*, 2008). Consistent with this, *Sprouty-1* protein expression was significantly (P<0.05) decreased in WT+TAC, compared with WT sham, LV. The downregulation of *Sprouty-1* protein in response to TAC, however, was reversed with increased PI3Kα signaling (**Figure 5.6B**). In addition, components of the TGF-β pathway, a potent miR-21 activator (Davis *et al.*, 2008; Cottonham *et al.*, 2010), including *tgfb2*, *tgfbr1* and *tgfbr2*, were upregulated with TAC, and suppressed with increased PI3Kα activity (**Figure 5.6A**). These results suggest that enhanced PI3Kα signaling inhibits cardiac fibrosis through reducing TGF-β signaling and the repression of the pro-fibrotic miR-21.

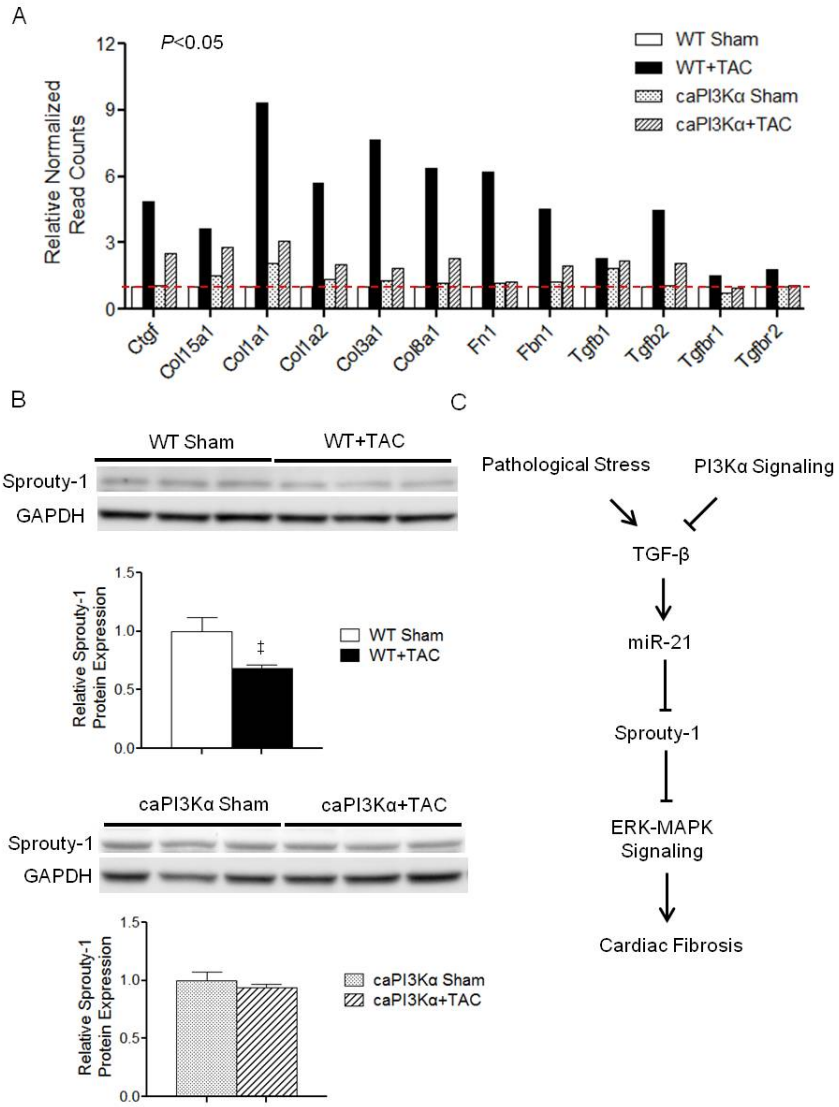

Figure 5. 6 Enhanced PI3Kα signaling in pathological hypertrophy attenuates TGF-β and miR-21 expression, in pathological hypertrophy, maintaining Sprouty-1 protein expression and reducing fibrosis.

(A) Averaged normalized read count of genes linked to fibrosis (*Ctgf, Col15a1, Col1a1, Col1a2, Col3a1, Col8a1, Fn1* and *Fbn1*) or the TGF-β pathway (*Tgfb1, Tgfb2, Tgfbr1* and *Tgfbr2*) in WT sham, WT+TAC, caPI3Kα sham and caPI3Kα+TAC LV. Normalized read count data were expressed relative to the mean WT sham value. (B) Representative Western blot of fractionated LV proteins from WT sham, WT+TAC, caPI3Kα sham and caPI3Kα+TAC LV (n=4-5 in each group) probed with anti-sprouty1 and anti-GAPDH antibodies. The expression levels of each protein on each blot were measured and normalized to the expression of GAPDH of the same sample on the same blot. Protein expression data were expressed relative to the mean value of WT sham LV samples. The mean ± SEM relative expression level of *Sprouty*-1 was significantly (‡P<0.05) lower in WT+TAC than in WT sham, LV. The downregulation of the *Sprouty*-1 protein with TAC, however, was abrogated with enhanced PI3Kα signaling. (D) Schematic of proposed mechanism underlying PI3Kα-mediated suppression of cardiac fibrosis in pathological hypertrophy induced by pressure-overload.

5.4 Discussion

5.4.1 MicroRNA sequencing revealed protective mirna expression signature of enhaned PI3Kα signaling

The comparative analyses of miRNA expression in WT sham, WT+TAC, caPI3Kα sham and caPI3Kα+TAC LV samples allowed the identification of the "protective PI3Kα microRNome" in the setting of pathological hypertrophy. As described above and detailed in **Online Supplemental Table S5.6**, the increased expression of many of these miRNAs have been shown to contribute to various myocardial pathologies. For example, miR-199a-5p, miR-214 and miR-212 have all been shown to be upregulated in murine models of pathological hypertrophy (van Rooij *et al.*, 2006; Cheng *et al.*, 2007; Sayed *et al.*, 2007) and in human failing hearts (van Rooij *et al.*, 2006; Thum *et al.*, 2007; van Rooij *et al.*, 2008), and overexpression of miR-199a-5p, miR-214 or miR-212 in murine myocytes led to hypertrophic growth and activation of fetal gene program (van Rooij *et al.*, 2006; Jentzsch *et al.*, 2011). The observation that enhanced PI3Kα signaling suppresses the expression of these disease-causing miRNAs suggests that the anti-pathological-hypertrophy effects of PI3Kα signaling are mediated, at least in part, by normalizing the expression of these "pathological miRNAs". Previous attempts to modulate the pathological expression of these miRNAs have consisted largely of eliminating or reducing them, one or two miRNAs at a time. Interestingly, however, this approach seems to have only very small to moderate beneficial effects likely reflecting the inherent complexity of the signaling networks involved (Matkovich *et al.*; van Rooij, 2011). The observation that enhanced PI3Kα signaling results in the marked and simultaneous suppression of multiple "pathological miRNAs" suggests a novel therapeutic approach: modulating the expression of multiple disease-causing miRNAs concurrently. This strategy has the potential of impacting multiple signaling pathways

which would be expected to have a greater effect on disease progression and severity than knocking down individual miRNAs.

The analytical approach developed and used here allowed the identification of 13 novel miRNA* of known mature miRNA genes and 11 novel miRNAs. Importantly, of the >10 million sequence reads analyzed, up to 896 clusters were predicted to be putative mouse miRNAs. Of these, 246 clusters were detected at >100 reads, and 26 putative miRNAs met all the criteria of “novel miRNA”, of these, 15 were updated in the most recent (November 2011) miRNAbase, leaving 11 truely novel miRNAs. The low yield of novel miRNAs identified in these experiments has two interpretations. First, a large fraction of the “putative miRNA” reads may represent low-abundance hairpin species that were occasionally processed by the Drosha-Dicer miRNA biogenesis machinery. Secondly, it is possible that most mouse miRNAs have already been identified and annotated, as recent studies using large-scale cloning approaches to identify novel mammalian miRNAs yielded only a few uncharacterized, low-abundance miRNAs (Landgraf *et al.*, 2007; Basso *et al.*, 2009). Importantly, however, we cannot exclude the possibility that the stringent criteria used might have filtered out some miRNAs expressed at very low levels but that, nevertheless, are of biological significance. Regardleess, additional experiments are needed to determine the functional roles of the novel miRNAs identified in the studies here.

In the miRNA sequencing experiments detailed here, a small number (~10-20) of highly abundant miRNAs were identified that account for the majority of the mature miRNA species expressed in the adult mouse LV (**Figure 5.1C,D**). Although this observation is similar to previously published miRNA-Seq findings in the mouse heart (Rao *et al.*, 2009), the relative abundances of the highly expressed miRs in the previous report by

Rao et al were different than those determined here. The most abundant miRNA in Rao et al (Rao *et al.*, 2009), which accounted for ~40% of the total miRNA reads, was miR-1. Here, however, miR-1 ranked #20 in abundance and accounted for only ~1% of the total miRNA reads (**Figure 5.1C and Online Supplemental Table S5.3**). Although the use of different sequencing platforms or library construction approaches might be expected to cause minor read count differences (Fehniger *et al.*, 2010), it is unlikely that either could contribute significantly to the differences observed in these two studies. It seems more likely the apparent discrepancy in the findings may reflect the fact that whole heart samples were used by Rao et al (Rao *et al.*, 2009), whereas only LV was used in the studies here. Because of the highly sensitive and quantitative nature of deep sequencing experiments (Pais *et al.*, 2011), regional differences in relative miRNA expression levels will impact quantitative analyses.

5.4.2 Combined miRNA-Seq and mRNA-Seq analyses provide a transcriptome framework to explore novel mechanisms underlying the pathobiology of cardiac hypertrophy

The mechanisms through which miRNAs regulate biological process are translational inhibition or mRNA degradation of the miRNA targets (Ambros, 2004; van Rooij, 2011). It has been argued recently that mRNA destabilization accounts for most of miRNA-mediated gene modulation (Baek *et al.*, 2008; Selbach *et al.*, 2008), and that up to 84% of the protein level changes caused by miRNA regulation can be attributed to altered mRNA expression (Guo *et al.*, 2010). To understand the functional impact of miRNA regulation, therefore, it is pivotal to examine the target mRNA expression levels concomitantly in the same biological context.

Combining miRNA-Seq and mRNA-Seq datasets allows direct assessment of the reciprocal expression of a given miRNA and its known/predicted target transcripts. Using this approach, miR-21 was identified as a potential candidate through which increased PI3Kα signaling protects against cardiac fibrosis induced by TAC. A mechanistic model was proposed on the basis of these findings (**Figure 5.6C**): upon pressure-overload, the TGF-β signaling pathway is activated and promotes the expression of miR-21 in cardiac fibroblasts, resulting in the translational suppression of the protein, *Sprouty-1*, which tonically suppresses the activation of pro-fibrotic ERK-MAPK signaling; ERK-MAPK signaling, therefore, is released from tonic inhibition by *Sprouty-1*, resulting in increased cardiac fibrosis. The augmentation of cardiac PI3Kα signaling, however, abrogates the activation of TGF-β signaling, leading to blunted miR-21 expression and the maintenance of *Sprouty-1* expression, keeping the ERK-MAPK signaling inhibited and preventing the development of cardiac fibrosis. Additional *in vitro* and *in vivo* experiments are needed to test this hypothesis directly.

In addition, the mRNA-seq experiments also uncovered functional transcriptome changes that suggest possible mechanisms underlying the protective effects of PI3Kα signaling against pathological hypertrophy (**Figure 5.5**). On the transcriptional level, pressure-overload impairs cardiac functioning through: (1) suppressing the expression of genes required for normal cardiac functioning, including genes involved in regulating mitochondrial function, oxidative-reduction, and lipid metabolism; and, (2) maladaptively upregulating the fetal gene program, inflammation, stress-response and extracellular matrix genes. The results here demonstrate that increased PI3Kα signaling ameliorates the aberrant expression of genes that are upregulated and genes that are downregulated, thereby providing multiple cardioprotective effects.

In conclusion, the studies presented here utilized next-generation sequencing technologies for comprehensive cardiac miRNA and mRNA expression profiling in mouse LV and identified multiple miRNAs and mRNAs that were abnormally expressed in pathological hypertrophy and normalized with enhanced PI3Kα signaling. Several novel miRNAs of potential significance in cardiac hypertrophy were also identified. Combined miRNA and mRNA analyses revealed that increased PI3Kα signaling reduces cardiac fibrosis in pathological hypertrophy through modulating TGF-β signaling and attenuating miR-21 expression. In addition, the TAC-induced maladaptive remodeling were ameliorated with increased PI3Kα signaling and were associated with the normalization of the pathological, disease-causing miRNAs including miR-199a-5p, miR-214 and miR-212. These results demonstrate not only the strength and robustness of next-generation sequencing in exploring the cardiac transcriptome architecture and dynamics in physiological and pathological contexts, but also the potential molecular mechanisms underlying the cardioprotective effects of increased PI3Kα signaling in the setting of pathological hypertrophy.

Chapter 6: Conclusions

6.1 Overview

Repolarizing K^+ currents, including voltage-gated K^+ (Kv) and inwardly rectifying (Kir) currents, are the major determinants of myocardial action potential repolarization. Alterations in the expression of myocardial repolarizing K^+ currents can lead to changes in resting membrane properties, in the shapes and durations of action potentials, as well as the myocardial excitability. Considerable evidence has shown that electrical remodeling, particularly the reductions in densities of repolarizing K^+ currents, occurs in LV dysfunction, including pathological cardiac hypertrophy (Mayet *et al.*, 1996; McIntyre & Fry, 1997) and heart failure (Beuckelmann *et al.*, 1993), leading to arrhythmogenic ventricular action potential prolongation, increased dispersion of repolarization, and subsequently increased propensity for life-threatening arrhythmias and sudden cardiac death (Tomaselli *et al.*, 1994; Haider *et al.*, 1998). Despite advances in pharmacological and device therapies for LV dysfunction to inhibit the maladaptive, pathological changes, ion channel remodeling, one of the fundamental mechanisms underlying the increased arrhythmogenecity with various myocardial diseases, has not been successfully targeted (Jessup & Brozena, 2003).

Exercise training-induced physiological hypertrophy, in contrast to pathological LVH or heart failure, is not associated with electrical abnormalities or increased arrhythmia risk (Mayet *et al.*, 1999; Biffi *et al.*, 2008). In fact, aerobic exercise training has been shown to reduce repolarization abnormalities and sudden-death rate in heart failure patients (Ali *et al.*, 1999), as well as in animal models of LV dysfunction (Lachance *et al.*, 2009). These observations clearly suggest that electrical remodeling occurs in response to exercise training to maintain the normal myocardial function. Considerable evidence

suggests that aerobic exercise provides multiple beneficial effects on the myocardium, including increased myocardial perfusion (Hambrecht *et al.*, 2000b), improved myocardial energy metabolism (O'Neill *et al.*, 2007), reduced myocardial fibrosis (McMullen *et al.*, 2003), and/or maintained calcium handling (Medeiros *et al.*, 2008), many of which have been attributed to increased PI3Kα signaling in response to exercise training.

The studies here were conducted to test directly the hypothesis that beneficial ion channel remodeling occurs with exercise training and enhanced PI3Kα activity, and to explore the signaling mechanisms underlying this exercise training- (PI3Kα-) mediated electrical remodeling. The hypothesis that increased PI3Kα signaling will counteract the adverse electrophysiological remodeling, including decreased K^+ current densities, impaired repolarization, and increased risk of lethal ventricular arrhythmias, associated with pathological hypertrophy and heart failure, was also tested. Finally, combined miRNA- and mRNA-sequencing analyses were applied to explore the mechanisms by which enhanced PI3Kα signaling provides cardioprotective effects, minimizing pathological remodeling, in a mouse model of TAC-induced pathological hypertrophy.

6.2 Exercise training and PI3Kα activation lead to transcriptional upregulation of myocardial ion channel subunits independent of cellular hypertrophy and Akt

The results presented here demonstrate that physiological hypertrophy, induced by chronic exercise (swim) training or transgenic increases in PI3Kα signaling, is associated with increases in myocardial repolarizing K^+, as well as depolarizing Na^+ and Ca^{2+}, currents, reflecting increased expression of the transcripts encoding the underlying ion

channel subunits. The transcriptional upregulation of ion channel subunits with physiological hypertrophy is in proportion to increased myocyte size and the global increases in RNA and protein expression, resulting in the maintenance of ionic current densities and myocardial electrical excitability. Further experiments revealed that exercise training and enhanced PI3Kα signaling-mediated transcriptional upregulation of myocardial ion channel subunits is independent of cellular hypertrophy and Akt signaling.

Interestingly, recent studies in a mouse model of TAC-induced pathological hypertrophy have shown repolarizing K^+ channel subunit expression levels are not increased in proportion to the increased total RNA synthesis and the hypertrophic growth and, as a result, K^+ current densities are decreased (Marionneau *et al.*, 2008b). The disconnect between the global increases in RNA synthesis and the transcriptional regulationof ion channel subunits in TAC-induced hypertrophy (Hannan *et al.*, 2003), together with the hypertrophy-independent transcriptional upregulation of channel subunits in response to exercise training or increased PI3Kα signaling imply a unique regulatory mechanism coordinating myocardial ion channel gene expression, that is independent of the general transcriptional machinery that is robustly activated in response to hypertrophic stimuli, such as pressure overload or exercise training.

In addition, it has been recently shown that PI3Kα activation is critical in mediating myocardial metabolic remodeling in physiological hypertrophy, including increased capacity to oxidize fatty acids/glucose and increased mitochondrial biogenesis, and that these metabolic remodeling effects are also Akt-independent (O'Neill *et al.*, 2007). Taken together, these results demonstrate that PI3Kα signaling exerts distinct biological effects

on the myocardium through divergent downstream pathways: Akt1-dependent physiological cardiac growth, Akt2-dependent insulin-sensitization and cellular survival, as well as Akt-independent metabolic and electrical remodeling. The signaling mechanisms of how PI3Kα mediates the Akt-independent metabolic and electrical effects are not well-understood; although it has been suggested that PKCλ/ζ could be the potential downstream effecter that is required for PI3Kα-mediated metabolic remodeling (O'Neill *et al.*, 2007). Further studies are required to identify the downstream signaling effectors that mediate myocardial electrical remodeling in response to PI3Kα activation.

6.3 Enhancing myocardial PI3Kα activity as a novel therapeutic approach to ameliorate arrhythmogenic LV dysfunction

The increased incidence of life-threatening ventricular arrhythmias in patients with pathological hypertrophy and heart failure is a consequence of complex pathological remodeling in cardiac structural (Akar *et al.*, 2004), neurohumoral (Vaseghi & Shivkumar, 2008) and electrophysiological properties (Beuckelmann *et al.*, 1993; Kaab *et al.*, 1998; Li *et al.*, 2002; Akar *et al.*, 2005; Marionneau *et al.*, 2008b). Traditional approaches used in the clinical management of heart failure, specifically pharmacological (Kober *et al.*, 1995; Pitt *et al.*, 1999) and device therapies (Moss *et al.*, 2009), are largely aimed at inhibiting the maladaptive neurohumoral signaling and structural abnormalities accompanying LV dysfunction. Targeting the electrophysiological derangements using anti-arrhythmic agents has proven to be ineffective and, indeed, has been associated with increased, rather than decreased, mortality (CAST, 1989). The results presented here demonstrate that increased PI3Kα signaling in pathological hypertrophy and heart failure helps to normalize ventricular

repolarization and maintain electrical functioning through the transcriptional upregulation of repolarizing K^+ channels, a mechanism of action *distinct* from classic heart failure therapeutics.

A simple and practical approach to increasing cardiac PI3Kα signaling is aerobic exercise training (McMullen *et al.*, 2003; Yang *et al.*, 2010). Indeed, aerobic exercise training has been shown to improve LV function and prolong survival in heart failure patients (Coats, 2011), as well as in animal models of heart failure (McMullen *et al.*, 2007; Lachance *et al.*, 2009). These results suggest a novel proactive, physiologic therapeutic approach against the increased arrhythmogenecity with LV dysfunction, which may synergize with traditional heart failure therapeutics and improve patient outcomes.

6.4 Deep sequencing revealed mechanisms underlying the protective effects of increased PI3Kα signaling in pathological hypertrophy/heart failure

PI3Kα signaling plays multiple roles in the myocardium, including the regulatioin of myocyte growth, hypertrophy, proliferation, survival, metabolism, aging and regeneration (Cantley, 2002; Sussman *et al.*, 2011). Accumulating evidence suggests that augmentation of PI3Kα signaling is beneficial in various cardiac diseases, including pathological hypertrophy (McMullen *et al.*, 2007; Yang *et al.*, 2012), myocardial infarction (Lin *et al.*, 2010), diabetic cardiomyopathy (Huynh *et al.*), atrial fibrillation (Pretorius *et al.*, 2009), and heart failure (McMullen *et al.*, 2007; Yang *et al.*, 2012), normalizing the detrimental molecular and structural remodeling resulting from pathological stimuli. The mechanisms underlying the cardioprotective effects provided by increased PI3Kα signaling, however, remain poorly understood.

The studies presented here utilized next-generation sequencing technologies for a comprehensive cardiac miRNA and mRNA expression profiling in pathological and physiological hypertrophy. These analyses identified multiple miRNAs and mRNAs that were aberrantly expressed in pathological hypertrophy but normalized with enhanced PI3Kα signaling, revealing the "protective PI3Kα microRNome and mRNome". The combined miRNA and mRNA analyses, for example, revealed that increased PI3Kα signaling reduces cardiac fibrosis in pathological hypertrophy through modulating TGF-β signaling and miR-21 expression. In addition, TAC-induced pathological remodeling is blunted with enhanced PI3Kα signaling and is associated with the repression of pathological, disease-causing miRNAs including miR-199a-5p, miR-214 and miR-212. Several novel miRNAs of potential significance in cardiac hypertrophy were also identified.

6.5 Impact of studies

The studies completed and presented here have revealed that electrical remodeling distinguishes exercise training-induced physiological, from stress-induced pathological, cardiac hypertrophy. While pathological hypertrophy is associated with abnormal electrical functioning, including arrhythmogenic action potential prolongation and increased repolarization dispersion (Mayet *et al.*, 1996; McIntyre & Fry, 1997), physiological hypertrophy is not associated with electrical abnormalities or increased arrhythmia risk. The experiments here revealed that the electrophysiological differences between pathological and physiological hypertrophy resulted from the differences in the transcriptional regulation of repolarizing K^+ channel subunits: transcripts encoding K^+ channel subunits fail to upregulate in proportion to cellular hypertrophy with pathological hypertrophy, resulting in reduced K^+ current densities and subsequent arrhythmogenic

changes. In contrast, K^+ channel subunit transcripts are upregulated in parallel with the increase in myocyte size with physiological hypertrophy, maintaining K^+ current densities and electrical functioning. The results here also demonstrate that PI3Kα signaling plays a critical role in mediating the electrical remodeling observed with physiological hypertrophy, and that PI3Kα signaling-mediated electrical remodeling is actually independent of cellular hypertrophy and Akt. These studies provide novel insights in the role of PI3Kα signaling pathway in the transcriptional regulation of myocardial ion channels.

The results presented here also demonstrate that increased PI3Kα signaling in pathological hypertrophy and heart failure can normalize ventricular repolarization and maintain electrical functioning through the transcriptional upregulation of repolarizing K^+ channels. These results suggest that enhancing myocardial PI3Kα signaling, either through exercise training or pharmacologic agents, could directly address the electrophysiological basis of life-threatening arrhythmias associated with pathological LVH and heart failure. These observations, therefore, could lead to the development of novel heart failure treatments via a mechanism of action distinct from classic heart failure therapeutics.

Finally, the studies here established a molecular and bioinformatic pipeline that permits comprehensive quantification and analyses of myocardial miRNA and mRNA expression with next-generation sequencing, and applied this approach to define the impact of enhanced PI3Kα signaling on myocardial transcriptome structure in the setting of pressure overload-induced pathological hypertrophy. The results from these studies not only demonstrate the strength and robustness of next-generation sequencing in efforts to define the cardiac transcriptome architecture and dynamics in physiological and

pathological contexts, but also reveal the protective transcriptome signature of enhanced PI3Kα signaling in pathological hypertrophy, as well as the potential molecular mechanisms underlying the cardioprotective effects of increased PI3Kα signaling. The approach described provides a comprehensive yet straightforward set of methods to quantify and analyze myocardial transcritpome, methods that could be exploited in studies on normal and disease human hearts to provide important new insights into disease mechanisms and novel therapeutic targets.

6.6 Future directions

Increasing evidence suggests that myocardial Kv and Kir channels function in macromolecular complexes, comprising pore-forming α subunits, a number of cytosolic and transmembrane accessory subunits, as well as regulatory, cytoskeletal, and signaling proteins (Sanguinetti *et al.*, 1996; Shi *et al.*, 1996; Manganas & Trimmer, 2000; Aimond *et al.*, 2005; Nerbonne & Kass, 2005; Radicke *et al.*, 2005; Radicke *et al.*, 2006; Niwa & Nerbonne, 2010; Pongs & Schwarz, 2010). Various signaling molecules have been shown to modulate functional K^+ current expression through regulating channel activity, channel subunit stability or trafficking, including calmodulin kinase II (CaMKII) (Li *et al.*, 2006), cAMP-dependent protein kinase (PKA) (Anderson *et al.*, 2000; Gallego *et al.*, 2005), protein kinase C (PKC) (Schrader *et al.*, 2009), and extracellular signal regulated kinase (ERK) (Schrader *et al.*, 2006; Schrader *et al.*, 2009). Interestingly, many of these signaling molecules also play critical roles in regulating the development of cardiac hypertrophy (Frey & Olson, 2003; Dorn & Force, 2005) and, like PI3Kα, have been shown to modulate K^+ channel subunit expression transcriptionally. For example, in neonatal rat ventricle, activation of PKC negatively regulates *Kcnip2* (KChIP2) expression , and this PKC-dependent transcriptional suppression of KChIP2 was shown to be mediated by the ERK pathway (Jia & Takimoto, 2006). In addition, calcineurin (Rossow *et al.*, 2006) and NFAT (Amberg *et al.*, 2004; Rossow *et al.*, 2004), two downstream targets of Gq/11 protein kinase, the signaling nexus mediating pathological hypertrophy, have been shown to negatively regulate K^+ channel (Kv1.5, Kv2.1, Kv4.2 and Kv4.3) transcript expression. The links between these hypertrophy-related signaling pathways and the transcriptional networks regulating the expression of K^+ channel subunit genes, however, have not been defined. Future studies focused on determining how the signaling pathways activated on pathological hypertrophy prevent the transcriptional upregulation of the transcripts encoding ion channels subunits in

proportion to the global increase in mRNA/protein expression. The studies completed here demonstrate that transcriptional upregulation of K^+ channel subunits induced by enhanced PI3Kα signaling is Akt-independent. These results argue for further research focused on dissecting the downstream signaling mechanisms through which enhanced PI3Kα activities mediates electrical remodeling. Further studies aimed at delineating the links between cellular signaling pathways and the transcriptional (and post-transcriptional) regulation of K^+ channel (and other ion channel) genes are also needed. Insights gained from these studies could provide more direct and specific strategies to reverse ion channel dysregulation, and the resulting generation of arrhythmogenic substrates, in cardiomyopathy and heart failure.

The studies completed here also demonstrate that enhancing cardiac PI3Kα signaling mitigates the increased arrhythmogenicity associated with pathological hypertrophy and heart failure, observations which suggest that possible therapeutic potential of pharmacological agents that activate PI3Kα signaling in human failing hearts. Clearly, studies aimed at exploring this hypothesis directly are needed. Interestingly, growth hormone (GH) and IGF-1 , two endogenous neurohumoral agonists that can activate cellular PI3Kα signaling, have been tested as experimental heart failure therapeutics in animal models (Yang *et al.*, 1995; Duerr *et al.*, 1996; Cittadini *et al.*, 1997) and human patients (Fazio *et al.*, 1996; Osterziel *et al.*, 1998; Genth-Zotz *et al.*, 1999). Animal studies have demonstrated that the administration of GH or IGF-1 confers beneficial effects on cardiac structural remodeling, contractile function and survival in heart failure (Yang *et al.*, 1995; Duerr *et al.*, 1996; Cittadini *et al.*, 1997). Initial human studies also showed that recombinant GH therapy resulted in improvements in LV performance, hemodynamics, exercise capacity and clinical symptoms in patients with moderate to

advanced heart failure (Fazio *et al.*, 1996; Osterziel *et al.*, 1998; Genth-Zotz *et al.*, 1999). Subsequent randomized, placebo-controlled trials, however, failed to confirm significant beneficial effects of chronic GH therapy in heart failure patients (Isgaard *et al.*, 1998; Smit *et al.*, 2001; Acevedo *et al.*, 2003). The lack of beneficial effects of GH administration in these larger studies may reflect the development of GH resistance, which has been described in patients with heart failure and other chronic illnesses (Anker *et al.*, 1997; Van den Berghe *et al.*, 1999). Using IGF-1, instead of GH, would avoid the issue of GH resistance, although, to date, there have been no studies that have investigated the impact of direct IGF-1 administration in patients with heart failure. Importantly, none of the studies conducted to date have investigated the effects of increased GH/IGF-1 on cardiac electrical functioning in the setting of LV dysfunction (Fazio *et al.*, 1996; Osterziel *et al.*, 1998; Genth-Zotz *et al.*, 1999). Future studies, therefore, should also include an emphasis on investigating the effect(s) of increasing IGF-1 signaling on electrical remodeling and arrhythmia risk in animal models and patients with LV dysfunction. The results presented here also argue for further research focused on developing pharmacological agents or biological approaches to activate PI3Kα signaling directly in the human heart, as well as on detailing the effects of these manipulations on arrhythmia vulnerability and sudden cardiac death.

Additional studies here applied next-generation sequencing technologies in myocardial transcriptome profiling. These analyses identified miRNAs and mRNAs that are implicated in the molecular mechanisms underlying PI3Kα-mediated cardioprotective effects. Future studies should focus on investigating the mechanisms through which PI3Kα signaling modulates the aberrantly expressed miRNAs and mRNAs involved in pathological myocardial remodeling. It was also recently reported that deep sequencing

can be exploited for in-depth, genome-wide, analyses of the expression of cardiac transcript isoforms, as well as for the identification of novel spliced exons, alternative terminal exons, novel genes, long noncoding RNAs (lncRNAs) and long intergenic noncoding RNAs (lincRNAs) (Lee *et al.*, 2011), further demonstrating the power and feasibility of applying deep sequencing methods to detail the complex cardiac transcriptome at individual exon and transcript levels. Taken together, these results argue that next-gen sequencing approaches could be used to re-evaluate cardiac transcriptome remodeling in human cardiovascular diseases, such as heart failure and cardiomyopathy, to advance our understanding of the mechanisms underlying disease processes, as well as to identify novel therapeutic targets.

References

Abbott GW, Xu X & Roepke TK. (2007). Impact of ancillary subunits on ventricular repolarization. *J Electrocardiol* **40,** S42-46.

Acevedo M, Corbalan R, Chamorro G, Jalil J, Nazzal C, Campusano C & Castro P. (2003). Administration of growth hormone to patients with advanced cardiac heart failure: effects upon left ventricular function, exercise capacity, and neurohormonal status. *Int J Cardiol* **87,** 185-191.

Adamson PB & Vanoli E. (2001). Early autonomic and repolarization abnormalities contribute to lethal arrhythmias in chronic ischemic heart failure: characteristics of a novel heart failure model in dogs with postmyocardial infarction left ventricular dysfunction. *J Am Coll Cardiol* **37,** 1741-1748.

Aimond F, Kwak SP, Rhodes KJ & Nerbonne JM. (2005). Accessory Kvbeta1 subunits differentially modulate the functional expression of voltage-gated K+ channels in mouse ventricular myocytes. *Circ Res* **96,** 451-458.

Akar FG, Laurita KR & Rosenbaum DS. (2000). Cellular basis for dispersion of repolarization underlying reentrant arrhythmias. *J Electrocardiol* **33 Suppl,** 23-31.

Akar FG, Spragg DD, Tunin RS, Kass DA & Tomaselli GF. (2004). Mechanisms underlying conduction slowing and arrhythmogenesis in nonischemic dilated cardiomyopathy. *Circ Res* **95,** 717-725.

Akar FG & Tomaselli GF. (2005). Conduction abnormalities in nonischemic dilated cardiomyopathy: basic mechanisms and arrhythmic consequences. *Trends Cardiovasc Med* **15,** 259-264.

Akar FG, Wu RC, Juang GJ, Tian Y, Burysek M, Disilvestre D, Xiong W, Armoundas AA & Tomaselli GF. (2005). Molecular mechanisms underlying K+ current downregulation in canine tachycardia-induced heart failure. *Am J Physiol Heart Circ Physiol* **288,** H2887-2896.

Ali A, Mehra MR, Malik FS, Lavie CJ, Bass D & Milani RV. (1999). Effects of aerobic exercise training on indices of ventricular repolarization in patients with chronic heart failure. *Chest* **116,** 83-87.

Allen DL, Harrison BC, Maass A, Bell ML, Byrnes WC & Leinwand LA. (2001). Cardiac and skeletal muscle adaptations to voluntary wheel running in the mouse. *J Appl Physiol* **90,** 1900-1908.

Amberg GC, Rossow CF, Navedo MF & Santana LF. (2004). NFATc3 regulates Kv2.1 expression in arterial smooth muscle. *J Biol Chem* **279,** 47326-47334.

Ambros V. (2004). The functions of animal microRNAs. *Nature* **431,** 350-355.

Anderson AE, Adams JP, Qian Y, Cook RG, Pfaffinger PJ & Sweatt JD. (2000). Kv4.2 phosphorylation by cyclic AMP-dependent protein kinase. *J Biol Chem* **275,** 5337-5346.

Anker SD, Chua TP, Ponikowski P, Harrington D, Swan JW, Kox WJ, Poole-Wilson PA & Coats AJ. (1997). Hormonal changes and catabolic/anabolic imbalance in chronic heart failure and their importance for cardiac cachexia. *Circulation* **96,** 526-534.

Baek D, Villen J, Shin C, Camargo FD, Gygi SP & Bartel DP. (2008). The impact of microRNAs on protein output. *Nature* **455,** 64-71.

Barr CS, Naas A, Freeman M, Lang CC & Struthers AD. (1994). QT dispersion and sudden unexpected death in chronic heart failure. *Lancet* **343,** 327-329.

Barry DM, Xu H, Schuessler RB & Nerbonne JM. (1998). Functional knockout of the transient outward current, long-QT syndrome, and cardiac remodeling in mice expressing a dominant-negative Kv4 alpha subunit. *Circ Res* **83,** 560-567.

Basso K, Sumazin P, Morozov P, Schneider C, Maute RL, Kitagawa Y, Mandelbaum J, Haddad J, Jr., Chen CZ, Califano A & Dalla-Favera R. (2009). Identification of the human mature B cell miRNome. *Immunity* **30,** 744-752.

Beuckelmann DJ, Nabauer M & Erdmann E. (1993). Alterations of K+ currents in isolated human ventricular myocytes from patients with terminal heart failure. *Circ Res* **73,** 379-385.

Biffi A, Maron BJ, Di Giacinto B, Porcacchia P, Verdile L, Fernando F, Spataro A, Culasso F, Casasco M & Pelliccia A. (2008). Relation between training-induced left ventricular hypertrophy and risk for ventricular tachyarrhythmias in elite athletes. *Am J Cardiol* **101,** 1792-1795.

Brugada R, Hong K, Dumaine R, Cordeiro J, Gaita F, Borggrefe M, Menendez TM, Brugada J, Pollevick GD, Wolpert C, Burashnikov E, Matsuo K, Wu YS, Guerchicoff A, Bianchi F, Giustetto C, Schimpf R, Brugada P & Antzelevitch C. (2004). Sudden death associated with short-QT syndrome linked to mutations in HERG. *Circulation* **109,** 30-35.

Brunet A, Bonni A, Zigmond MJ, Lin MZ, Juo P, Hu LS, Anderson MJ, Arden KC, Blenis J & Greenberg ME. (1999). Akt promotes cell survival by phosphorylating and inhibiting a Forkhead transcription factor. *Cell* **96,** 857-868.

Brunet S, Aimond F, Li H, Guo W, Eldstrom J, Fedida D, Yamada KA & Nerbonne JM. (2004). Heterogeneous expression of repolarizing, voltage-gated K+ currents in adult mouse ventricles. *J Physiol* **559,** 103-120.

Bryant SM, Wan X, Shipsey SJ & Hart G. (1998). Regional differences in the delayed rectifier current (IKr and IKs) contribute to the differences in action potential duration in basal left ventricular myocytes in guinea-pig. *Cardiovasc Res* **40,** 322-331.

Buerger A, Rozhitskaya O, Sherwood MC, Dorfman AL, Bisping E, Abel ED, Pu WT, Izumo S & Jay PY. (2006). Dilated cardiomyopathy resulting from high-level myocardial expression of Cre-recombinase. *J Card Fail* **12,** 392-398.

Callaghan B, Koh SD & Keef KD. (2004). Muscarinic M2 receptor stimulation of Cav1.2b requires phosphatidylinositol 3-kinase, protein kinase C, and c-Src. *Circ Res* **94,** 626-633.

Cantley LC. (2002). The phosphoinositide 3-kinase pathway. *Science* **296,** 1655-1657.

CAST. (1989). Preliminary report: effect of encainide and flecainide on mortality in a randomized trial of arrhythmia suppression after myocardial infarction. The Cardiac Arrhythmia Suppression Trial (CAST) Investigators. *N Engl J Med* **321,** 406-412.

Cheng Y, Ji R, Yue J, Yang J, Liu X, Chen H, Dean DB & Zhang C. (2007). MicroRNAs are aberrantly expressed in hypertrophic heart: do they play a role in cardiac hypertrophy? *Am J Pathol* **170,** 1831-1840.

Cho H, Mu J, Kim JK, Thorvaldsen JL, Chu Q, Crenshaw EB, 3rd, Kaestner KH, Bartolomei MS, Shulman GI & Birnbaum MJ. (2001a). Insulin resistance and a diabetes mellitus-like syndrome in mice lacking the protein kinase Akt2 (PKB beta). *Science* **292,** 1728-1731.

Cho H, Thorvaldsen JL, Chu Q, Feng F & Birnbaum MJ. (2001b). Akt1/PKBalpha is required for normal growth but dispensable for maintenance of glucose homeostasis in mice. *J Biol Chem* **276,** 38349-38352.

Cittadini A, Grossman JD, Napoli R, Katz SE, Stromer H, Smith RJ, Clark R, Morgan JP & Douglas PS. (1997). Growth hormone attenuates early left ventricular remodeling and improves cardiac function in rats with large myocardial infarction. *J Am Coll Cardiol* **29,** 1109-1116.

Coats AJ. (2011). Clinical utility of exercise training in chronic systolic heart failure. *Nat Rev Cardiol* **8,** 380-392.

Coats AJ, Adamopoulos S, Radaelli A, McCance A, Meyer TE, Bernardi L, Solda PL, Davey P, Ormerod O, Forfar C & et al. (1992). Controlled trial of physical training in chronic heart failure. Exercise performance, hemodynamics, ventilation, and autonomic function. *Circulation* **85,** 2119-2131.

Costantini DL, Arruda EP, Agarwal P, Kim KH, Zhu Y, Zhu W, Lebel M, Cheng CW, Park CY, Pierce SA, Guerchicoff A, Pollevick GD, Chan TY, Kabir MG, Cheng SH, Husain M, Antzelevitch C, Srivastava D, Gross GJ, Hui CC, Backx PH & Bruneau BG. (2005). The homeodomain transcription factor Irx5 establishes the mouse cardiac ventricular repolarization gradient. *Cell* **123,** 347-358.

Cottonham CL, Kaneko S & Xu L. (2010). miR-21 and miR-31 converge on TIAM1 to regulate migration and invasion of colon carcinoma cells. *J Biol Chem* **285,** 35293-35302.

Covarrubias M, Wei AA & Salkoff L. (1991). Shaker, Shal, Shab, and Shaw express independent K+ current systems. *Neuron* **7,** 763-773.

D'Angelo DD, Sakata Y, Lorenz JN, Boivin GP, Walsh RA, Liggett SB & Dorn GW, 2nd. (1997). Transgenic Galphaq overexpression induces cardiac contractile failure in mice. *Proc Natl Acad Sci U S A* **94,** 8121-8126.

Davis BN, Hilyard AC, Lagna G & Hata A. (2008). SMAD proteins control DROSHA-mediated microRNA maturation. *Nature* **454,** 56-61.

DeBosch B, Sambandam N, Weinheimer C, Courtois M & Muslin AJ. (2006a). Akt2 regulates cardiac metabolism and cardiomyocyte survival. *J Biol Chem* **281,** 32841-32851.

DeBosch B, Treskov I, Lupu TS, Weinheimer C, Kovacs A, Courtois M & Muslin AJ. (2006b). Akt1 is required for physiological cardiac growth. *Circulation* **113,** 2097-2104.

Dobrzynski H, Billeter R, Greener ID, Tellez JO, Chandler NJ, Flagg TP, Nichols CG, Lopatin AN & Boyett MR. (2006). Expression of Kir2.1 and Kir6.2 transgenes under the control of the alpha-MHC promoter in the sinoatrial and atrioventricular nodes in transgenic mice. *J Mol Cell Cardiol* **41,** 855-867.

Dorn GW, 2nd & Force T. (2005). Protein kinase cascades in the regulation of cardiac hypertrophy. *J Clin Invest* **115,** 527-537.

Duerr RL, McKirnan MD, Gim RD, Clark RG, Chien KR & Ross J, Jr. (1996). Cardiovascular effects of insulin-like growth factor-1 and growth hormone in chronic left ventricular failure in the rat. *Circulation* **93,** 2188-2196.

Etzion S, Etzion Y, DeBosch B, Crawford PA & Muslin AJ. (2010). Akt2 deficiency promotes cardiac induction of Rab4a and myocardial beta-adrenergic hypersensitivity. *J Mol Cell Cardiol* **49,** 931-940.

Fazio S, Sabatini D, Capaldo B, Vigorito C, Giordano A, Guida R, Pardo F, Biondi B & Sacca L. (1996). A preliminary study of growth hormone in the treatment of dilated cardiomyopathy. *N Engl J Med* **334,** 809-814.

Fehniger TA, Wylie T, Germino E, Leong JW, Magrini VJ, Koul S, Keppel CR, Schneider SE, Koboldt DC, Sullivan RP, Heinz ME, Crosby SD, Nagarajan R, Ramsingh G, Link DC, Ley TJ & Mardis ER. (2010). Next-generation sequencing identifies the natural killer cell microRNA transcriptome. *Genome Res* **20,** 1590-1604.

Foeger NC, Wang W, Mellor RM & Nerbonne JM. (2012). The accessory K(+) channel interacting protein 2 stabilizes Kv4 protein and is required for the generation of native fast transient outward K(+) currents (Submitted).

Fozzard HA. (1991). Excitation-contraction coupling in the heart. *Adv Exp Med Biol* **308,** 135-142.

Frey N & Olson EN. (2003). Cardiac hypertrophy: the good, the bad, and the ugly. *Annu Rev Physiol* **65,** 45-79.

Furukawa T, Kimura S, Furukawa N, Bassett AL & Myerburg RJ. (1992). Potassium rectifier currents differ in myocytes of endocardial and epicardial origin. *Circ Res* **70,** 91-103.

Gallego M, Setien R, Puebla L, Boyano-Adanez Mdel C, Arilla E & Casis O. (2005). alpha1-Adrenoceptors stimulate a Galphas protein and reduce the transient outward K+ current via a cAMP/PKA-mediated pathway in the rat heart. *Am J Physiol Cell Physiol* **288,** C577-585.

Garofalo RS, Orena SJ, Rafidi K, Torchia AJ, Stock JL, Hildebrandt AL, Coskran T, Black SC, Brees DJ, Wicks JR, McNeish JD & Coleman KG. (2003). Severe diabetes, age-dependent loss of adipose tissue, and mild growth deficiency in mice lacking Akt2/PKB beta. *J Clin Invest* **112,** 197-208.

Genth-Zotz S, Zotz R, Geil S, Voigtlander T, Meyer J & Darius H. (1999). Recombinant growth hormone therapy in patients with ischemic cardiomyopathy : effects on hemodynamics, left ventricular function, and cardiopulmonary exercise capacity. *Circulation* **99,** 18-21.

Gillis AM, Mathison HJ, Kulisz E & Lester WM. (2000). Dispersion of ventricular repolarization and ventricular fibrillation in left ventricular hypertrophy: influence of selective potassium channel blockers. *J Pharmacol Exp Ther* **292,** 381-386.

Golub TR, Slonim DK, Tamayo P, Huard C, Gaasenbeek M, Mesirov JP, Coller H, Loh ML, Downing JR, Caligiuri MA, Bloomfield CD & Lander ES. (1999). Molecular classification of cancer: class discovery and class prediction by gene expression monitoring. *Science* **286,** 531-537.

Griffiths-Jones S. (2006). miRBase: the microRNA sequence database. *Methods Mol Biol* **342,** 129-138.

Griffiths-Jones S, Grocock RJ, van Dongen S, Bateman A & Enright AJ. (2006). miRBase: microRNA sequences, targets and gene nomenclature. *Nucleic Acids Res* **34,** D140-144.

Guo H, Ingolia NT, Weissman JS & Bartel DP. (2010). Mammalian microRNAs predominantly act to decrease target mRNA levels. *Nature* **466,** 835-840.

Guo W, Jung WE, Marionneau C, Aimond F, Xu H, Yamada KA, Schwarz TL, Demolombe S & Nerbonne JM. (2005). Targeted deletion of Kv4.2 eliminates I(to,f) and results in electrical and molecular remodeling, with no evidence of ventricular hypertrophy or myocardial dysfunction. *Circ Res* **97,** 1342-1350.

Guo W, Li H, Aimond F, Johns DC, Rhodes KJ, Trimmer JS & Nerbonne JM. (2002). Role of heteromultimers in the generation of myocardial transient outward K+ currents. *Circ Res* **90,** 586-593.

Guo W, Li H, London B & Nerbonne JM. (2000). Functional consequences of elimination of i(to,f) and i(to,s): early afterdepolarizations, atrioventricular block, and ventricular

arrhythmias in mice lacking Kv1.4 and expressing a dominant-negative Kv4 alpha subunit. *Circ Res* **87,** 73-79.

Guo W, Xu H, London B & Nerbonne JM. (1999). Molecular basis of transient outward K+ current diversity in mouse ventricular myocytes. *J Physiol* **521 Pt 3,** 587-599.

Hackenberg M, Rodriguez-Ezpeleta N & Aransay AM. miRanalyzer: an update on the detection and analysis of microRNAs in high-throughput sequencing experiments. *Nucleic Acids Res* **39,** W132-138.

Hackenberg M, Sturm M, Langenberger D, Falcon-Perez JM & Aransay AM. (2009). miRanalyzer: a microRNA detection and analysis tool for next-generation sequencing experiments. *Nucleic Acids Res* **37,** W68-76.

Haider AW, Larson MG, Benjamin EJ & Levy D. (1998). Increased left ventricular mass and hypertrophy are associated with increased risk for sudden death. *J Am Coll Cardiol* **32,** 1454-1459.

Hambrecht R, Hilbrich L, Erbs S, Gielen S, Fiehn E, Schoene N & Schuler G. (2000a). Correction of endothelial dysfunction in chronic heart failure: additional effects of exercise training and oral L-arginine supplementation. *J Am Coll Cardiol* **35,** 706-713.

Hambrecht R, Wolf A, Gielen S, Linke A, Hofer J, Erbs S, Schoene N & Schuler G. (2000b). Effect of exercise on coronary endothelial function in patients with coronary artery disease. *N Engl J Med* **342,** 454-460.

Hannan RD, Jenkins A, Jenkins AK & Brandenburger Y. (2003). Cardiac hypertrophy: a matter of translation. *Clin Exp Pharmacol Physiol* **30,** 517-527.

Harrison BC, Bell ML, Allen DL, Byrnes WC & Leinwand LA. (2002). Skeletal muscle adaptations in response to voluntary wheel running in myosin heavy chain null mice. *J Appl Physiol* **92,** 313-322.

Harrison DG, Marcus ML, Dellsperger KC, Lamping KG & Tomanek RJ. (1991). Pathophysiology of myocardial perfusion in hypertension. *Circulation* **83,** III14-18.

Heidecker B, Kasper EK, Wittstein IS, Champion HC, Breton E, Russell SD, Kittleson MM, Baughman KL & Hare JM. (2008). Transcriptomic biomarkers for individual risk assessment in new-onset heart failure. *Circulation* **118,** 238-246.

Hilgemann DW, Feng S & Nasuhoglu C. (2001). The complex and intriguing lives of PIP2 with ion channels and transporters. *Sci STKE* **2001,** RE19.

Himmel B & Nagel G. (2004). Protein kinase-independent activation of CFTR by phosphatidylinositol phosphates. *EMBO Rep* **5,** 85-90.

Hombach V. (2002). Electrocardiogram of the failing heart. *Card Electrophysiol Rev* **6,** 209-214.

Hoshijima M & Chien KR. (2002). Mixed signals in heart failure: cancer rules. *J Clin Invest* **109,** 849-855.

Houghton JL, Carr AA, Prisant LM, Rogers WB, von Dohlen TW, Flowers NC & Frank MJ. (1992). Morphologic, hemodynamic and coronary perfusion characteristics in severe left ventricular hypertrophy secondary to systemic hypertension and evidence for nonatherosclerotic myocardial ischemia. *Am J Cardiol* **69,** 219-224.

Huynh K, McMullen JR, Julius TL, Tan JW, Love JE, Cemerlang N, Kiriazis H, Du XJ & Ritchie RH. Cardiac-specific IGF-1 receptor transgenic expression protects against cardiac fibrosis and diastolic dysfunction in a mouse model of diabetic cardiomyopathy. *Diabetes* **59,** 1512-1520.

Isgaard J, Bergh CH, Caidahl K, Lomsky M, Hjalmarson A & Bengtsson BA. (1998). A placebo-controlled study of growth hormone in patients with congestive heart failure. *Eur Heart J* **19,** 1704-1711.

Jentzsch C, Leierseder S, Loyer X, Flohrschutz I, Sassi Y, Hartmann D, Thum T, Laggerbauer B & Engelhardt S. (2011). A phenotypic screen to identify hypertrophy-modulating microRNAs in primary cardiomyocytes. *J Mol Cell Cardiol*.

Jessup M & Brozena S. (2003). Heart failure. *N Engl J Med* **348,** 2007-2018.

Jia Y & Takimoto K. (2006). Mitogen-activated protein kinases control cardiac KChIP2 gene expression. *Circ Res* **98,** 386-393.

Kaab S, Dixon J, Duc J, Ashen D, Nabauer M, Beuckelmann DJ, Steinbeck G, McKinnon D & Tomaselli GF. (1998). Molecular basis of transient outward potassium current downregulation in human heart failure: a decrease in Kv4.3 mRNA correlates with a reduction in current density. *Circulation* **98,** 1383-1393.

Kanno S & Saffitz JE. (2001). The role of myocardial gap junctions in electrical conduction and arrhythmogenesis. *Cardiovasc Pathol* **10,** 169-177.

Kaplan ML, Cheslow Y, Vikstrom K, Malhotra A, Geenen DL, Nakouzi A, Leinwand LA & Buttrick PM. (1994). Cardiac adaptations to chronic exercise in mice. *Am J Physiol* **267,** H1167-1173.

Kemi OJ, Ceci M, Wisloff U, Grimaldi S, Gallo P, Smith GL, Condorelli G & Ellingsen O. (2008). Activation or inactivation of cardiac Akt/mTOR signaling diverges physiological from pathological hypertrophy. *J Cell Physiol* **214,** 316-321.

Kim J, Wende AR, Sena S, Theobald HA, Soto J, Sloan C, Wayment BE, Litwin SE, Holzenberger M, LeRoith D & Abel ED. (2008). Insulin-like growth factor I receptor signaling is required for exercise-induced cardiac hypertrophy. *Mol Endocrinol* **22,** 2531-2543.

Kober L, Torp-Pedersen C, Carlsen JE, Bagger H, Eliasen P, Lyngborg K, Videbaek J, Cole DS, Auclert L & Pauly NC. (1995). A clinical trial of the angiotensin-converting-enzyme inhibitor trandolapril in patients with left ventricular dysfunction after myocardial

infarction. Trandolapril Cardiac Evaluation (TRACE) Study Group. *N Engl J Med* **333,** 1670-1676.

Kodirov SA, Brunner M, Nerbonne JM, Buckett P, Mitchell GF & Koren G. (2004). Attenuation of I(K,slow1) and I(K,slow2) in Kv1/Kv2DN mice prolongs APD and QT intervals but does not suppress spontaneous or inducible arrhythmias. *Am J Physiol Heart Circ Physiol* **286,** H368-374.

Kong W, Po S, Yamagishi T, Ashen MD, Stetten G & Tomaselli GF. (1998). Isolation and characterization of the human gene encoding Ito: further diversity by alternative mRNA splicing. *Am J Physiol* **275,** H1963-1970.

Koziris LP, Hickson RC, Chatterton RT, Jr., Groseth RT, Christie JM, Goldflies DG & Unterman TG. (1999). Serum levels of total and free IGF-I and IGFBP-3 are increased and maintained in long-term training. *J Appl Physiol* **86,** 1436-1442.

Kuo HC, Cheng CF, Clark RB, Lin JJ, Lin JL, Hoshijima M, Nguyen-Tran VT, Gu Y, Ikeda Y, Chu PH, Ross J, Giles WR & Chien KR. (2001). A defect in the Kv channel-interacting protein 2 (KChIP2) gene leads to a complete loss of I(to) and confers susceptibility to ventricular tachycardia. *Cell* **107,** 801-813.

Lachance D, Plante E, Bouchard-Thomassin AA, Champetier S, Roussel E, Drolet MC, Arsenault M & Couet J. (2009). Moderate exercise training improves survival and ventricular remodeling in an animal model of left ventricular volume overload. *Circ Heart Fail* **2,** 437-445.

Landgraf P, Rusu M, Sheridan R, Sewer A, Iovino N, Aravin A, Pfeffer S, Rice A, Kamphorst AO, Landthaler M, Lin C, Socci ND, Hermida L, Fulci V, Chiaretti S, Foa R, Schliwka J, Fuchs U, Novosel A, Muller RU, Schermer B, Bissels U, Inman J, Phan Q, Chien M, Weir DB, Choksi R, De Vita G, Frezzetti D, Trompeter HI, Hornung V, Teng G, Hartmann G, Palkovits M, Di Lauro R, Wernet P, Macino G, Rogler CE, Nagle JW, Ju J, Papavasiliou FN, Benzing T, Lichter P, Tam W, Brownstein MJ, Bosio A, Borkhardt A, Russo JJ, Sander C, Zavolan M & Tuschl T. (2007). A mammalian microRNA expression atlas based on small RNA library sequencing. *Cell* **129,** 1401-1414.

Langmead B, Trapnell C, Pop M & Salzberg SL. (2009). Ultrafast and memory-efficient alignment of short DNA sequences to the human genome. *Genome Biol* **10,** R25.

Le Blanc C, Mironneau C, Barbot C, Henaff M, Bondeva T, Wetzker R & Macrez N. (2004). Regulation of vascular L-type Ca2+ channels by phosphatidylinositol 3,4,5-trisphosphate. *Circ Res* **95,** 300-307.

Lee JH, Gao C, Peng G, Greer C, Ren S, Wang Y & Xiao X. (2011). Analysis of transcriptome complexity through RNA sequencing in normal and failing murine hearts. *Circ Res* **9,** 1332-1341.

Levy D, Anderson KM, Savage DD, Balkus SA, Kannel WB & Castelli WP. (1987). Risk of ventricular arrhythmias in left ventricular hypertrophy: the Framingham Heart Study. *Am J Cardiol* **60,** 560-565.

Levy D, Garrison RJ, Savage DD, Kannel WB & Castelli WP. (1990). Prognostic implications of echocardiographically determined left ventricular mass in the Framingham Heart Study. *N Engl J Med* **322,** 1561-1566.

Li GR, Lau CP, Ducharme A, Tardif JC & Nattel S. (2002). Transmural action potential and ionic current remodeling in ventricles of failing canine hearts. *Am J Physiol Heart Circ Physiol* **283,** H1031-1041.

Li H, Guo W, Mellor RL & Nerbonne JM. (2005). KChIP2 modulates the cell surface expression of Kv 1.5-encoded K(+) channels. *J Mol Cell Cardiol* **39,** 121-132.

Li H, Guo W, Yamada KA & Nerbonne JM. (2004). Selective elimination of I(K,slow1) in mouse ventricular myocytes expressing a dominant negative Kv1.5alpha subunit. *Am J Physiol Heart Circ Physiol* **286,** H319-328.

Li J, Marionneau C, Zhang R, Shah V, Hell JW, Nerbonne JM & Anderson ME. (2006). Calmodulin kinase II inhibition shortens action potential duration by upregulation of K+ currents. *Circ Res* **99,** 1092-1099.

Lin RC, Weeks KL, Gao XM, Williams RB, Bernardo BC, Kiriazis H, Matthews VB, Woodcock EA, Bouwman RD, Mollica JP, Speirs HJ, Dawes IW, Daly RJ, Shioi T, Izumo S, Febbraio MA, Du XJ & McMullen JR. (2010). PI3K(p110 alpha) protects against myocardial infarction-induced heart failure: identification of PI3K-regulated miRNA and mRNA. *Arterioscler Thromb Vasc Biol* **30,** 724-732.

Litovsky SH & Antzelevitch C. (1988). Transient outward current prominent in canine ventricular epicardium but not endocardium. *Circ Res* **62,** 116-126.

Liu G, Friggeri A, Yang Y, Milosevic J, Ding Q, Thannickal VJ, Kaminski N & Abraham E. miR-21 mediates fibrogenic activation of pulmonary fibroblasts and lung fibrosis. *J Exp Med* **207,** 1589-1597.

London B, Guo W, Pan X, Lee JS, Shusterman V, Rocco CJ, Logothetis DA, Nerbonne JM & Hill JA. (2001a). Targeted replacement of KV1.5 in the mouse leads to loss of the 4-aminopyridine-sensitive component of I(K,slow) and resistance to drug-induced qt prolongation. *Circ Res* **88,** 940-946.

London B, Guo W, Pan X, Lee JS, Shusterman V, Rocco CJ, Logothetis DA, Nerbonne JM & Hill JA. (2001b). Targeted replacement of Kv1.5 in the mouse leads to loss of the 4-aminopyridine-sensitive component of $I_{K,slow}$ and resistance to drug-induced QT prolongation. *Circ Res* **88,** 940-946.

Loots GG & Ovcharenko I. (2004). rVISTA 2.0: evolutionary analysis of transcription factor binding sites. *Nucleic Acids Res* **32,** W217-221.

Lopatin AN & Nichols CG. (2001). Inward rectifiers in the heart: an update on I(K1). *J Mol Cell Cardiol* **33,** 625-638.

Lopes CM, Zhang H, Rohacs T, Jin T, Yang J & Logothetis DE. (2002). Alterations in conserved Kir channel-PIP2 interactions underlie channelopathies. *Neuron* **34,** 933-944.

Lorell BH & Carabello BA. (2000). Left ventricular hypertrophy: pathogenesis, detection, and prognosis. *Circulation* **102,** 470-479.

Loussouarn G, Park KH, Bellocq C, Baro I, Charpentier F & Escande D. (2003). Phosphatidylinositol-4,5-bisphosphate, PIP2, controls KCNQ1/KCNE1 voltage-gated potassium channels: a functional homology between voltage-gated and inward rectifier K+ channels. *EMBO J* **22,** 5412-5421.

Luo J, McMullen JR, Sobkiw CL, Zhang L, Dorfman AL, Sherwood MC, Logsdon MN, Horner JW, DePinho RA, Izumo S & Cantley LC. (2005). Class IA phosphoinositide 3-kinase regulates heart size and physiological cardiac hypertrophy. *Mol Cell Biol* **25,** 9491-9502.

Mammarella A, Paradiso M, Basili S, De Matteis A, Cardarello CM, Di Franco M, Donnarumma L, Labbadia G & Paoletti V. (2000). Morphologic left ventricular patterns and prevalence of high-grade ventricular arrhythmias in the normotensive and hypertensive elderly. *Adv Ther* **17,** 222-229.

Manganas LN & Trimmer JS. (2000). Subunit composition determines Kv1 potassium channel surface expression. *J Biol Chem* **275,** 29685-29693.

Mann DL. (2011). The emerging role of innate immunity in the heart and vascular system: for whom the cell tolls. *Circ Res* **108,** 1133-1145.

Marguerat S & Bahler J. (2010). RNA-seq: from technology to biology. *Cell Mol Life Sci* **67,** 569-579.

Marionneau C, Aimond F, Brunet S, Niwa N, Finck B, Kelly DP & Nerbonne JM. (2008a). PPARalpha-mediated remodeling of repolarizing voltage-gated K+ (Kv) channels in a mouse model of metabolic cardiomyopathy. *J Mol Cell Cardiol* **44,** 1002-1015.

Marionneau C, Brunet S, Flagg TP, Pilgram TK, Demolombe S & Nerbonne JM. (2008b). Distinct cellular and molecular mechanisms underlie functional remodeling of repolarizing K+ currents with left ventricular hypertrophy. *Circ Res* **102,** 1406-1415.

Marionneau C, Couette B, Liu J, Li H, Mangoni ME, Nargeot J, Lei M, Escande D & Demolombe S. (2005). Specific pattern of ionic channel gene expression associated with pacemaker activity in the mouse heart. *J Physiol* **562,** 223-234.

Masiha S, Sundstrom J & Lind L. (2012). Inflammatory markers are associated with left ventricular hypertrophy and diastolic dysfunction in a population-based sample of elderly men and women. *J Hum Hypertens*.

Matkovich SJ, Van Booven DJ, Eschenbacher WH & Dorn GW, 2nd. RISC RNA sequencing for context-specific identification of in vivo microRNA targets. *Circ Res* **108,** 18-26.

Matkovich SJ, Zhang Y, Van Booven DJ & Dorn GW, 2nd. (2010). Deep mRNA sequencing for in vivo functional analysis of cardiac transcriptional regulators: application to Galphaq. *Circ Res* **106,** 1459-1467.

Mayet J, Kanagaratnam P, Shahi M, Senior R, Doherty M, Poulter NR, Sever PS, Handler CE, Thom SA & Foale RA. (1999). QT dispersion in athletic left ventricular hypertrophy. *Am Heart J* **137,** 678-681.

Mayet J, Shahi M, McGrath K, Poulter NR, Sever PS, Foale RA & Thom SA. (1996). Left ventricular hypertrophy and QT dispersion in hypertension. *Hypertension* **28,** 791-796.

McIntyre H & Fry CH. (1997). Abnormal action potential conduction in isolated human hypertrophied left ventricular myocardium. *J Cardiovasc Electrophysiol* **8,** 887-894.

McLenachan JM, Henderson E, Morris KI & Dargie HJ. (1987). Ventricular arrhythmias in patients with hypertensive left ventricular hypertrophy. *N Engl J Med* **317,** 787-792.

McLerie M & Lopatin AN. (2003). Dominant-negative suppression of I(K1) in the mouse heart leads to altered cardiac excitability. *J Mol Cell Cardiol* **35,** 367-378.

McMullen JR, Amirahmadi F, Woodcock EA, Schinke-Braun M, Bouwman RD, Hewitt KA, Mollica JP, Zhang L, Zhang Y, Shioi T, Buerger A, Izumo S, Jay PY & Jennings GL. (2007). Protective effects of exercise and phosphoinositide 3-kinase(p110alpha) signaling in dilated and hypertrophic cardiomyopathy. *Proc Natl Acad Sci U S A* **104,** 612-617.

McMullen JR & Jennings GL. (2007). Differences between pathological and physiological cardiac hypertrophy: novel therapeutic strategies to treat heart failure. *Clin Exp Pharmacol Physiol* **34,** 255-262.

McMullen JR, Shioi T, Huang WY, Zhang L, Tarnavski O, Bisping E, Schinke M, Kong S, Sherwood MC, Brown J, Riggi L, Kang PM & Izumo S. (2004). The insulin-like growth factor 1 receptor induces physiological heart growth via the phosphoinositide 3-kinase(p110alpha) pathway. *J Biol Chem* **279,** 4782-4793.

McMullen JR, Shioi T, Zhang L, Tarnavski O, Sherwood MC, Kang PM & Izumo S. (2003). Phosphoinositide 3-kinase(p110alpha) plays a critical role for the induction of physiological, but not pathological, cardiac hypertrophy. *Proc Natl Acad Sci U S A* **100,** 12355-12360.

Medeiros A, Rolim NP, Oliveira RS, Rosa KT, Mattos KC, Casarini DE, Irigoyen MC, Krieger EM, Krieger JE, Negrao CE & Brum PC. (2008). Exercise training delays cardiac dysfunction and prevents calcium handling abnormalities in sympathetic hyperactivity-induced heart failure mice. *J Appl Physiol* **104,** 103-109.

Mende U, Kagen A, Cohen A, Aramburu J, Schoen FJ & Neer EJ. (1998). Transient cardiac expression of constitutively active Galphaq leads to hypertrophy and dilated cardiomyopathy by calcineurin-dependent and independent pathways. *Proc Natl Acad Sci U S A* **95,** 13893-13898.

Messerli FH, Ventura HO, Elizardi DJ, Dunn FG & Frohlich ED. (1984). Hypertension and sudden death. Increased ventricular ectopic activity in left ventricular hypertrophy. *Am J Med* **77,** 18-22.

Mitchell GF, Jeron A & Koren G. (1998). Measurement of heart rate and Q-T interval in the conscious mouse. *Am J Physiol* **274,** H747-751.

Mortazavi A, Williams BA, McCue K, Schaeffer L & Wold B. (2008). Mapping and quantifying mammalian transcriptomes by RNA-Seq. *Nat Methods* **5,** 621-628.

Moss AJ, Hall WJ, Cannom DS, Klein H, Brown MW, Daubert JP, Estes NA, 3rd, Foster E, Greenberg H, Higgins SL, Pfeffer MA, Solomon SD, Wilber D & Zareba W. (2009). Cardiac-resynchronization therapy for the prevention of heart-failure events. *N Engl J Med* **361,** 1329-1338.

Muslin AJ & DeBosch B. (2006). Role of Akt in cardiac growth and metabolism. *Novartis Found Symp* **274,** 118-126; discussion 126-131, 152-115, 272-116.

Nabauer M, Beuckelmann DJ, Uberfuhr P & Steinbeck G. (1996). Regional differences in current density and rate-dependent properties of the transient outward current in subepicardial and subendocardial myocytes of human left ventricle. *Circulation* **93,** 168-177.

Nakatani K, Sakaue H, Thompson DA, Weigel RJ & Roth RA. (1999). Identification of a human Akt3 (protein kinase B gamma) which contains the regulatory serine phosphorylation site. *Biochem Biophys Res Commun* **257,** 906-910.

Nass RD, Aiba T, Tomaselli GF & Akar FG. (2008). Mechanisms of disease: ion channel remodeling in the failing ventricle. *Nat Clin Pract Cardiovasc Med* **5,** 196-207.

Nattel S, Maguy A, Le Bouter S & Yeh YH. (2007). Arrhythmogenic ion-channel remodeling in the heart: heart failure, myocardial infarction, and atrial fibrillation. *Physiol Rev* **87,** 425-456.

Nerbonne JM. (2004). Studying cardiac arrhythmias in the mouse--a reasonable model for probing mechanisms? *Trends Cardiovasc Med* **14,** 83-93.

Nerbonne JM & Guo W. (2002). Heterogeneous expression of voltage-gated potassium channels in the heart: roles in normal excitation and arrhythmias. *J Cardiovasc Electrophysiol* **13,** 406-409.

Nerbonne JM & Kass RS. (2005). Molecular physiology of cardiac repolarization. *Physiol Rev* **85,** 1205-1253.

Neri Serneri GG, Boddi M, Modesti PA, Cecioni I, Coppo M, Padeletti L, Michelucci A, Colella A & Galanti G. (2001). Increased cardiac sympathetic activity and insulin-like growth factor-I formation are associated with physiological hypertrophy in athletes. *Circ Res* **89,** 977-982.

Nichols CG & Lopatin AN. (1997). Inward rectifier potassium channels. *Annu Rev Physiol* **59,** 171-191.

Nichols CG, Makhina EN, Pearson WL, Sha Q & Lopatin AN. (1996). Inward rectification and implications for cardiac excitability. *Circ Res* **78,** 1-7.

Niwa N & Nerbonne JM. (2010). Molecular determinants of cardiac transient outward potassium current (I(to)) expression and regulation. *J Mol Cell Cardiol* **48,** 12-25.

Nordin C, Siri F & Aronson RS. (1989). Electrophysiologic characteristics of single myocytes isolated from hypertrophied guinea-pig hearts. *J Mol Cell Cardiol* **21,** 729-739.

O'Connor CM, Whellan DJ, Lee KL, Keteyian SJ, Cooper LS, Ellis SJ, Leifer ES, Kraus WE, Kitzman DW, Blumenthal JA, Rendall DS, Miller NH, Fleg JL, Schulman KA, McKelvie RS, Zannad F & Pina IL. (2009). Efficacy and safety of exercise training in patients with chronic heart failure: HF-ACTION randomized controlled trial. *JAMA* **301,** 1439-1450.

O'Neill BT, Kim J, Wende AR, Theobald HA, Tuinei J, Buchanan J, Guo A, Zaha VG, Davis DK, Schell JC, Boudina S, Wayment B, Litwin SE, Shioi T, Izumo S, Birnbaum MJ & Abel ED. (2007). A conserved role for phosphatidylinositol 3-kinase but not Akt signaling in mitochondrial adaptations that accompany physiological cardiac hypertrophy. *Cell Metab* **6,** 294-306.

Oikarinen L, Nieminen MS, Viitasalo M, Toivonen L, Jern S, Dahlof B, Devereux RB & Okin PM. (2004). QRS duration and QT interval predict mortality in hypertensive patients with left ventricular hypertrophy: the Losartan Intervention for Endpoint Reduction in Hypertension Study. *Hypertension* **43,** 1029-1034.

Olson EN & Schneider MD. (2003). Sizing up the heart: development redux in disease. *Genes Dev* **17,** 1937-1956.

Osterziel KJ, Strohm O, Schuler J, Friedrich M, Hanlein D, Willenbrock R, Anker SD, Poole-Wilson PA, Ranke MB & Dietz R. (1998). Randomised, double-blind, placebo-controlled trial of human recombinant growth hormone in patients with chronic heart failure due to dilated cardiomyopathy. *Lancet* **351,** 1233-1237.

Pais H, Moxon S, Dalmay T & Moulton V. (2011). Small RNA discovery and characterisation in eukaryotes using high-throughput approaches. *Adv Exp Med Biol* **722,** 239-254.

Panama BK, Latour-Villamil D, Farman GP, Zhao D, Bolz SS, Kirshenbaum LA & Backx PH. (2011). Nuclear factor kappaB downregulates the transient outward potassium current I(to,f) through control of KChIP2 expression. *Circ Res* **108,** 537-543.

Pelliccia A, Maron BJ, Culasso F, Di Paolo FM, Spataro A, Biffi A, Caselli G & Piovano P. (2000). Clinical significance of abnormal electrocardiographic patterns in trained athletes. *Circulation* **102,** 278-284.

Peng XD, Xu PZ, Chen ML, Hahn-Windgassen A, Skeen J, Jacobs J, Sundararajan D, Chen WS, Crawford SE, Coleman KG & Hay N. (2003). Dwarfism, impaired skin development, skeletal muscle atrophy, delayed bone development, and impeded adipogenesis in mice lacking Akt1 and Akt2. *Genes Dev* **17,** 1352-1365.

Petkova-Kirova PS, Gursoy E, Mehdi H, McTiernan CF, London B & Salama G. (2006). Electrical remodeling of cardiac myocytes from mice with heart failure due to the overexpression of tumor necrosis factor-alpha. *Am J Physiol Heart Circ Physiol* **290,** H2098-2107.

Pfeffer MA, Braunwald E, Moye LA, Basta L, Brown EJ, Jr., Cuddy TE, Davis BR, Geltman EM, Goldman S, Flaker GC & et al. (1992). Effect of captopril on mortality and morbidity in patients with left ventricular dysfunction after myocardial infarction. Results of the survival and ventricular enlargement trial. The SAVE Investigators. *N Engl J Med* **327,** 669-677.

Philip-Couderc P, Tavares NI, Roatti A, Lerch R, Montessuit C & Baertschi AJ. (2008). Forkhead transcription factors coordinate expression of myocardial KATP channel subunits and energy metabolism. *Circ Res* **102,** e20-35.

Pitt B, Zannad F, Remme WJ, Cody R, Castaigne A, Perez A, Palensky J & Wittes J. (1999). The effect of spironolactone on morbidity and mortality in patients with severe heart failure. Randomized Aldactone Evaluation Study Investigators. *N Engl J Med* **341,** 709-717.

Pluim BM, Zwinderman AH, van der Laarse A & van der Wall EE. (2000). The athlete's heart. A meta-analysis of cardiac structure and function. *Circulation* **101,** 336-344.

Po S, Roberds S, Snyders DJ, Tamkun MM & Bennett PB. (1993). Heteromultimeric assembly of human potassium channels. Molecular basis of a transient outward current? *Circ Res* **72,** 1326-1336.

Pongs O & Schwarz JR. (2010). Ancillary subunits associated with voltage-dependent K+ channels. *Physiol Rev* **90,** 755-796.

Pretorius L, Du XJ, Woodcock EA, Kiriazis H, Lin RC, Marasco S, Medcalf RL, Ming Z, Head GA, Tan JW, Cemerlang N, Sadoshima J, Shioi T, Izumo S, Lukoshkova EV, Dart AM, Jennings GL & McMullen JR. (2009). Reduced phosphoinositide 3-kinase (p110alpha) activation increases the susceptibility to atrial fibrillation. *Am J Pathol* **175,** 998-1009.

Priori SG, Pandit SV, Rivolta I, Berenfeld O, Ronchetti E, Dhamoon A, Napolitano C, Anumonwo J, di Barletta MR, Gudapakkam S, Bosi G, Stramba-Badiale M & Jalife J. (2005). A novel form of short QT syndrome (SQT3) is caused by a mutation in the KCNJ2 gene. *Circ Res* **96,** 800-807.

Putzke C, Wemhoner K, Sachse FB, Rinne S, Schlichthorl G, Li XT, Jae L, Eckhardt I, Wischmeyer E, Wulf H, Preisig-Muller R, Daut J & Decher N. (2007). The acid-sensitive potassium channel TASK-1 in rat cardiac muscle. *Cardiovasc Res* **75,** 59-68.

Qin D, Huang B, Deng L, El-Adawi H, Ganguly K, Sowers JR & El-Sherif N. (2001). Downregulation of K(+) channel genes expression in type I diabetic cardiomyopathy. *Biochem Biophys Res Commun* **283,** 549-553.

Radicke S, Cotella D, Graf EM, Banse U, Jost N, Varro A, Tseng GN, Ravens U & Wettwer E. (2006). Functional modulation of the transient outward current Ito by KCNE beta-subunits and regional distribution in human non-failing and failing hearts. *Cardiovasc Res* **71,** 695-703.

Radicke S, Cotella D, Graf EM, Ravens U & Wettwer E. (2005). Expression and function of dipeptidyl-aminopeptidase-like protein 6 as a putative beta-subunit of human cardiac transient outward current encoded by Kv4.3. *J Physiol* **565,** 751-756.

Rao PK, Kumar RM, Farkhondeh M, Baskerville S & Lodish HF. (2006). Myogenic factors that regulate expression of muscle-specific microRNAs. *Proc Natl Acad Sci U S A* **103,** 8721-8726.

Rao PK, Toyama Y, Chiang HR, Gupta S, Bauer M, Medvid R, Reinhardt F, Liao R, Krieger M, Jaenisch R, Lodish HF & Blelloch R. (2009). Loss of cardiac microRNA-mediated regulation leads to dilated cardiomyopathy and heart failure. *Circ Res* **105,** 585-594.

Reimand J, Kull M, Peterson H, Hansen J & Vilo J. (2007). g:Profiler--a web-based toolset for functional profiling of gene lists from large-scale experiments. *Nucleic Acids Res* **35,** W193-200.

Rials SJ, Wu Y, Xu X, Filart RA, Marinchak RA & Kowey PR. (1997). Regression of left ventricular hypertrophy with captopril restores normal ventricular action potential duration, dispersion of refractoriness, and vulnerability to inducible ventricular fibrillation. *Circulation* **96,** 1330-1336.

Roberts RE. (2003). Alpha 2 adrenoceptor-mediated vasoconstriction in porcine palmar lateral vein: role of phosphatidylinositol 3-kinase and EGF receptor transactivation. *Br J Pharmacol* **138,** 107-116.

Roden DM, Balser JR, George AL, Jr. & Anderson ME. (2002). Cardiac ion channels. *Annu Rev Physiol* **64,** 431-475.

Rose J, Armoundas AA, Tian Y, DiSilvestre D, Burysek M, Halperin V, O'Rourke B, Kass DA, Marban E & Tomaselli GF. (2005). Molecular correlates of altered expression of potassium currents in failing rabbit myocardium. *Am J Physiol Heart Circ Physiol* **288,** H2077-2087.

Rossow CF, Dilly KW & Santana LF. (2006). Differential calcineurin/NFATc3 activity contributes to the Ito transmural gradient in the mouse heart. *Circ Res* **98,** 1306-1313.

Rossow CF, Minami E, Chase EG, Murry CE & Santana LF. (2004). NFATc3-induced reductions in voltage-gated K+ currents after myocardial infarction. *Circ Res* **94,** 1340-1350.

Sanguinetti MC, Curran ME, Zou A, Shen J, Spector PS, Atkinson DL & Keating MT. (1996). Coassembly of K(V)LQT1 and minK (IsK) proteins to form cardiac I(Ks) potassium channel. *Nature* **384,** 80-83.

Sanguinetti MC, Jiang C, Curran ME & Keating MT. (1995). A mechanistic link between an inherited and an acquired cardiac arrhythmia: HERG encodes the IKr potassium channel. *Cell* **81,** 299-307.

Sayed D, Hong C, Chen IY, Lypowy J & Abdellatif M. (2007). MicroRNAs play an essential role in the development of cardiac hypertrophy. *Circ Res* **100,** 416-424.

Schrader LA, Birnbaum SG, Nadin BM, Ren Y, Bui D, Anderson AE & Sweatt JD. (2006). ERK/MAPK regulates the Kv4.2 potassium channel by direct phosphorylation of the pore-forming subunit. *Am J Physiol Cell Physiol* **290,** C852-861.

Schrader LA, Ren Y, Cheng F, Bui D, Sweatt JD & Anderson AE. (2009). Kv4.2 is a locus for PKC and ERK/MAPK cross-talk. *Biochem J* **417,** 705-715.

Schram G, Pourrier M, Melnyk P & Nattel S. (2002). Differential distribution of cardiac ion channel expression as a basis for regional specialization in electrical function. *Circ Res* **90,** 939-950.

Selbach M, Schwanhausser B, Thierfelder N, Fang Z, Khanin R & Rajewsky N. (2008). Widespread changes in protein synthesis induced by microRNAs. *Nature* **455,** 58-63.

Serra-Grima R, Estorch M, Carrio I, Subirana M, Berna L & Prat T. (2000). Marked ventricular repolarization abnormalities in highly trained athletes' electrocardiograms: clinical and prognostic implications. *J Am Coll Cardiol* **36,** 1310-1316.

Shi G, Nakahira K, Hammond S, Rhodes KJ, Schechter LE & Trimmer JS. (1996). Beta subunits promote K+ channel surface expression through effects early in biosynthesis. *Neuron* **16,** 843-852.

Shioi T, Kang PM, Douglas PS, Hampe J, Yballe CM, Lawitts J, Cantley LC & Izumo S. (2000). The conserved phosphoinositide 3-kinase pathway determines heart size in mice. *EMBO J* **19,** 2537-2548.

Smit JW, Janssen YJ, Lamb HJ, van der Wall EE, Stokkel MP, Viergever E, Biermasz NR, Bax JJ, Vliegen HW, de Roos A, Romijn JA & Roelfsema F. (2001). Six months of recombinant human GH therapy in patients with ischemic cardiac failure does not influence left ventricular function and mass. *J Clin Endocrinol Metab* **86,** 4638-4643.

Snyders DJ. (1999). Structure and function of cardiac potassium channels. *Cardiovasc Res* **42,** 377-390.

Sussman MA, Volkers M, Fischer K, Bailey B, Cottage CT, Din S, Gude N, Avitabile D, Alvarez R, Sundararaman B, Quijada P, Mason M, Konstandin MH, Malhowski A, Cheng Z, Khan M & McGregor M. (2011). Myocardial AKT: the omnipresent nexus. *Physiol Rev* **91,** 1023-1070.

Swynghedauw B, Chevalier B, Charlemagne D, Mansier P & Carre F. (1997). Cardiac hypertrophy, arrhythmogenicity and the new myocardial phenotype. II. The cellular adaptational process. *Cardiovasc Res* **35,** 6-12.

ter Keurs HE. (2011). Electromechanical coupling in the cardiac myocyte; stretch-arrhythmia feedback. *Pflugers Arch* **462,** 165-175.

Thum T, Galuppo P, Wolf C, Fiedler J, Kneitz S, van Laake LW, Doevendans PA, Mummery CL, Borlak J, Haverich A, Gross C, Engelhardt S, Ertl G & Bauersachs J. (2007). MicroRNAs in the human heart: a clue to fetal gene reprogramming in heart failure. *Circulation* **116,** 258-267.

Thum T, Gross C, Fiedler J, Fischer T, Kissler S, Bussen M, Galuppo P, Just S, Rottbauer W, Frantz S, Castoldi M, Soutschek J, Koteliansky V, Rosenwald A, Basson MA, Licht JD, Pena JT, Rouhanifard SH, Muckenthaler MU, Tuschl T, Martin GR, Bauersachs J & Engelhardt S. (2008). MicroRNA-21 contributes to myocardial disease by stimulating MAP kinase signalling in fibroblasts. *Nature* **456,** 980-984.

Tomaselli GF, Beuckelmann DJ, Calkins HG, Berger RD, Kessler PD, Lawrence JH, Kass D, Feldman AM & Marban E. (1994). Sudden cardiac death in heart failure. The role of abnormal repolarization. *Circulation* **90,** 2534-2539.

Tomaselli GF & Marban E. (1999). Electrophysiological remodeling in hypertrophy and heart failure. *Cardiovasc Res* **42,** 270-283.

Tsuji Y, Opthof T, Kamiya K, Yasui K, Liu W, Lu Z & Kodama I. (2000). Pacing-induced heart failure causes a reduction of delayed rectifier potassium currents along with decreases in calcium and transient outward currents in rabbit ventricle. *Cardiovasc Res* **48,** 300-309.

Valen G. (2011). Innate immunity and remodelling. *Heart Fail Rev* **16,** 71-78.

Van den Berghe G, Wouters P, Bowers CY, de Zegher F, Bouillon R & Veldhuis JD. (1999). Growth hormone-releasing peptide-2 infusion synchronizes growth hormone, thyrotrophin and prolactin release in prolonged critical illness. *Eur J Endocrinol* **140,** 17-22.

van der Heyden MA, Wijnhoven TJ & Opthof T. (2006). Molecular aspects of adrenergic modulation of the transient outward current. *Cardiovasc Res* **71,** 430-442.

van Rooij E. (2011). The art of microRNA research. *Circ Res* **108,** 219-234.

van Rooij E, Sutherland LB, Liu N, Williams AH, McAnally J, Gerard RD, Richardson JA & Olson EN. (2006). A signature pattern of stress-responsive microRNAs that can evoke cardiac hypertrophy and heart failure. *Proc Natl Acad Sci U S A* **103,** 18255-18260.

van Rooij E, Sutherland LB, Thatcher JE, DiMaio JM, Naseem RH, Marshall WS, Hill JA & Olson EN. (2008). Dysregulation of microRNAs after myocardial infarction reveals a role of miR-29 in cardiac fibrosis. *Proc Natl Acad Sci U S A* **105,** 13027-13032.

Vaseghi M & Shivkumar K. (2008). The role of the autonomic nervous system in sudden cardiac death. *Prog Cardiovasc Dis* **50,** 404-419.

Viard P, Butcher AJ, Halet G, Davies A, Nurnberg B, Heblich F & Dolphin AC. (2004). PI3K promotes voltage-dependent calcium channel trafficking to the plasma membrane. *Nat Neurosci* **7,** 939-946.

Volk T, Nguyen TH, Schultz JH, Faulhaber J & Ehmke H. (2001a). Regional alterations of repolarizing K+ currents among the left ventricular free wall of rats with ascending aortic stenosis. *J Physiol* **530,** 443-455.

Volk T, Nguyen THD, Schultz JH, Faulhaber J & Ehmke H. (2001b). Regional alterations of repolarizing K+ currents among the left ventricular free wall of rats with ascending aortic stenosis. *Journal of Physiology-London* **530,** 443-455.

Wang S, Aurora AB, Johnson BA, Qi X, McAnally J, Hill JA, Richardson JA, Bassel-Duby R & Olson EN. (2008). The endothelial-specific microRNA miR-126 governs vascular integrity and angiogenesis. *Dev Cell* **15,** 261-271.

Wang W, Niwa N & Nerbonne JM. (2012). Multiple components of the macroscopic steady state repolarizing K(+) currents, Iss, in adult mouse ventricular myocytes. (Submitted).

Wang Y, Cheng J, Chen G, Rob F, Naseem RH, Nguyen L, Johnstone JL & Hill JA. (2007). Remodeling of outward K+ currents in pressure-overload heart failure. *J Cardiovasc Electrophysiol* **18,** 869-875.

Wang Z, Feng J, Shi H, Pond A, Nerbonne JM & Nattel S. (1999). Potential molecular basis of different physiological properties of the transient outward K+ current in rabbit and human atrial myocytes. *Circ Res* **84,** 551-561.

Weeks KL & McMullen JR. (2011). The athlete's heart vs. the failing heart: can signaling explain the two distinct outcomes? *Physiology (Bethesda)* **26,** 97-105.

Xu H, Barry DM, Li H, Brunet S, Guo W & Nerbonne JM. (1999a). Attenuation of the slow component of delayed rectification, action potential prolongation, and triggered activity in mice expressing a dominant-negative Kv2 alpha subunit. *Circ Res* **85,** 623-633.

Xu H, Guo W & Nerbonne JM. (1999b). Four kinetically distinct depolarization-activated K+ currents in adult mouse ventricular myocytes. *J Gen Physiol* **113,** 661-678.

Yang KC, Foeger NC, Marionneau C, Jay PY, McMullen JR & Nerbonne JM. (2010). Homeostatic regulation of electrical excitability in physiological cardiac hypertrophy. *J Physiol* **588,** 5015-5032.

Yang KC, Jay PY, McMullen JR & Nerbonne JM. (2012). Enhanced cardiac PI3Kalpha signaling mitigates arrhythmogenic electrical remodeling in pathological hypertrophy and heart failure. *Cardiovasc Res* **93,** 252-262.

Yang R, Bunting S, Gillett N, Clark R & Jin H. (1995). Growth hormone improves cardiac performance in experimental heart failure. *Circulation* **92,** 262-267.

Yano N, Tseng A, Zhao TC, Robbins J, Padbury JF & Tseng YT. (2008). Temporally controlled overexpression of cardiac-specific PI3Kalpha induces enhanced myocardial contractility--a new transgenic model. *Am J Physiol Heart Circ Physiol* **295,** H1690-1694.

Yeh JK, Aloia JF, Chen M, Ling N, Koo HC & Millard WJ. (1994). Effect of growth hormone administration and treadmill exercise on serum and skeletal IGF-I in rats. *Am J Physiol* **266,** E129-135.

Zaritsky JJ, Eckman DM, Wellman GC, Nelson MT & Schwarz TL. (2000). Targeted disruption of Kir2.1 and Kir2.2 genes reveals the essential role of the inwardly rectifying K(+) current in K(+)-mediated vasodilation. *Circ Res* **87,** 160-166.

Zaritsky JJ, Redell JB, Tempel BL & Schwarz TL. (2001). The consequences of disrupting cardiac inwardly rectifying K(+) current (I(K1)) as revealed by the targeted deletion of the murine Kir2.1 and Kir2.2 genes. *J Physiol* **533,** 697-710.

Zhang S, Weinheimer C, Courtois M, Kovacs A, Zhang CE, Cheng AM, Wang Y & Muslin AJ. (2003). The role of the Grb2-p38 MAPK signaling pathway in cardiac hypertrophy and fibrosis. *J Clin Invest* **111,** 833-841.

Zobel C, Cho HC, Nguyen TT, Pekhletski R, Diaz RJ, Wilson GJ & Backx PH. (2003). Molecular dissection of the inward rectifier potassium current (IK1) in rabbit cardiomyocytes: evidence for heteromeric co-assembly of Kir2.1 and Kir2.2. *J Physiol* **550,** 365-372.